Aluminum microstructure evolution and effects on mechanical properties in quenching and aging process

by

Guannan Guo

A dissertation submitted to the faculty of the

Worcester Polytechnic Institute

in partial fulfillment of the requirements for the degree of

Doctor of Philosophy

in

Manufacturing Engineering

by

August 2017

Approved：

Richard D. Sisson, Advisor

George F. Fuller Professor Mechanical Engineering

Director of Manufacturing and Materials Engineering

Yiming Rong, Co-Advisor

John W. Higgins Professor of Mechanical Engineering

Associate Director of Manufacturing and Materials Engineering Program

Director of Computer-aided manufacturing Laboratory (CAM Lab.)

Abstract

High strength aluminum alloys are recently widely used in aircraft, automobile and construction industry fields. Typical T6 heat treatment process can be applied to improve the heat treatable aluminum alloy in order to facilitate the formation of prime strengthening precipitate phases. Critical steps in T6 heat treatment process include solution treatment, quenching and aging. Due to high thermal gradients in quenching process and aging process, large thermal stress will remain in the matrix and may bring unexpected deformation or distortion in further machining. Therefore, in order to predict the thermal stress effects, constitutive model and precipitate hardening model are needed to simulate the mechanical properties of alloy.

In this dissertation, an optimized constitutive model, which is used to describe the mechanical behavior during quenching and intermediate period of quenching and aging process, was given based on constitutive models with Zenor-Holloman parameter. Modification for constitutive model is based on the microstructure model, which is developed for the quenching and aging processes. Quench factor analysis method was applied to describe the microstructure evolution and volume fraction of primary precipitate phases during quenching process. Some experimental phenomena are discussed and explained by precipitate distributions. Classical precipitate hardening models were reviewed and two models were selected for Al-Cu-Mn alloy aging treatment. Thermal growth model and Euler algorithm were used to improve the accuracy and the selected precipitate hardening models were validated by yield stress and microstructure observations of Al-Cu-Mn aging response experiments.

Acknowledgements

Firstly, I would like to express my sincere gratitude to my advisor Prof. Richard D. Sisson for the continuous support of my PhD study and related research, for his patience, motivation, and immense knowledge. He helped me to finish my final defense and his guidance helped me in all the time of research and writing of this thesis. I could not have imagined having a better advisor and mentor for my PhD study. I also thank Prof. Rong who accepted me as PhD candidate firstly and gave me opportunities to work in General Motors and Tsinghua University, where I accomplished my most important projects of my PhD thesis.

Besides my advisors, I would like to thank the rest of my thesis committee: Prof. Liang Prof. Wang, for their insightful comments and encouragement, but also for the hard questions which incented me to widen my research from various perspectives.

My thanks also goes to Dr. Wang from General Motor who provided me an opportunity to join their team as intern, and who gave access to the laboratory and research facilities. Without they precious support it would not be possible to conduct this research.

I thank my fellow colleagues in for the stimulating discussions, my friends and all people who help me in research, lab and academic works. In particular, I am grateful to my wife Jia Wang and my family for supporting me spiritually throughout writing this thesis and my life in general.

Contents

Introduction

With the development of aerospace and aircraft technology, widely applications of high-strength aluminum alloy can satisfy the demand of high strength, high corrosion resistance and high toughness. [1] Since most of the applied aluminum alloys are heat-treatable, appropriate heat treatment processes can dramatically improve their strength, ductility and other mechanical properties. Al-Cu-based alloys have good mechanical properties at both low and high temperature ranges and are thus widely used in manufacturing industries. Several high-tech components, particularly in aerospace and aircraft industries with high standards of structural stability and mechanical properties under severe conditions, are composed of Al-Cu-based alloy. Heat-treatable Al-5%Cu-0.4%Mn alloys, denoted as ZL205A, not only improve the ductility, but also increase the yield strength by refining the primary strengthening θ' phase (Al_2Cu) size and by homogenizing the distribution of precipitate particles in the T6 heat treatment process. Nowadays, ZL205A are widely used to make structural components in aerospace, aircraft and automobile industries. The common failure of work piece made by ZL205A is crack propagation in quenching process, where local deformation expands beyond maximum ductility. Microstructure variation in heat treatment process including recovery, recrystallization and rearranged dislocations can increase the ductility, which is usually accompanied with reduction of strength. [2-6] Quenching process can also affect the microstructure of ZL205A, and the morphology and distribution of precipitates formed in this process also have significant effects on ductility. The primary phases in ZL205A include Al_2Cu, $Al_{20}Cu_2Mn_3$ and Al_3Ti phases, where Al_2Cu are generally considered to be primary strengthening phases in most Al-Cu based alloys. In order to obtain fine and uniform distribution Al_2Cu precipitates particles; Mn additions introduced into system are used for refining small Al_2Cu particles by increasing nucleation sites for nucleus. Besides, it can also accelerate the formation of Al_3Ti by improving recrystallization resistance, which in turn leads to good strength at elevated temperatures. [7,8] Moreover, different intermetallic phases have different impact on the ductility of materials. [9-11]

Since ductility has closed relationship with precipitates under different temperatures, the outcome of microstructure characteristics of heat treatment process should be

quantified in order to better predict and monitor mechanical behaviors. Several researchers have studied the effects of the T6 heat treatment on the yield strength of aluminum alloys with similar chemical concentration and their mechanical behavior at both high and low temperatures. [12,13] More works should have discussed mechanical properties such as strain and flow stress variation during the quenching process, where the factor of large temperature gradients should be considered. The cooling rate varies a lot among different locations due to the large and complex structure of the components, creating additional thermal stresses in the matrix. Although maintaining materials at low temperature would eliminate the effects of the natural aging process on the precipitates, the reheating process to the artificial aging temperature may allow some precipitate particles to nucleate and grow ahead of the aging process. Previous studies of flow stress in quenching ignored the phase effects on aluminum alloy, while assuming microstructure was identical and homogeneous. [14, 15] However, the precipitation process can be initiated during quenching process for aluminum alloy, [16] which cannot be avoided in all alternative methods. [17] Al_2Cu precipitates nucleation occurred from super-solid solution due to different solubility of solute elements and aluminum, which was accelerated by inherited vacancies from casting process. The vacancies aggravated the reduction of elongation and ductility of materials. [18] It is also reported that Al_2Cu phase formed in interface layer severely affected bond strength of clad composite and a number of micro-cracks caused by hard and brittle Al_2Cu phase, which made a contribution to low elongation. [19] Besides, T dispersoids have great thermal stability and easily nucleate during casting and solutionizing periods, which hardly dissolve into the matrix during consequent reheating and aging process. Due to complexity of structure and actual quenching methods, formation of T dispersoids before and during quenching process can hardly be avoided. [20] Therefore, there is an attempt to clarify the microstructure evolution of ZL205A during the reheating process and reveal the comprehensive effects of microstructure on deformation and fracture behaviors in this thesis.

The first component of this thesis is concerned of the mechanical properties of ZL205A (Al-Cu-Mn alloy) such as flow stress over a wide temperature range. A modified constitutive model has been developed in terms of temperature effects on phase transformation. Microstructure observations of dislocations and precipitate phases at different periods of heat treatment process are used to determine the effects

on flow stress and ductility. Isothermal tensile tests have been accomplished over a wide range of applicable temperatures and strain rates. Arrhenius-type constitutive model has been developed and calibrated with experimental data. Therefore, a better constitutive model can be used to simulate ZL205A mechanical behaviors under wide temperature ranges and to monitor quenching deformations. Besides, the corresponding microstructure observation and analysis helps explain the strain sensitivity and strain hardening trends varied at low or high temperature, and unexpected variation of the ductility of the alloy.

Another component of this thesis is focused on the precipitate hardening models of A356. Since A 300 series, aluminum–silicon series alloys have good fluidity, high strength and maintaining reasonable ductility, this kind of alloys are widely used in automobile manufacturing fields such as engine block, cylinder head and suspension components. Typically, silicon gives good fluidity and magnesium provides high strength by forming precipitates through proper heat treatment. T6 heat treatment is generally used in A356 production in order to obtain higher yield strength, while with the scarification of ductility. Besides, after aging process, the sizes of components made by A356 could expand, which leads to serious distortion. One possible reason is the growth of precipitate particles and the phase transformation of precipitate phase from coherent phases to incoherent stable phases. Therefore, a microstructure model of precipitate particles should be established. Many well-known precipitate-hardening models followed similar strengthening mechanism that the interactive motion behaviors of mobile dislocations and precipitate particles determine the contribution to final strengthening effects. [21-27]The particles could be sheared or surrounded by motive dislocations, which leads to the increase of dislocation density. The increasing dislocation density provides more inhibitions to plastic deformation. Since the criteria of separating these two strengthening modes are the precipitate particle size, accurate microstructure models of the precipitate particles should be studied through aging process.

During the aging process, the aging temperature and time are two critical values to simulate precipitate particles evolution under thermal dynamic principles and volume diffusion of solute element. For the microstructure part of these precipitate hardening models, there are two major methods to deal with precipitate particles evolution.

When assuming all particles as spherical shape, the radius of precipitate particles can either obtained as representative of mean value of all particles, which is called mean value approach method; [21, 23, 25, 26] or categorized particles into small groups with similar radius, which is called discrete value approach method. [28] Besides, when actual morphology of precipitate particles was considered, there would be different strengthening effects on different orientations, and different growth kinetics on different orientations which makes calculation of single particle more complicated than spherical particle assumption. The volume fraction of primary precipitate phase is usually increased exponentially and remains constant when reaching peak aging state. However, the prolonging aging process can activate the phase transformation of precipitate particles from semi-coherent phase to incoherent stable phase, which reduces the strengthening effects. Therefore, there is a need to review classical precipitate hardening models and find appropriate models to model the distortion of component made of A356 during aging. In this thesis, a microstructure model of precipitate phase of A356 is discussed when applying thermal growth model to the primary strengthening phases. The results of modified volume fraction of precipitate phases are used in the selected precipitate hardening models and a thorough comparison with experimental data of A356 aging data is given.

Ref:

1 MacAllister, G. K. "Effect of cooling rates on the mechanical properties of A206. 0-T4 and A206. 0-T71 aluminum alloy castings." *AFS Transactions* 97 (1987): 775-786.

2 Besson J (2009) Continuum models of ductile fracture: A review. International Journal of Damage Mechanics 19: 3–52.

3 Lin YC and Chen X-M (2011) A critical review of experimental results and constitutive descriptions for metals and alloys in hot working. Materials and Design 32: 1733–1759.

4 Liu HJ, Fujii H, Maeda M, et al. (2003) Tensile properties and fracture locations of friction-stir-welded joints of 2017-T351 aluminum alloy. Journal of Materials Processing Technology 142: 692–696.

5 Westermann I, Pedersen KO, Børvik T, et al. (2016) Work-hardening and ductility of artificially aged AA6060 aluminium alloy. Mechanics of Materials 97: 100–117.

6 Zhou J, Gao X, Hayden M, et al. (2012) Modeling the ductile fracture behavior of an aluminum alloy 5083- H116 including the residual stress effect. Engineering Fracture Mechanics 85: 103–116.

7 Birol Y (2007) Response to thermal exposure of the mechanically alloyed Al–Ti/C powders. Journal of Materials Science 42: 5123–5128.

8 Chang W-S and Muddle BC (1997) Trialuminide intermetallic alloys for elevated temperature applications—Overview. Metals and Materials 3: 1–15.

9 Simmons GW, Pao PS and Wei RP (1978) Fracture mechanics and surface chemistry studies of subcritical crack growth in AISI 4340 steel. Metallurgical Transactions A 9: 1147–1158.

10 Vasudevan AK and Doherty R (1987) Grain boundary ductile fracture in precipitation hardened aluminum alloys. Acta Metallurgica 35: 1193–1219.

11 Zehnder AT and Rosakis AJ (1990) Dynamic fracture initiation and propagation in 4340 steel under impact loading. International Journal of Fracture 43: 271–285.

12 X. YANG, J. ZHU, Z. NONG, M. YE, Z. LAI, and Y. LIU: 'Constitutive Behavior of As-quenched Al-Cu-Mn Alloy', *Modern Physics Letters B*, 2013, **27**, 1-8.

13 M. L. Newman: 'Modeling the behavior of a type-319 aluminum alloy during quenching', University of Illinois at Urbana-Champaign, Illinois, 2002.

14 X. Y. Liu, Q. L. Pan, Y. B. He, W. B. Li, W. J. Liang, and Z. M. Yin: 'Flow behavior and microstructural evolution of Al–Cu–Mg–Ag alloy during hot compression deformation', *Materials Science and Engineering A*, 2009, **500**(1-2), 150-154.

15 H.-Y. Li, Y.-H. Li, X.-F. Wang, J.-J. Liu, and Y. Wu: 'A comparative study on modified Johnson Cook, modified Zerilli–Armstrong and Arrhenius-type constitutive models to predict the hot deformation behavior in 28CrMnMoV steel', *Materials & Design*, 2013, **49**, 493-501.

16 J. Evancho and J. Staley: 'Kinetics of precipitation in aluminum alloys during continuous cooling', *Metallurgical Transactions*, 1974, **5**(1), 43-47.

17 C. M. Estey, S. L. Cockcroft, D. M. Maijer, and C. Hermesmann: 'Constitutive behaviour of A356 during the quenching operation', *Materials Science and Engineering A*, 2004, **383**(2), 245-251.

18 H.-J. Liu and H.-J. Zhang: 'Repair welding process of friction stir welding groove defect', *Transactions of Nonferrous Metals Society of China*, 2009, **19**(3), 563-567.

19 J. Lee, D. Bae, W. Chung, K. Kim, J. Lee, and Y. Cho: 'Effects of annealing on the mechanical and interface properties of stainless steel/aluminum/copper clad-metal sheets', *Journal of Materials Processing Technology*, 2007, **187**, 546-549.

20 S. Cheng, Y. H. Zhao, Y. T. Zhu, and E. Ma: 'Optimizing the strength and ductility of fine structured 2024 Al alloy by nano-precipitation', *Acta Materialia*, 2007, **55**(17), 5822-5832.

21 H.R Shercliff and M.F. Ashby, *Acta mater,* Vol 38, No. 10, pp. 1789-1802, 1990

22 M. Perez, M. Dumont and D. Acevedo-Reyes, *Acta mater* 56(2008) 2119-2132

23 A. Deschamps, *Acta mater*, Vol 47, No. 1, pp 281-292, 1999

24 A. Deschamps, *Acta mater*, Vol 47, No. 1, pp 293-305, 1999

25 S. Esmaeili, *Acta mater* 51 (2003) 2245-2257,

26 A. Bahrami, *Metallurgical and Materials Transactions A,* 09 August 2012

27 Liu, Gang, et al. "Modeling the strengthening response to aging process of heat-treatable aluminum alloys containing plate/disc-or rod/needle-shaped precipitates." *Materials Science and Engineering: A* 344.1 (2003): 113-124

28 S. Esmaeili, D.J. Lloyd, *Metallurgical and Materials Transactions A*, Vol 34A, March 2003.

Literature reviews

1 Additional elements effects on microstructure and mechanical properties of Al-Cu system alloy

Since precipitate phases are critical factors related with final yield strength and other properties, optimizing morphology and distribution of precipitate phase facilitate well strengthening effects on Al-Cu alloy. Additional elements such as Mg, Mn, Si and Sn are introduced into Al-Cu system can adjust Al_2Cu nucleation and growth by affecting nucleation kinetics, volumetric misfit strain, shear strain and interfacial energy of θ' precipitate phases. For example, $\{1\ 0\ 0\}_\alpha$ plate of metastable Al_2Cu in 2XXX series aluminum alloy play the dominate role in strengthening, and $\{1\ 1\ 1\}_\alpha$ plates of metastable Al_2Cu are founded in Al-Cu alloys microalloyed with Mg and Ag. Li-modified Al-Cu alloys has $\{1\ 1\ 1\}_\alpha$ plates of T1 (Al_2CuLi) to strength and AA2195 is considered to be strengthened by uniform distribution of T_1 plates of large aspect ratio. [1, 2, 3] Sn (roughly 0.01~0.02at%) is introduced into Al-Cu system to increase the transaction from θ'' to θ' and perform rational orientation and uniform θ' precipitate phases. It was reported that for Al-1.7at%Cu, 0.01at% Sn dramatically shorten the time to reach peak hardness and increase peak hardness, and solute Sn is more effective to involve into θ' nucleation than Sn phases. [4] Sc is also an important solute element that is used to improve Al-Cu mechanical properties. Al_3Sc dispersoids are specially referred to the Al_3Sc particles formed in high temperature processing of the alloy, such as homogenization, hot-rolling or extrusion, which are considered to stabilize the grain boundary of Al and hence inhibit the recrystallization. Al_3Sc precipitates referred to those formed during aging process after solution treatment, however, due to the limited decomposition of Al_3Sc from super solid solution, the strengthening contribution from Al_3Sc usually be restricted, and Al_3Sc hardly coexisted with other strengthening precipitates due to its temperature regime. [5]

Among the additional elements, manganese is introduced into Al-Cu system to obtain fine-grain polycrystalline and improve its strength especially at high temperature. Mn addition had already been proved to refine θ'-Al_2Cu and retard Orowan coarsening. Related DSC analysis of compare between Al-Cu alloy with and without Mn addition is accomplished by previous researchers, which proved the formation of θ'-Al_2Cu is largely postponed but dominantly enhance the strength just before peak aged.

Diffusivity of Mn is closed to Cu that leads to easily attracting Cu atoms toward Mn atoms. Thus, quenched vacancy or clusters formed after quenching or beginning of aging does not efficiently work to form GP zones. [6] T dispersoids have great thermal stability and provide preferred nucleation sites for other possible precipitate phases. Even though addition of Mn can efficiently reduce the coarsening stage of θ'-Al_2Cu, consideration of phase transformation from θ'-Al_2Cu to stable phase losing its coherency and strengthening should be included. However, the introduction of Mn into system also brings undesirable effects on mechanical properties, especially on the resistance to crack growth. [7, 8] T dispersoids formed as grain boundaries also decrease the binding capacity of neighbor grains, which leads to micro voids or cracks easily occurred. Thus, for solution treatment, quenching and aging periods, the evolution of T dispersoids or precipitates should be taken into consideration in order to predict deformation behaviors of ZL205 alloy.

2 Heat treatment processes effects on microstructure and strengthening mechanism of aluminum alloy

1) Casting

Typical heat treatment process concludes casting, solutionizing, quenching and aging steps for most of heat treatable aluminum alloy. Casting process is critical to the whole heat treatment process since most of microstructure characteristics of matrix are set in this period. Secondary dendrite arm spacing, SDAS, is often applied to evaluate the coarseness of the microstructure after casting. [9] Dendrite structure has lower copper content in central part. Moving toward the outside of the arms, which corresponds to metal freezing later, the copper content increases and combines with Al to form the Al-α + Al_2Cu eutectic mixture. [10] DAS can also affect micro-segregation of alloy element and distribution of second precipitate phase or micro-porosity. Cooling rate of solidification process is the critical parameter that determines length of DAS. Proper selection of pouring temperature, cooling conditions and chemical distribution should be considered in order to guarantee satisfied casting quality. Besides, due to long freezing range of Al-Cu based casting alloys, micro-porosities are easily formed during solidification. The different cooling rates of raw casting component lead to different thermal shrinkages. Micro-pores

cannot be filled with liquid alloy immediately and be left in the as-cast structure. With the help of proper squeeze casting method, pressure are applied during casting process to accelerate liquid alloy flow into micro-pores and fill them, which can dramatically reduces such defects. [11]

For Al-Cu based alloy, homogeneous Cu distribution is important for Al-Cu based alloy. Due to gravity casting and solubility of copper element, copper segregation serious, while Mn or Mg segregation hardly occurs because of fully dissolved in α-Al matrix. Inverse segregation is usually found in cast Al-Cu alloys owing to long freezing range, which leads to large dendrite arm spacing with slow cooling rate. Low temperature gradients also lead to coarsening dendrite skeleton and shrinkage induced fluid transports the solute rich liquid away from the center of the casting back to the surface. Such casting microstructures as dendrite arm and additional element segregations will further affect following up mechanical properties in quenching and aging such as precipitate phase morphology and distribution. For as-cast aluminum alloys, yield strength is believed to be affected by copper content in α-Al grains and increased amounts of intermetallic compounds, especially the fine intermetallic presented at the α-Al grain boundaries. Since present project focus on quenching and aging effects on mechanical properties, fine α-Al grains and short DAS are needed to eliminate casting defects and negative effects on following heat treatment process. Casting process parameters such as temperature gradient and cooling rate should be well controlled.

2) Solutionizing

Method that introducing additional elements into the aluminum matrix in order to produce second precipitate phases is termed as solutionizing. Particles formed at casting and homogenization process will dissolve and additional solute elements will diffuse into the matrix in solution treatment. These additional elements can affect the pre-quenching process microstructure and also play as nucleation sites for further precipitation in aging to strengthen the aluminum alloys leading to the significant increase of ductility and decrease of yield strength because of less pining of the fine intermetallic presented at the α-Al phase boundaries. It is worth to note that the solute content in the primary α-Al phase is increased after solutionizing, which means solution strengthening is enhanced. However, the alternations in microstructure from

other phases and at grain boundaries are more significant and effective, resulting in a reduction of the yield strength and an increase of elongation. [12] In order to obtain the fine super solid solution for quenching and homogenization nucleation sites for aging, the effects of solutionizing on microstructure and mechanical properties should be discussed and the process parameters of solution treatment should be optimized.

The objective of choosing proper solution process parameters is to maximum solute element in aluminum alloys in the aluminum matrix. Solution temperature, which is determined by solute element content, should be in the range that avoids overheating or local melting and accelerates the dissolution of particles formed in pre-heating and casting process as much as possible. Upper limit of the solution temperature is usually closed to the eutectic temperature when considering the effects of grain growth, surface effects and economy of operation. Solution time required in solutionizing should guarantee sufficient dissolution and make the maximum solute elements solve into matrix. It is dependent on the types of products, alloy systems, casting or fabricating procedures used and thickness insofar as it influences pre-existing microstructure. From the microstructure aspect, the coarseness of as-cast microstructure determines the time needed for solution treatment. The finer as-cast microstructure, the shorter solution time is needed. From the macrostructure aspect, the larger the section thickness is, the longer holding time required, while thin products just need several minutes to finish the solution treatment. Excessive diffusion should be avoided when prolonging the solution time and particular mechanical properties decreased with increasing solution time should be also controlled. Since current project aims at studying thin wall components made by ZL205, the solution process will be finished very soon to avoid unexpected coarsening and mechanical properties reduction.

3) Quenching

Quenching process is used to obtain super saturated solid solution in order to facilitate the further precipitation in aging. Different quenchants such as oil, water or polymer solution are used to cooling materials to room temperature when providing suitable cooling rate. Microstructure formation and distribution occurred in varied quenching conditions have great effects on aluminum quenching behaviors and further effects on aging process. Fink and Willey pioneered attempts to describe the effect of quenching

on properties of aluminum alloys. [13] They applied isothermal quenching techniques to develop C-Curve for particular aluminum alloys. Even though their method worked well when the cooling rates are uniform, it is failed to predict the effect of quenching on aluminum alloys properties when the cooling rate varied considerably during the quench. Since the properties are highly dependent on the microstructure evolution, and such microstructure evolution determined by the material, quenching temperature and time needs to be predicted by quenching process parameters. [14, 15, 16] Quench factor analysis method is put forward to predict the volume fraction of precipitate phase in quenching process instead of average cooling rate method. Time elapsed during non-isothermal quenching process are divided into several short time steps, which can be considered as isothermal quenching process. [17-21] Since quenching process typically lasts very short, the growth or coarsening of these intermetallic dispersoids or precipitate particles can be ignored. However, lack of considering dispersoids formed in quenching process brings overestimation of primary precipitate hardening phase's volume fraction in simulation and negative effects on mechanical properties.

4) Aging

Result of strengthening is dislocation motion is blocked by the formed precipitate particles during the aging process due to change of solubility of alloy element. Since the mechanical properties are concerned and highly dependent on the precipitate phase distribution, the size and volume fraction of precipitate phases should know at the peak-aged state. T6 heat treatment is widely used in heat treatable aluminum alloy production to obtain peak yield strength. Binary Al–Cu alloy has following aging sequence: $\alpha \rightarrow \alpha$ + GP zones $\rightarrow \alpha + \theta'' \rightarrow \alpha + \theta' \rightarrow \alpha + \theta$ [22, 23, and 24]. The aluminum solid solution is indicated by α, the metastable phases are indicated by θ', θ'' and the stable precipitates by θ.

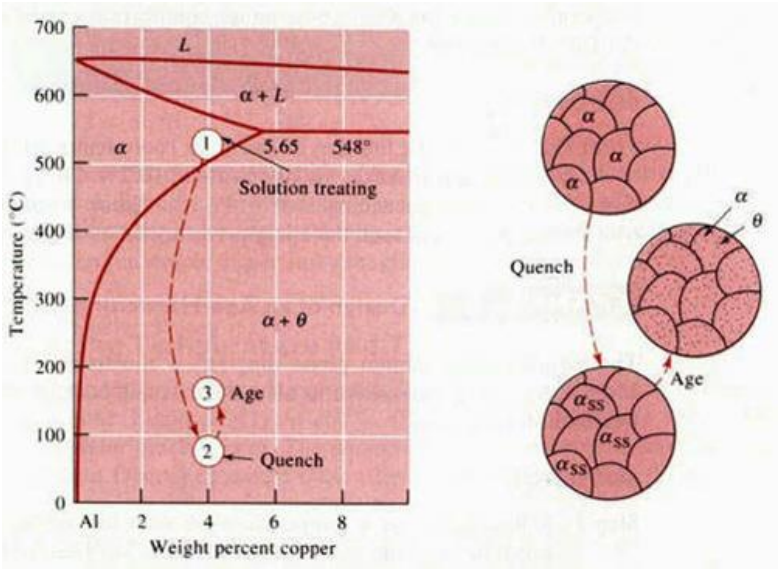

Figure 2.1 The aluminum rich end of Al-Cu phase diagram

The super saturation of vacancies allows solute elements diffusion and lead to the formation of GP zones. GP zone is firstly nucleated from the super solid solution; the dislocation among the matrix can offer proper nucleation sites for GP zone, also the grain boundary and other defects in the matrix can be available nucleation sites. Typically the thickness of the GP zone is one or two atom layers and GP zone is fully coherent with the matrix. After the formation of the GP zone, the next step is the formation of transit phase. Some reports show that there exist GP II zone between GP zone and the transit phase based on different material. GP II zone will generally follow GP zones by forming a second layer parallel to the GP zone on the plane. [25] Other authors consider GP II zones as an ordered phase with two Cu layers separated by three Al layers. Mentioning about transit phase, there will be not only one phase formation at this period, and the previous transit phase can transform to another type of transit phase, with the change of composition and morphology. Meanwhile, the orientation and morphology of the transit phase also alter their contribution to precipitate strengthen. [26, 27] To simulate precipitate hardening the assumption of the particle size should not be spherical shape, size and volume fraction of these transit phases should be modeled precisely. They may alter the shape of precipitates phase, magnitude and anisotropy of the interfacial energy, the different elastic constants of matrix and precipitate and crystal structure. Detailed simulation models will be given in the next section and compared.

Transit phase is considered to generate from GP zone and consume the original GP zone space at the same time. The coherency relationship with the matrix now turns to semi-coherent, which will produce large lattice deformation and strengthen the material. The final phenomena in the aging process is the stable second phase nucleation, growth and coarsening. Transit phase cannot maintain stable at room temperature or in-service condition and spontaneously transform to the stable phase. The non-coherent boundary and complicate semi-coherent boundary with the matrix decrease the strength of the material. The formation of the stable phase will consume the precipitate phase and the strength effect is reduced.

3 Strengthening mechanism of deformation and constitutive models

Deformation of ZL205A is one of the concerns in my proposal especially in heat treatment process. Dislocation motions in matrix allow for deformation of material. When the dislocation motion is inhibited and dislocation density is increased, the movement of dislocation will be restricted due to the pile up of dislocation. Any strengthening method is aiming at either improving the dislocation density or hindering moving dislocations. [28] Work hardening mechanism, solid solution mechanism, precipitate hardening mechanism and grain boundary mechanism are general strengthening mechanisms, which will be discussed with actual heat treatment periods to tailor their effects on yield strength and flow stress.

Work hardening method is usually used to improve strength and hardness in cold deformation by introducing more dislocation that increasing dislocation density. The interactive action with encountered dislocations will impede dislocation motion by stress field generated by dislocations. Besides, cross dislocation lines may play as pin point that also increase the barrier to the motion of dislocations. Cold working in the interval between quenching and aging is considered to accelerate the aging response, providing numerous sites for heterogeneous nucleation of precipitates. [29] In current proposal, a cold working is avoided in order not to introduce work hardening effects into heat treatment process from solutionizing to reheating process. Therefore, the variation of aluminum grain size and precipitation formed in natural aging or reheating process will be only related with temperature variations.

Solid solution strengthening is important for aluminum alloy since lots of additional elements can be introduced into aluminum matrix to form substitution or interstitial solid solution. The solute atoms can cause lattice distortion to increase yield strength by impeding dislocation motion. Meanwhile, the stress fields caused by solute atoms can interact with dislocations. Depends on actual size of solute elements, they can interfere with neighbor dislocations by playing as potential obstacles. During solution treatment process of current proposal, the major solute elements are Cu and Mn atoms. T dispersoids, which has chemical compositions of $Al_{20}Cu_2Mn_3$, are easily formed with great thermal stability making them hardly dissolve in further reheating process. Cu atoms can be observed to fully dissolve into matrix to obtain fine and homogeneous solid solution。 Segregation of Cu and some vacancies can be expected to be eliminated during solution treatment. Therefore, solution-strengthening effects on yield strength and flow stress may be highly related with T dispersoids size and volume fraction.

Precipitate hardening methods are widely used to strengthening heat treatable aluminum alloy by precipitating second phases from super solid solution, when solubility of solute element reduce during aging process. Precipitate particles play the similar functions as solutes that pinning the motion of dislocations. With the continuous of aging process, the precipitate phases will lose their coherency relationship with the matrix so that the strengthening effects are weakened. Besides, there are two interactive motions between precipitate particles and dislocations. When the size of particles are small, the dislocation line will be cut when passing by the particles; and when the size of particles are relative large, dislocation lines will be looped or bowed leaving a closed dislocation ring. Both methods increase the dislocation density that also increases the barrier of dislocation motion. In this project, working hardening mechanism can be neglected because there is no significant cold working occurred before or after the experiments. Grain boundaries effects on strengthening are also remain the same based on the observation of stabilized aluminum grain size during heat treatment process and isothermal tensile tests. Thus, solid solution strengthening especially in quenching and reheating process and precipitate hardening strengthening in aging process are major strengthening mechanism that governing yield strength and flow stress.

In this study, constitutive models are studied to provide accurate deformation at wide range of strain rates and temperatures when considering solid solution and precipitate strengthening, and dynamic recrystallization and recovery softening mechanism. Therefore, a proper constitutive model that combines the effects of process parameters and thermal dynamic would be useful. Strain, strain rate and temperature are three critical parameters determine softening and hardening effects on deformation behaviors of aluminum alloy. Thermal softening and strain hardening are considered separately so that the production of both factors and strain factor gives the variation of flow stress. In this situation, the work of plastic deformation all converses to heat. However, high strain rate leads to insufficient time for inner heat to disperse, which leads to the competence between the thermal softening and strain hardening at particular temperature and strain rate. Johnson-Cook empirical constitutive models are selected to predict flow stress of ZL205 at high strain rate with wide temperature range, which is proved to be successful in predicting such deformation behaviors, while some of parts are not fully discussed. [30, 31] Related researches pointed out that at higher strain rate, the flow stress would monotonously increase as temperature rises, which is opposite to the variation at lower strain rate. [32] Dynamic strain aging mechanism is used to explain this unusual phenomenon considering the new-formed solute atoms that affect dislocation motion. This similar phenomenon founded in ZL205 proved sensitivities of ZL205 to deformation time since the deformation period is much longer than high strain rate situations, which does not have plenty time for aging. Solute atoms transportation at some particular states may also be controlled by forest dislocation, which is usually observed at low temperature deformation circumstance. Therefore, the microstructure state of ZL205 alloy in selected strain rate and temperature range should be examined firstly, and temperature terms in constitutive models may be more complicate than the ones descripted in Johnson-Cook model.

At low temperature range, the flow stress of materials usually has proportional relationship with dislocation density, and mobile dislocation are easily tangled or seized with forest dislocation thus reduce ductility and improve strength. The microstructure at low temperature range is usually considered to be stable and no phase transformation or precipitation is considered in this circumstance. While at high

temperature range, the factors that affect flow stress can be divided into two subclasses, one is related with temperature and another is independent on temperature. The maximum threshold stress is presented as maximum glide resistance force. When the stress is larger than maximum threshold stress, continuous glide will occur. Strain rate at this condition can be obtained from the product of Burgers vector, dislocation density and velocity. However, the stress could be smaller than maximum threshold stress and jerky glide, which is considered to be discrete glide compared with continuous glide, will dominate the mechanical behaviors. Under this circumstance, the total mobile dislocation density is composed of mobile dislocation and potential dislocation, which will be activated by thermal fluctuation. The increment of strain contributed by thermal fluctuation can be given as [33]:

$$\delta\gamma = \gamma_0 \delta P_t \qquad (2.1)$$

where γ_0 is average strain together with dislocations taking part in process and δP_t represents the possibility of released contributed by thermal fluctuation. Then the product of frequency factor and Boltzmann factor presented as Arrhenius term can be obtained as:

$$P_t = v_G \exp\left(-\frac{\Delta G}{kT}\right) \qquad (2.2)$$

Equation 2.2 follows the assumption that thermal fluctuation exceeding in magnitude is only described by Boltzmann distribution and $\frac{\Delta G}{kT}$ should be small in order to neglect the possibility of backward jumps. At last, thermal activation process is a statistical process, which means the average value when counting dislocation density is meaningful. Other factors like stress released by recovery and inhibited by mechanical stress are also make a contribution to the increment of strain. When the value of thermal fluctuation term is larger than other factors, the stress-strain curve can directly give information about ΔG effects. In addition, ΔG used in this section is not as the same as the common symbol G in thermodynamics. ΔG is called activation free enthalpy and defined by:

$$\Delta G = \Delta F - \Delta W \qquad (2.1)$$

where ΔF is the Helmholtz free energy necessary for activation and ΔW is the additional work that brought dislocation from stable position to unstable position.

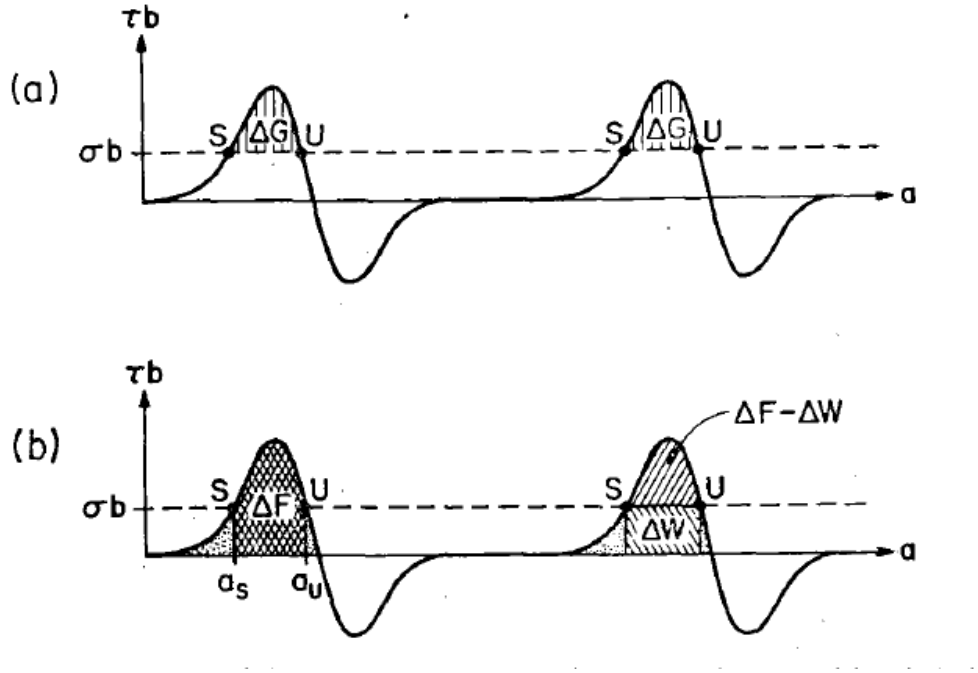

Figure 2.2 A glide diagram explanation of ΔG, ΔF, and ΔW quantities.

Phenomenological description of activation energy when consider all obstacles are box-shaped can be given as:

$$\Delta G = F_0\left(1 - \frac{\sigma}{\hat{\tau}}\right) \qquad (2.2)$$

where F_0 represents total energy to activate glide without external energy. Short-range obstacles are especially sensitive to thermal activation, therefore above equation can be replace by a useful form:

$$\Delta G = F_0\{\left(1 - (\frac{\sigma}{\hat{\tau}})^p\right)\}^q \qquad (2.3)$$

where two adjust parameters p and q are used to describe the profile of stress. Empirically, 1/2 is chosen for p and 2/3 is chosen for q. In discrete glide system, the glide resistance may be assumed to be proportional to the shear modulus and activation area proportional to the square of the Burgers vector, thus the value of activation energy ΔG can be calculated as:

$$\Delta G = \mu b^3 g\left(\frac{\sigma}{\mu}\right) \qquad (2.4)$$

where μ is the shear modulus, which can be taken as a function of temperature and b is Burgers vector. Above all, the strain rate is highly depended on activation energy for hot deformation when thermal activation mechanism is the primary cause during high temperature deformation of materials:

$$\dot{\gamma} = \gamma_0 v_G \exp\left(-\frac{\Delta G}{kT}\right) \quad (2.5)$$

Then, when activation energy of hot deformation can be assumed to be constant above half of the melting point temperature, and pre-exponential term of dislocation participated into process is considered at various flow stress state, the above equation can be written as:

$$\dot{\varepsilon} = AF(\sigma)\exp\left(-\frac{Q}{RT}\right) \quad (2.6)$$

$$F(\sigma) = \begin{cases} \sigma^n & \alpha\sigma < 0.8 \\ exp(\beta\sigma) & \alpha\sigma > 1{,}2 \\ [\sinh(\alpha\sigma)]^n & for\ all\ \alpha\sigma \end{cases} \quad (2.7)$$

And Zener-Holloman parameter is used to represent the relationship of strain rate and temperature:

$$Z = \dot{\varepsilon}\exp\left(-\frac{Q}{RT}\right) \quad (2.8)$$

Since constitutive equations used Zener-Holloman parameters well describe the mechanical behaviors at different stress level by empirical relationship and apply thermal activation mechanism to quantify the mechanical behaviors at high temperature, it will be a good choice to apply in Al-Cu aluminum alloy system since there will be precipitation and recovery occurred at high temperature deformation that brings extra obstacle to dislocation motion, which is needed thermal activation mechanism to predict the effects of precipitates and Al grain size. Arrhenius-type equations have been applied to describe the compression deformation behaviors of aluminum alloys especially at high temperature deformation or forming process. [34-38] Hyperbolic law in Arrhenius-type equations gives both excellent descriptions at high or low flow stress. Zener-Hollmon parameter gave the temperature compensate strain rate in an exponent-type that helps give a comprehensive description of all stresses level. [39] The model has been widely used to predict aluminum alloy such as 2124-T851, A356, Al-Cu-Mg alloy and Sn modified Al-Cu-Mg alloy. However, tensile properties of aluminum alloy are lack of discussion. Previous study have already pointed that the hot tensile deformation is the competence of work hardening, dynamic softening and develops of microvoids or cracks. Microvoids or intermetallic compounds may form before quenching which play as possible crack source and large thermal gradient in quenching process can produce residual stress that destroying the thermal stability of aluminum components. At low deformation temperature, dynamic

recrystallization softening hardly occurs and non-uniform microstructure combined with large dislocation clusters caused by strain hardening will bring serious stress concentration. While at high deformation temperature, dynamic recrystallization softening will be enhanced by thermal activated mechanism.

For ZL205 aluminum alloy used in my project, Al grains, Al_2Cu precipitate phase, Mn and Zr additions formed as dispersoids may have effects on mechanical properties such as fracture, hardness and strength. The variation change in microstructure will dramatically affect the deformation mechanism and activation energy of hot deformation should be related with temperature and strain rate. [40-43] In as-cast Al-Cu aluminum alloy, larger grains usually bring coarser boundary, which leads to significant deduction of ultimate tensile strength. Eutectic phase will produce fracture soon because of fragility and thickness. Deformation can increase as the grain size increase when the particles are small because not enough coarsening, however, larger particles under other casting processes such as rheocast leads to excessively coarseness of grain boundaries and therefore fracture occurs before large deformation. Elongation properties also share the similar behaviors as deformation induced by variation of grain boundaries or sizes. [44] Different distribution of Al_2Cu precipitate phase caused by different casting methods or additional elements also has an effect on mechanical properties. Discontinuous but better distribution of the eutectic phase caused by dendritic material microstructure presents better mechanical properties due to finer control of this hard and fragile phase than smaller size but continuous and thick eutectic boundaries. T dispersoids formed in casting and solutionizing also play important role on mechanical properties in Al-Cu alloy with Mn additions by stabilizing grain size at elevated temperatures and retarding recovery. [45] Formation of T dispersoids at grain boundaries decreases the binding capacity of neighbor grains, which leads to micro voids or cracks easily occurred. Such micro voids or cracks may play as deformation source during following tension test and easily get fracture. It had been reported that addition of Mn is used to form $Al_{20}Cu_2Mn_3$ dispersion to increase the resistance to recrystallization and improve damage tolerance by help homogenize slip. [46] T dispersoids phases also entangled with dislocations and could be potential dislocation source. Zr additions can form Al_3Zr that also inhibit recrystallization. Previous studies have already proved the T phase formed in Al-Cn-Mn system at grain boundaries dramatically reduce the binding capacity, which leads to easily crack

formation and propagation, and mathematical model of T phase distribution and morphology should be investigated and obtained by hot deformation process parameters. Therefore, combined effects of above microstructure on mechanical behaviors of ZL205 in whole temperature range should be studied.

4 Precipitate hardening models of aluminum alloys modified by thermal growth model

Many experiment data have been studied to discover the relationship between the precipitate and the component of alloy, aging time and temperature. In order to get a comprehensive law of precipitate hardening mechanism of aging, some previous models developed to describe the thermodynamic of precipitate particles' size, morphology and characteristics, for the size and volume fraction of precipitate phases directly impede the dislocation motions. Shercliff H.R and Ashby.M.F firstly made an attempt to combine the process parameters of aging process, such as composition of alloy, time and temperature, to predict the yield strength, and this method is successfully applied on 6000 series aluminum alloy. In the model, strengthening contribution is mainly composed of solute atoms, shearable precipitates and non-shearable precipitates. [47] A.Deschamps and his partners introduced microstructure evolution into the precipitate hardening model, described in detail the nucleation, growth and coarsening of the precipitate particles. [48] Because dislocations are preferred sites for transit phase nucleation and growth; the precipitates at dislocation were also discussed to modify the microstructure evolution model. Basic strength mechanisms are classified as precipitation shearing and bypassing based on the different size of the particles. And the morphology of the particles is assumed to be spheroid for convenient calculation. Following fundamental equation are mostly used in many precipitate hardening models for yield strength calculation:

$$\sigma_p = \frac{M\bar{F}}{bl} \tag{2.9}$$

Where M is the Taylor factor, b is the magnitude of Burgers vector and l is the mean effective particle spacing in the slip plane along the bending dislocation. [49] Based on dislocation strength mechanics and morphology, the main two parameters to determine the final yield strength after aging come to the radius and the volume fraction of the precipitates. And from these two parameters we can calculate the l and F then get the value of yield strength.

B. Raeisinia and W.J. Poole and etc. used the volume fraction of the different dominated precipitate strength particles to calculate yield strength. [50] However, they ignored the size of these particles and assume the homogeneous size of the precipitates phase. S. Esmaeili and D.J. Lloyd calculated the relative volume fraction of precipitates with aging time, and then dedicated the value of radius of particles. This paper considered the actual morphology of precipitates so that the simulation will be more accurate. [51] On the other hand, since the actual morphology of precipitates are not usually spheroid, G.Liu gave a more accurate and realistic description of the precipitates morphology, separating into plate/dis and rod/needle shape, then applied the peak-aged state to derive the volume fraction of these practices. And this method was proved to work well when applying to Al-Cu-Mg alloy and Al-Mg-Si alloy. [52] In M. Song paper, he put forward that at the first of the aging process, the dislocation cutting mechanism might play a prime role on dominating the strength. [53] Therefore, he made a modification of G. Liu model and considers the increment of yield strength is composed of cutting and bypassing mechanism.

However, in the precipitate hardening model, the microstructure evolution is assumed to be no contact with other growing atoms and therefore the growth will not affect the neighbor particles growth. In reality, at the beginning of the aging process, the solute atom has the maximum super solution and the diffusion rate of solute atom is large. With prolonging the aging time, the concentration of solute atoms and the precipitate phase growth rate will decrease, and this will bring the deviation of the model and experiment. Therefore, we need the accurate prediction of the growth rate of the precipitates in the aging process. In Deschamps and Brechet, they separated the whole microstructure evolution into nucleation, growth and coarsening three steps. They calculated different nucleation rates and growth rates for each step and use them to get the density and the radius of the precipitate particles. Although they gave a criteria to identify the critical radius to separate nucleation, pure growth and coarsening, it is difficulty in determining when the growth and coarsening happening. In my project, I firstly made attempt to follow the method described in Ford's patent studying Al-Cu system. In the patent, the growth rate can be obtained from the volume change and the phase fraction. The transformation among precipitate phases can produce the volume

change because of the diffusion of precipitate element from the different transit phases. When applied T6 heat treatment, thermal growth of the prime strengthen phase Al_2Cu (termed with θ' in the patent) is not completely growth to its maximum size when it turns to stable phase (termed with θ). And with the time prolonging, the θ will coarse and consume θ', which lead to reduce the thermal growth effect. This model can also predict the non-isothermal aging process. In the end, the dimension change vs. Cu fraction can be determined from the model. The relative parameters can get from TTT diagram and equilibrium state phase fraction. [54] In this project, S. Esmaeili's model and Myhr's model have been chosen to be the reference models and try to modify them with thermal growth model. As mentioned before, the data needed of both models are the volume fraction of the precipitates, which we can realize by TEM or SEM data.

Reference

1 Nie J F, Muddle B C. Strengthening of an Al–Cu–Sn alloy by deformation-resistant precipitate plates[J]. Acta Materialia, 2008, 56(14): 3490-3501.

2 Chester RJ. PhD thesis. Australia: Monash University; 1983.

3 I.J. Polmear, M.J. CouperMetall Trans A, 19A (1988), p. 1027

4 Bourgeois L, Dwyer C, Weyland M, et al. The magic thicknesses of θ′ precipitates in Sn-microalloyed Al–Cu[J]. Acta Materialia, 2012, 60(2): 633-644.

5 Chen B A, Pan L, Wang R H, et al. Effect of solution treatment on precipitation behaviors and age hardening response of Al–Cu alloys with Sc addition[J]. Materials Science and Engineering: A, 2011, 530: 607-617.

6 Takeda M, Komatsu A, Ohta M, et al. The influence of Mn on precipitation behavior in Al-Cu[J]. Scripta Materialia, 1998, 39(9): 1295-1300.

7 Lee W M, Zikry M A. Microstructural characterization of a high-strength aluminum alloy subjected to high strain-rate impact[J]. Metallurgical and Materials Transactions A, 2011, 42(5): 1215-1221.

8 Giummarra C, Thomas B, Rioja R J. New aluminum lithium alloys for aerospace applications[C]//Proceedings of the light metals technology conference. 2007.

9 R. Trivedi and W. Kurz, *Int. Mater. Rev.* **39**, 49 (1994).

10 Barros A S, Magno I A, Souza F A, et al. Measurements of microhardness during transient horizontal directional solidification of Al-Rich Al-Cu alloys: Effect of

thermal parameters, primary dendrite arm spacing and Al2Cu intermetallic phase[J]. Metals and Materials International, 2015, 21(3): 429-439.

11 Gan Y, Zhang D, Zhang W, et al. Effect of cooling rate on microstructure and mechanical properties of squeeze cast Al-Cu-Mg alloy[J]. International Journal of Cast Metals Research, 2015, 28(1): 50-58.

12 Yang H, Ji S, Fan Z. Effect of heat treatment and Fe content on the microstructure and mechanical properties of die-cast Al–Si–Cu alloys[J]. Materials & Design, 2015.

13 W.L. Fink and L.A. Willey: *Trans, AIME*, 1948, vol. 175, pp.414-27

14 Bratland, D. H., et al. "Overview No. 124 Modeling of precipitation reactions in industrial processing." *Acta Materialia* 45.1 (1997): 1-22.

15 Porter, David A., and Kenneth E. Easterling. *Phase Transformations in Metals and Alloys, (Revised Reprint)*. CRC press, 1992.

16 D.A. Porter and K.E. Easterling. Phase Transformation in Metals and Alloys, Van Nostrand Reinhold, Co. Ltd. Wokingham

17 Shang, B. C., et al. "Investigation of quench sensitivity and transformation kinetics during isothermal treatment in 6082 aluminum alloy." *Materials & Design* 32.7 (2011): 3818-3822.

18 Liu, Shengdan, et al. "Investigation of quench sensitivity of high strength Al–Zn–Mg–Cu alloys by time–temperature-properties diagrams." *Materials & Design* 31.6 (2010): 3116-3120.

19 Newkirk, J. W., and D. S. MacKenzie. "The Jominy end quench for light-weight alloy development." *Journal of materials engineering and performance* 9.4 (2000): 408-415.

20 Hömberg, Dietmar. "A numerical simulation of the Jominy end-quench test."*Acta Materialia* 44.11 (1996): 4375-4385.

21 Dolan, G. P., et al. "Quench factor analysis of aluminium alloys using the Jominy end quench technique." *Materials science and technology* 21.6 (2005): 687-692.

22 Hu S Y, Baskes M I, Stan M, et al. Atomistic calculations of interfacial energies, nucleus shape and size of θ′ precipitates in Al–Cu alloys[J]. Acta materialia, 2006, 54(18): 4699-4707.

23 Vaithyanathan V, Wolverton C, Chen L Q. Multiscale modeling of θ′ precipitation in Al–Cu binary alloys[J]. Acta Materialia, 2004, 52(10): 2973-2987.

24 Zhu A W, Starke Jr E A. Stress aging of Al–Cu alloys: computer modeling[J]. Acta materialia, 2001, 49(15): 3063-3069.

25 Eto T, Sato A, Mori T. Stress-oriented precipitation of GP Zones and θ′ in an Al-Cu alloy[J]. Acta Metallurgica, 1978, 26(3): 499-508.
26 Zhu A W, Starke E A. Strengthening effect of unshearable particles of finite size: a computer experimental study[J]. Acta materialia, 1999, 47(11): 3263-3269.
27 Zhu A W, Chen J, Starke E A. Precipitation strengthening of stress-aged Al–xCu alloys[J]. Acta Materialia, 2000, 48(9): 2239-2246.
28 Callister, William Jr, Materials Science and Engineering, An Introduction. John Wiley & Sons, NY, NY 1985
29 Ringer, S. P., B. C. Muddle, and I. J. Polmear. "Effects of cold work on precipitation in Al-Cu-Mg-(Ag) and Al-Cu-Li-(Mg-Ag) alloys." *Metallurgical and Materials Transactions A* 26.7 (1995): 1659-1671.
30 Alankar A, Wells M A. Constitutive behavior of as-cast aluminum alloys AA3104, AA5182 and AA6111 at below solidus temperatures[J]. Materials Science and Engineering: A, 2010, 527(29): 7812-7820.
31 Johnson G R, Cook W H. A constitutive model and data for metals subjected to large strains, high strain rates and high temperatures[C]//Proceedings of the 7th International Symposium on Ballistics. 1983, 21: 541-547.
32 XW Yang, Phd thesis, MULTI-FIELD COUPLING MODELS AND DEFORMATION PREDICTION OF ALUMINUM ALLOY LARGE COMPLICATED WORKPIECES DURING HEAT TREATMENT
33 U.F. Kocks, A.S. Argon, M.F. Ashby, Thermodynamics and Kinetics of Slip, 1975
34 Shi H, McLaren A J, Sellars C M, et al. Constitutive equations for high temperature flow stress of aluminium alloys[J]. Materials Science and Technology, 1997, 13(3): 210-216.
35 Nes E. Constitutive laws for steady state deformation of metals, a microstructural model[J]. Scripta metallurgica et materialia, 1995, 33(2): 225-231.
36 Sheppard T, Wood E P. Effect of section geometry on extrudability of Al–Cu–Mn alloy[J]. Metals Technology, 1980, 7(1): 58-66.
37 Shi L, Yang H, Guo L G, et al. Constitutive modeling of deformation in high temperature of a forging 6005A aluminum alloy[J]. Materials & Design, 2014, 54: 576-581.
38 Sellars C M, McTegart W J. On the mechanism of hot deformation[J]. Acta Metallurgica, 1966, 14(9): 1136-1138.

39 Chen S, Chen K, Peng G, et al. Effect of heat treatment on hot deformation behavior and microstructure evolution of 7085 aluminum alloy[J]. Journal of Alloys and Compounds, 2012, 537: 338-345.

40 Medina, Sebastián F., and Carlos A. Hernandez. "General expression of the Zener-Hollomon parameter as a function of the chemical composition of low alloy and microalloyed steels." *Acta materialia* 44.1 (1996): 137-148.

41 Deng, Ying, Zhimin Yin, and Jiwu Huang. "Hot deformation behavior and microstructural evolution of homogenized 7050 aluminum alloy during compression at elevated temperature." *Materials Science and Engineering: A* 528.3 (2011): 1780-1786.

42 Chen, Zhongwei, Pei Chen, and Cuiying Ma. "Microstructures and mechanical properties of Al-Cu-Mn alloy with La and Sm addition." *Rare Metals* 31.4 (2012): 332-335.

43 Chen, Zhongwei, Pei Chen, and Shishun Li. "Effect of Ce addition on microstructure of Al 20 Cu 2 Mn 3 twin phase in an Al–Cu–Mn casting alloy." *Materials Science and Engineering: A* 532 (2012): 606-609.

44 Zoqui E J, Robert M H. Structural modifications in rheocast Al–Cu alloys by heat treatment and implications on mechanical properties[J]. Journal of Materials Processing Technology, 1998, 78(1): 198-203.

45 Li Y, Liu ZY, Lin LH, Peng JT, Ning AL (2011) J Mater Sci 46:3708. doi:10.1007/s10853-010-5143-7

46 Mahon GJ, Howe JM, Vasudevan AK (1990) Acta Metall Mater 38:1503

47 Rometsch, P. A., and G. B. Schaffer. "An age hardening model for Al–7Si–Mg casting alloys." *Materials Science and Engineering: A* 325.1 (2002): 424-434.

48 Deschamps, A., F. Livet, and Y. Brechet. "Influence of predeformation on ageing in an Al–Zn–Mg alloy—I. Microstructure evolution and mechanical properties." *Acta Materialia* 47.1 (1998): 281-292.

49 Esmaeili S, Wang X, Lloyd D J, et al. On the precipitation-hardening behavior of the Al-Mg-Si-Cu alloy AA6111[J]. Metallurgical and Materials Transactions A, 2003, 34(3): 751-763.

50 A Model for Predicting the Yield Stress of AA6111 After Multistep Heat Treatments. B. RaeisiniaPooleW.J. Metallurgical and Materials Transactions A, 2006, 37A.

51 Esmaeili S, Lloyd D J. Modeling of precipitation hardening in pre-aged AlMgSi (Cu) alloys[J]. Acta materialia, 2005, 53(20): 5257-5271.
52 Modeling the strengthening response to aging process of heat-treatable aluminum alloys containing plate/disc- or rod/needle-shaped precipitates. G. LiuZhang, X.D. Ding, J. Sun, K.H. ChenG.J. Materials Science and Engineering, 2002.
53 Modeling the hardness and yield strength evolutions of aluminum alloy with rod/needle-shaped precipitates. SongMin. Materials Science and Engineering A, 2007.
54 Christopher Mark WolvertonMI(US)Saline, John Edmond AllisonArbor, MI(US)Ann. Method of Optimizing Heat Treatment of Alloys by Predicting Thermal Growth. US 6858103 B2 2005 Feb 22

Wang, W., Wang, G., Guo, G., & Rong, Y. (2016). *International Journal of Damage Mechanics*, 1056789516683540.

Competitive relationship between thermal effect and grain boundary precipitates on the ductility of an as-quenched Al-Cu-Mn alloy

Wenguang Wang[1,2]; Gang Wang[1,2,1]; Guannan Guo[3]; Yiming Rong[4]

Abstract

The ductility of an Al-Cu-Mn alloy is typically characterized by fracture strain, and is influenced by experimental temperature and its microstructure. Previous researches show that the ductility increases with the temperature and decreases with the strain rate. However, based on the results of isothermal tensile tests of as-quenched Al-Cu-Mn alloy in this paper, it was found that the ductility decreased apparently (approximately 90% under strain rate of 0.001/s) at a medium temperature range (573K – 673K), and gradually reincreased to its original level at higher temperature. A competitive relationship between temperature softening and grain boundary T precipitation was proposed to account for the unusual variation of ductility. In addition, a ductility model based on the competitive relationship was deduced to quantify the evolution of the fracture strain for the as-quenched Al-Cu-Mn alloy, and validated by the experimental results.

Keywords

Ductility; Grain boundary precipitation; Thermal softening; Quenching; Al-Cu-Mn alloy

[1]State Key Laboratory of Tribology & Institute of Manufacturing Engineering, Department of Mechanical Engineering, Tsinghua University, Beijing 100084, PR China
[2]Beijing Key Lab of Precision/Ultra-precision Manufacturing Equipments and Control, Tsinghua University, Beijing 100084, China
[3]Department of Manufacturing Engineering, Worcester Polytechnic Institute, Worcester, MA, 01609, USA
[4]Mechanical and Energy Engineering Department, South University of Science and Technology of China, Shenzhen, 518055, China
Corresponding author:
Gang Wang, State Key Laboratory of Tribology, Tsinghua University, Lee Shau Kee S&T Building A1003-3, Beijing, China. Email: gwang@tsinghua.edu.cn

Introduction

The Al-Cu-Mn aluminum alloy exhibits satisfactory mechanical properties at different temperatures, which makes it widely used as a structural component in the automobile and aero-astronautic industries (Belov et al., 2014; Li et al., 2011; Toleuova et al., 2012; Wang et al., 2016). In the production process, workpieces of Al-Cu-Mn cast alloy often fail due to the propagation of quenching cracks, where local deformation expands beyond fracture strain (Chen et al., 2012; Ye et al., 2014).

Ductility is generally affected by the experimental temperature, which is defined as the fracture strain. Deformed grains at an elevated temperature can be recovered and recrystallized with rearranging dislocations, thus generating a new set of un−deformed grains, which are normally accompanied by a reduction in the strength of the material and a simultaneous increase in the ductility(Besson, 2009; Lin and Chen, 2011; Liu et al., 2003; Westermann et al., 2016; Zhou et al., 2012). In addition, the microstructures of alloys, especially the pattern and precipitation position of intermetallic phases, have a significant influence on the ductility(Chen et al., 2015; Cvijović et al., 2011; Horstemeyer et al., 2000; Poole et al., 2005; Westermann et al., 2014). In general, the fracture strain increases with increasing temperature and decreases with increasing strain rate (Liu and Fu, 2014; Raj and Ashby, 1975; Rakin et al., 2004; Wang et al., 2010).

The main phases of Al-Cu-Mn alloy include Al_2Cu, $Al_{20}Cu_2Mn_3$, and Al_3Ti phases. Al_2Cu phases are the primary strengthening precipitate phases with fine and uniform distribution (Gao et al., 2016; Samuel, 1998; Samuel et al., 1995). Mn additions in the alloy can dramatically refine phases, retard Orowan coarsening, and improve recrystallization resistance by forming T dispersoids ($Al_{20}Cn_2Mn_3$)(Li et al., 1992; Zupanič et al., 2015). The trialuminide intermetallic Al_3Ti, which has a tetragonal structure and low symmetry, is one of the reasons for the poor ductility of the material, although it may improve the strength of Al alloys at elevated temperatures(Birol, 2007; Chang and Muddle, 1997). Generally, as a price to pay for strengthening the alloy by inhibiting the movement of dislocations, precipitate phases usually lead to a slight decline in the fracture strain. Moreover, different intermetallic phases have different impacts on the ductility of materials (Simmons et al., 1978; Vasudevan and Doherty, 1987; Zehnder and Rosakis, 1990).

In this paper, the stress-strain curves of the as-quenched Al-Cu-Mn cast alloy at different temperatures and strain rates were studied. An interesting experimental phenomenon was observed. The ductility of the alloy, beyond all expectation, did not increase as the temperature increased but showed some regularity. Therefore, this study attempted to explain the unexpected variation of the ductility of the alloy. The variation was explained through an experimental study and theoretical analysis on the different effects of temperature and intermetallic phases.

Materials and Methods

Al-5%Cu-0.4%Mn (called ZL205A via the Chinese national norm) is a typical cast Al-Cu-Mn aluminum alloy with high strength and ductility (tensile strength $R_m = 512MPa$; elongation at fracture $A_5 = 7.0\%$) after heat treatment. The detailed chemical compositions are given in Table 1. Inevitably, there are some impurities, including Fe, Si, Mg, and Zn.

Table 1. Main chemical composition of ZL205A alloy (in wt.%)

Element	*Cu*	*Mn*	*Ti*	*Zr*	*Cd*	*B*	*V*	*Al*
wt.%	*4.6-5.3*	*0.3-0.5*	*0.15-0.35*	*0.05-0.20*	*0.15-0.25*	*0.005-0.006*	*0.05-0.3*	*Bal.*

The material used for the tensile tests was produced by low-pressure die casting, which was then examined by non-destructive X-ray detection to guarantee that no serious casting defects would occur. Qualified samples were heat-treated, as shown in Figure 1. The samples were machined into rod shapes with two screw thread ends. The detailed dimensions are given in Figure 2. The samples were firstly solid solutionized at 813K for 10 hours in a Muffle furnace and then quenched at 298K (room temperature) in 11% UCON™ Quenchant A to obtain a supersaturated α-Al solid solution. Secondly, the samples were heated to test temperatures and held for five minutes to make the temperature uniform. Afterward, the samples were stretched in a tensile machine. The tensile tests were conducted at six different temperatures from room temperature to 773K (298K, 373K, 473K, 573K, 673K, 773K) and under three different strain rates (0.001/s, 0.01/s, 0.1/s). The parameter scopes were basically in accordance with the practical situation of heat treatment process. Three samples were used to guarantee good repeatability under every experimental condition.

After drawn to fracture, the samples were cooled down quickly at cold water to retain the microstructure during the tests. Then, the tensile samples were cut into proper dimensions and washed using an ultrasonic wave cleaning machine. Subsequently, the tensile fracture surfaces and inner microstructures were observed by a scanning electron microscope (SEM). The surfaces for inner microstructure observations over a distance of 5 millimeters from the fracture surfaces were polished without any chemical etching.

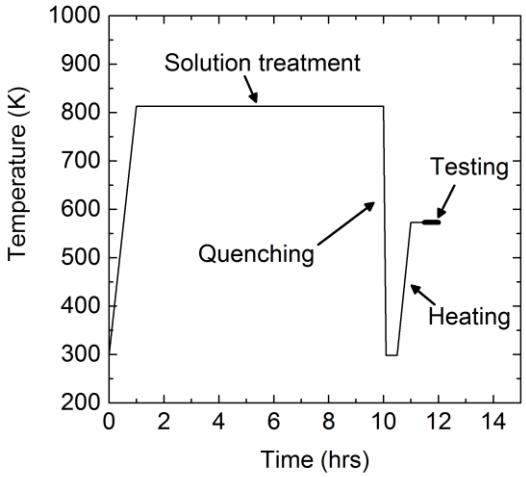

Figure 1. Thermal history used in the tensile tests

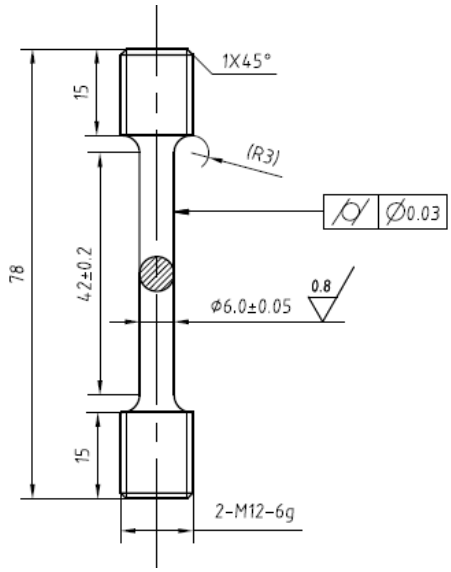

Figure 2. Dimensions of the tensile samples

An INSTRON™ 5985 equipment was used for the tensile tests, and a FEI Quanta™ 200 FEG machine equipped with Energy Disperse Spectroscopy (EDS) was employed for the inner microstructure observation and fractographic examination.

Results

3.1 Stress-strain curves and fracture strain variations

The true strain ε_t during the tensile deformation can be calculated as

$$e_t = \ln \frac{A_0}{A} \qquad (1)$$

where A_0 is the initial cross-sectional area and A is the instantaneous cross-sectional area. The uniform strain ε_u describes global deformation before necking of samples under uniaxial tension.

$$e_u = \ln \frac{A_0}{A_u} \qquad (2)$$

where, A_u is the cross-section area before necking. When fracture occurs, A_f is the cross-section area at fracture. Therefore, the fracture strain ε_f is defined as

$$e_f = \ln \frac{A_0}{A_f} \tag{3}$$

The local deformation that occurs post necking is much larger than the global response. Therefore, the true stress-strain curves were obtained in consideration of necking modification(Siebel and Schwaigerer, 1948; Majzoobi et al., 2015).

As shown in Figure 3(a), the true stress-strain curves of ZL205A under a strain rate of 0.001/s are significantly different in the temperature range from 298K to 773K. The flow stresses of the material obviously decrease as the experimental temperature increases. Furthermore, the fracture strains and uniform strains of the samples also vary hugely with the experimental temperature. Figure 3(b) demonstrates the change of the fracture strains and the uniform strains with error estimation. The error bars are obtained based on at least three credible repeated experimental tests under certain conditions. The overall shape of the fracture strain resembles a “spoon” shape. More precisely, the curve falls to a minimum value of only 2.55% at approximately 573K, while it is above 30.94% at the lower temperatures of 289K-373K and approximately 18% at a higher temperature of 737K.

Generally, three typical stages are observed in the curve, which are the low temperature stage (LTS) at 298K-373K, the middle temperature stage (MTS) at 573K-673K, and the high temperature stage (HTS) at 737K, as well as two transitional periods, i.e., one from LTS to MTS and the other from MTS to HTS. For test samples under the strain-rate of 0.001/s, the fracture strains are reduced by 28% from LTS to MTS and then rise sharply by approximately 15% from MTS to HTS. Therefore, the temperature played a significant role on the variation of ductility.

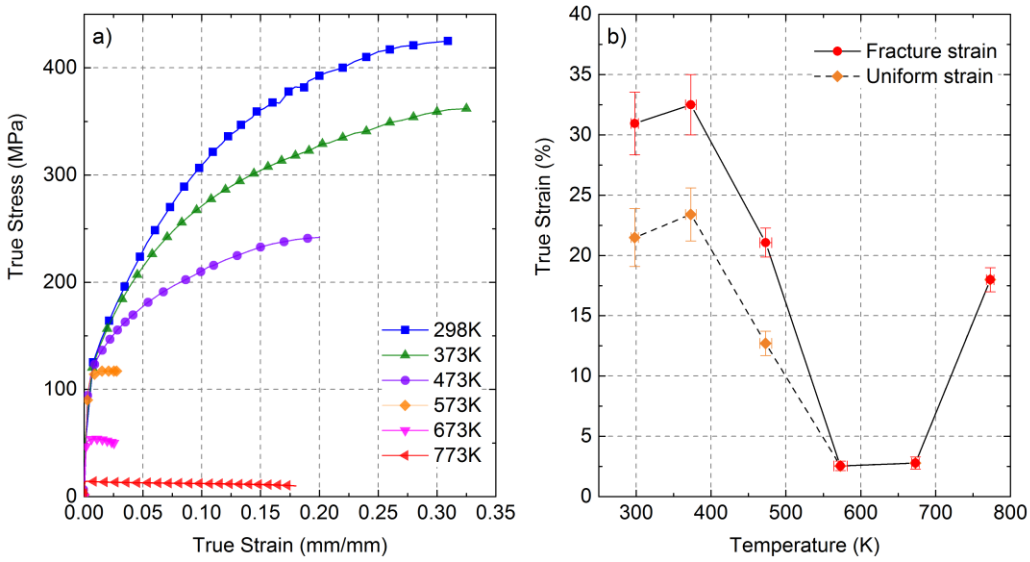

(a) True stress-strain curves (b) Uniform strain and fracture strain

Figure 3. Stress-strain curves of ZL205A at different temperatures with a strain rate of 0.001/s

The true stress-strain curves of ZL205A at different temperatures under strain-rates of 0.01/s and 0.1/s are given in Figure 4(a) and Figure 5(a), and their fracture strain and uniform strain curves are provided, respectively in Figure 4(b) and Figure 5(b). The flow stress, similar to that under the 0.001/s strain rate, becomes smaller with increasing temperature, except for at 573K. At that temperature, yield strengths and elastic moduli of the material are remarkably higher than at other temperatures. Additionally, the fracture strain patterns under 0.01/s and 0.1/s strain rates are also of spoon-shapes and reach a minimal value at 573K. Certainly, there are several thought-provoking differences among the fracture strain curves. The major difference among them is the variation of the depth of the "spoon" shape. The fracture strain minimum increases from 2.55% to 7.05% and to 12.2% with the strain rate increasing from 0.001/s to 0.01/s and to 0.1/s. Moreover, the fracture strain declines from LTS to MTS at the strain rate of 0.001/s, 0.01/s and 0.1/s is 28.39%, 20.04% and 10.36%, respectively. The fracture strain recovery from MTS to HTS basically declines slightly, i.e., 15.45%, 13.85%, and 11.3%. A higher strain rate increases the minimum of the fracture strains; meanwhile, the pattern of the fracture strains remains the same. Therefore, it is highly likely that temperature has a dominating effect on the variation of fracture strain; in addition, the influence of strain rate should not be ignored.

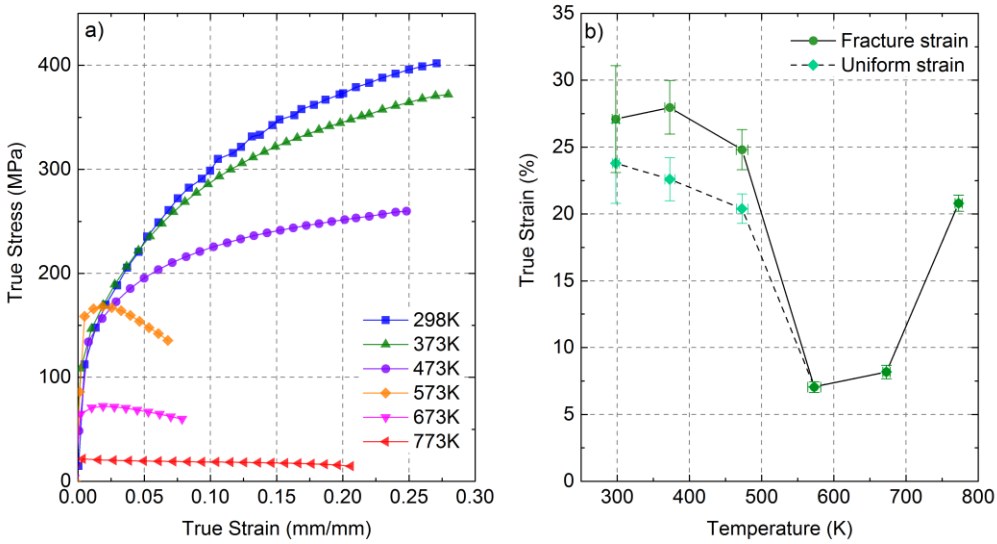

(a) True stress-strain curves (b) Uniform strain and fracture strain

Figure 4. Stress-strain curves of ZL205A at different temperatures with a strain rate of 0.01/s

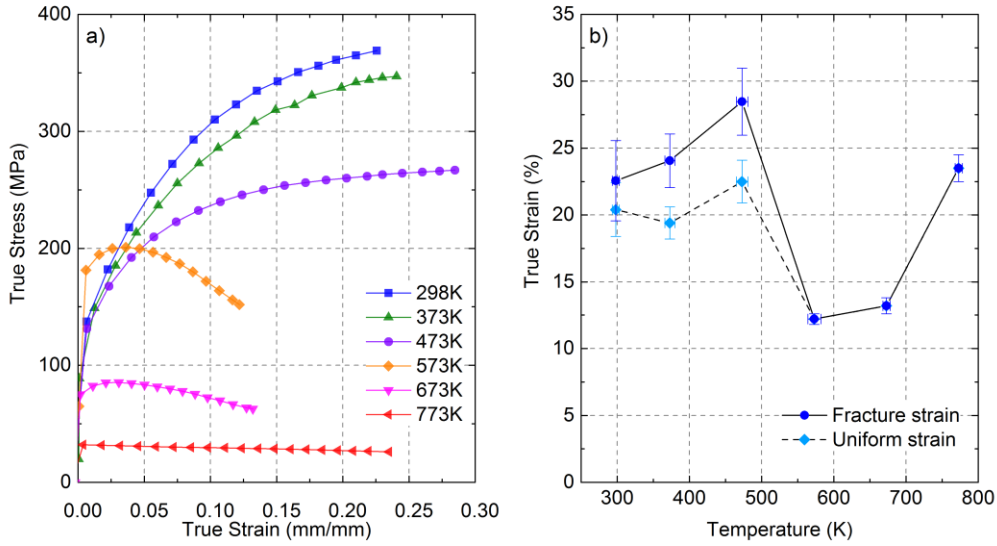

(a) True stress-strain curves (b) Uniform strain and fracture strain

Figure 5. Stress-strain curves of ZL205A at different temperatures with a strain rate of 0.1/s

Previous researchers(Estey et al., 2004; Shi et al., 2014; Yang et al., 2013) usually studied flow stresses of aluminum alloys through stress-strain curves under uniaxial compression because compressive tests can be easily conducted under precisely controlled heating and cooling rates. As a result, the variation in the fracture strains of alloys was rarely observed. Newman et al.(Newman et al., 2003) also studied the tensile behavior of the as-quenched W319 aluminum alloy. However, as their samples were not stretched to fracture, they also did not observe the unusual ductility variation

phenomenon. In this study, the variation of the ductility of the ZL205A cast aluminum alloy with the temperature and strain rate was observed, analyzed, and explained through fractography analysis and microstructure observations in the following sections.

3.2 Fractography analysis

Figure 6 and Figure 7 show fracture surfaces of test samples after fracture at LTS, MTS, and HTS. At LTS, the tensile sample exhibited “necking” before fracture and showed a smooth fracture feature at 45 degrees to the loading direction, as shown in Figure 6(a). Accordingly, the fracture surface at LTS shown in Figure 7(a) is mainly composed of dense small dimples, with some obvious and large dimples. These features are all typical characteristics of ductile fracture. The fracture feature plays an important role in the ductility (fracture strains) of a material, so that as-quenched ZL205A exhibits great ductility (fracture strain > 30.9%) and good strength at LTS.

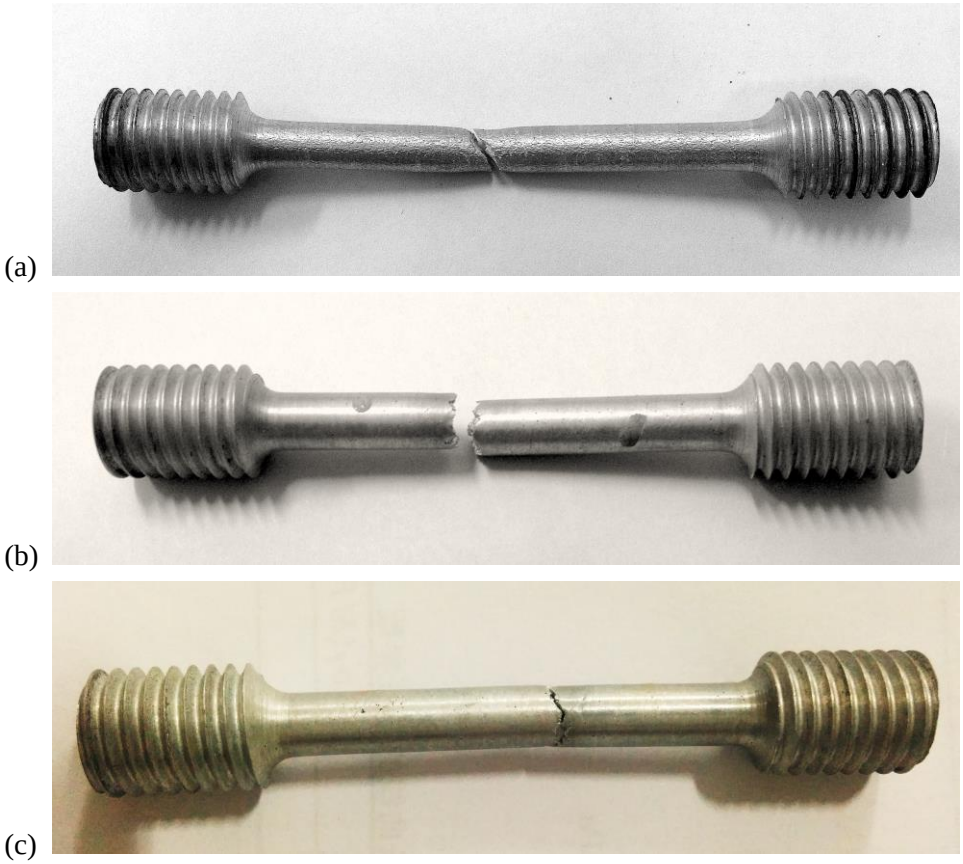

Figure 6. The samples after fracture under various tensile test conditions
(a) LTS; (b) MTS; (c) HTS

The fracture features of samples at MTS and HTS exhibit some similar characteristics but also have differences. The samples at both MTS and HTS show irregular serrated fracture edges, with no obvious “necking”, as shown in Figure 6(b) and 6(c). Moreover, the fracture surfaces, as shown in Figure 7(b) and 7(c), are clearly composed of rock candy patterns and cleavage patterns at both stages, which indicate intergranular fracture. However, the fracture strains at both stages vary greatly; i.e., the fracture strain is only 2.55% at MTS, but nearly 18% at HTS. The grain surfaces are flat and smooth; and fracture cleavage and grain boundaries are greatly evident and can be clearly recognized on the fracture surfaces at MTS. These are typical features of grain boundary brittle fracture (GBBF). On the contrary, at HTS, the grain surfaces are somewhat rough, and the boundaries are less clear than at MTS. Figure 8 shows a grain surface of the fracture surface under high magnification at HTS. There are many tiny dimples on the surface, indicating ductile fracture. Therefore, as-quenched ZL205A exhibits grain boundary ductile fracture (GBDF), which is different from the other temperature stages.

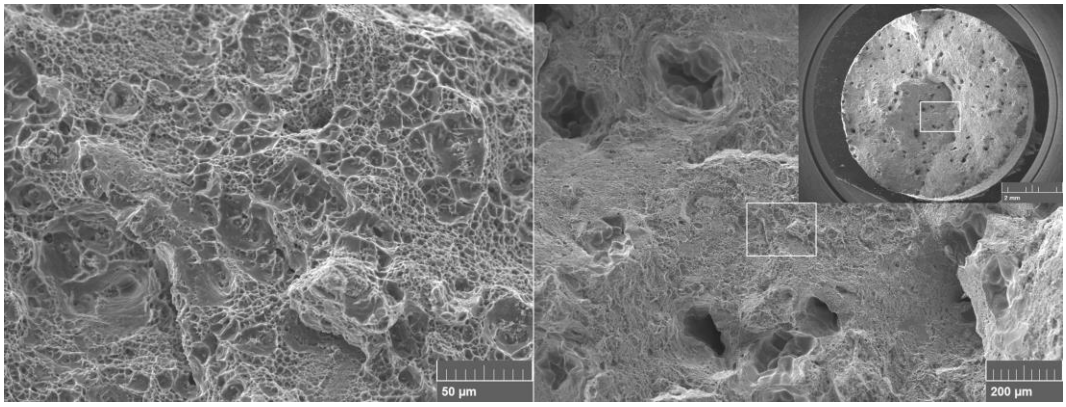

(a) At LTS (1000x, 200x, 32x)

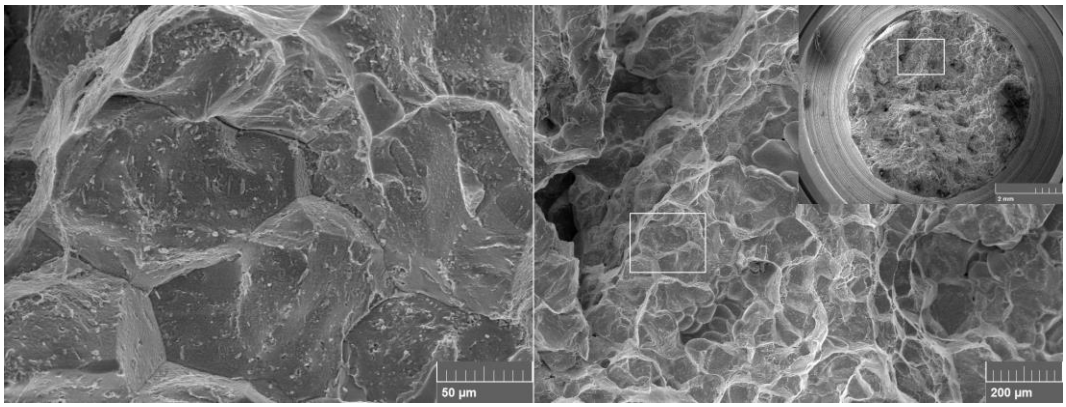

(b) At MTS (1000x, 200x, 32x)

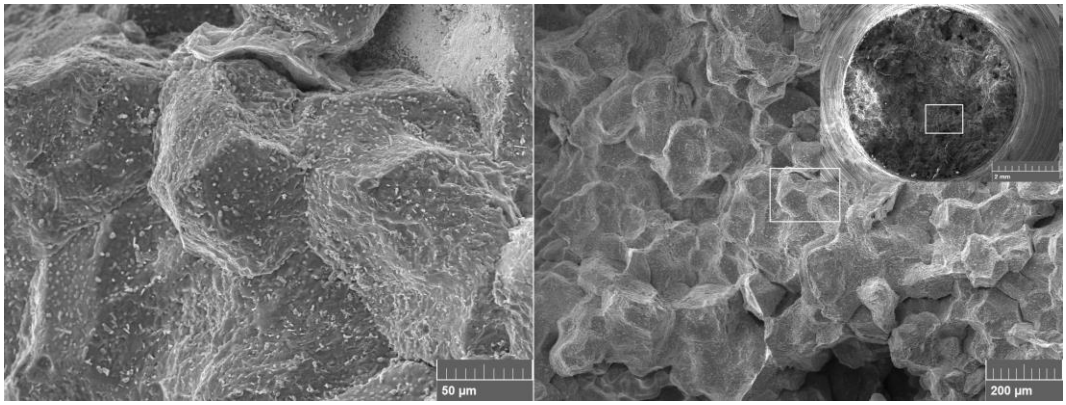

(c) At HTS (1000x, 200x, 32x)

Figure 7. Fracture surfaces of test samples by SEM

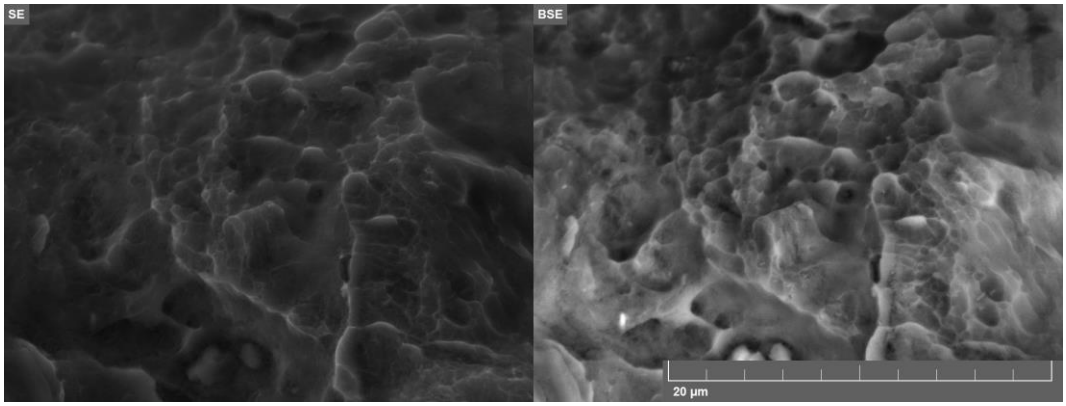

Figure 8. Fracture surfaces of test samples at HTS under high magnification SEM

3.3 Precipitation analysis and microstructure comparison

Various fracture modes in the test samples at different temperature stages, as described in Section 3.2, lead to significantly different fracture strains at the different temperature stages. As a typical high strength heat-treatable Al-Cu-Mn alloy, as-quenched ZL205A is likely to exhibit different precipitation behaviors at different temperatures, resulting in different microstructures and mechanical properties. Al, Cu, Mn, and Ti are the four most common alloying elements. The main intermetallic phases of ZL205A can be categorized into precipitation strengthening phases, e.g., Al_2Cu and $Al_{20}Cu_2Mn_3$ (T phase), and stable phases, e.g., Al_3Ti, which form upon solidification. The fracture surfaces and inner microstructures were observed using SEM by applying SE (second electron) and BSE (back-scatter electron) methods at the LTS, MTS and HTS stages to compare the microstructure and precipitation and clarify reasons for the variations in the fracture strain and ductility. **错误!未找到引用源。** shows the high magnification fracture surface of ZL205A at LTS. White particles are found inside small dimples, where the matrix is homogeneous, without significant Cu or Mn aggregation. These white particles are determined to be Al_3Ti by

EDS analysis. Apart from large vacancies caused by casting defects, Al_3Ti particles can reduce the bonding capacity of neighboring grains and, in turn, provide preferential positions of microvoids and crack nucleation(Birol, 2007; Milman et al., 2001).

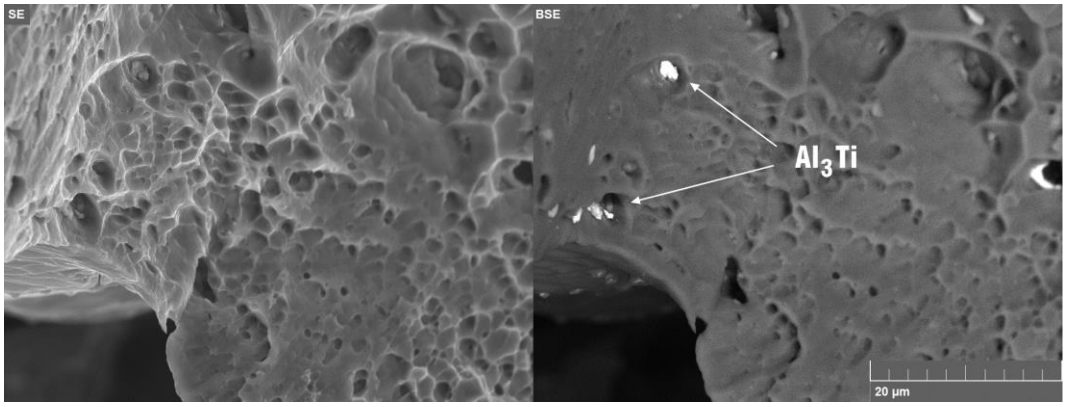

The inner structure of the samples near the fracture surface at LTS is shown in Figure 9. The general matrix (Zone I) is homogeneous, while a few precipitate phases, such as tiny Al_2Cu particles, are randomly distributed in the matrix. The loose structure (Zone II) observed at the grain boundary encompasses several white particles, which are also Al_3Ti particles. The inner microstructure observation is in good agreement with the fracture microstructure. The matrix at LTS is homogeneous and uniform with little precipitation, except for several white Al_3Ti particles accompanied by a loose structure. The “loose structure” is distributed around grain boundaries, without obvious directionality. Therefore, the “loose structure” around Al_3Ti particles is positively shrinkage micro-holes. As a result, in terms of the ductility, ZL205A at LTS performs well.

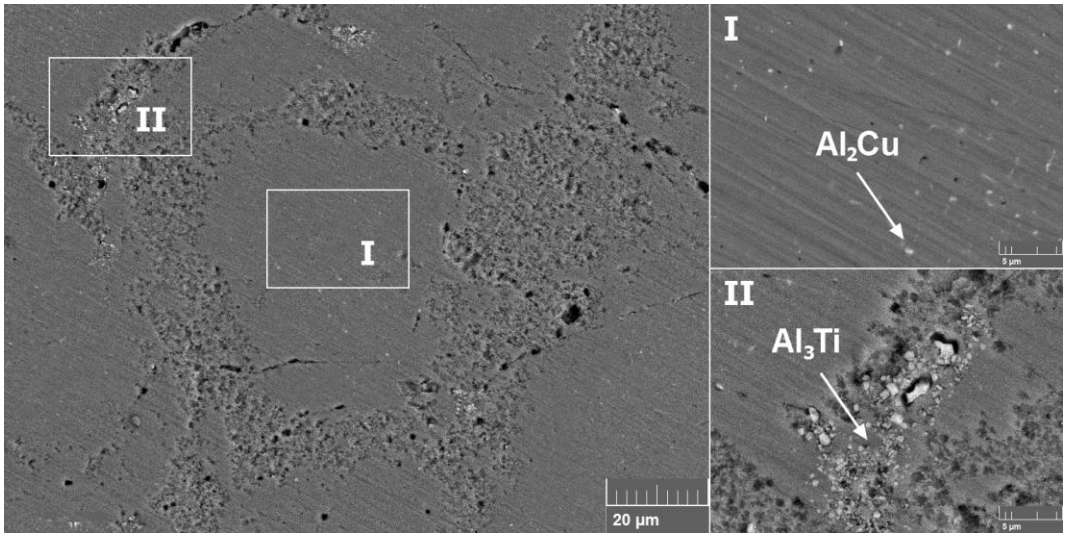

Figure 9. The inner microstructure of test samples at LTS

The inner structure of the samples near the fracture surface at LTS is shown in Figure 9. The general matrix (Zone I) is homogeneous, while a few precipitate phases, such as tiny Al_2Cu particles, are randomly distributed in the matrix. The loose structure (Zone II) observed at the grain boundary encompasses several white particles, which are also Al_3Ti particles. The inner microstructure observation is in good agreement with the fracture microstructure. The matrix at LTS is homogeneous and uniform with little precipitation, except for several white Al_3Ti particles accompanied by a loose structure. The "loose structure" is distributed around grain boundaries, without obvious directionality. Therefore, the "loose structure" around Al_3Ti particles is positively shrinkage micro-holes. As a result, in terms of the ductility, ZL205A at LTS performs well.

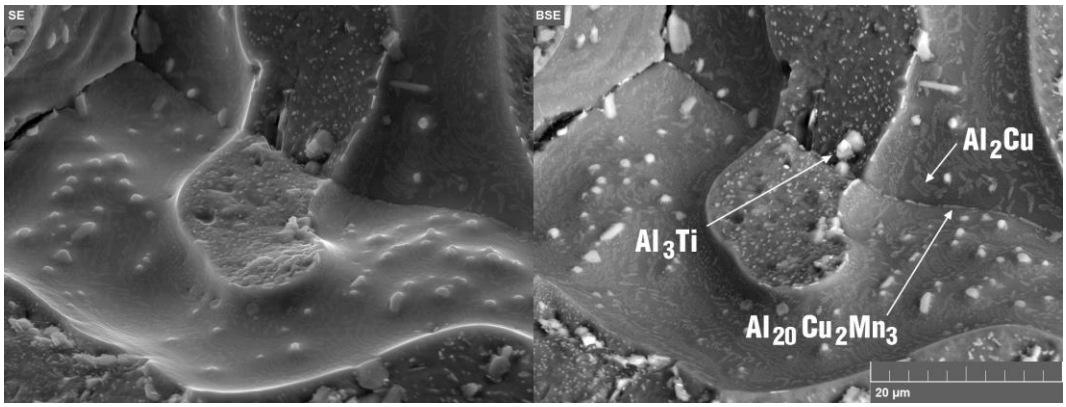

Figure 10. Microstructure observations of the fracture surface at MTS

The microstructure of the samples at MTS, as shown in Figure 11, shows the distribution of Al_2Cu dispersoids, T phases, and Al_3Ti particles. Al_2Cu dispersoids

homogeneously precipitate from the supersaturated solid solution, while T phases dominantly form at grain boundaries. Large T phase particles gather at the intercept point of grain boundaries, and the rest of the T phases still align with the grain boundaries. Al_3Ti particles are still associated with loose structures and vacancies. Moreover, the fracture strain dramatically decreases to 2~3% at MTS under the strain rate of 0.001/s. Al_3Ti, as mentioned before, will not change during heat treatment and therefore could not be the reason for the variation in the fracture strain and ductility. Al_2Cu, the main strengthening precipitation phase, can increase the strength of the alloy, while slightly decreasing its ductility. However, this reduction cannot possibly be the cause of the sharp drop in the fracture strain observed in the experiments. After the exclusion of other possibilities, T phases, gathering along the grain boundaries, are most likely to be the cause of the variation in the fracture strain. The grain boundary with T precipitates is an initial source of cracks and easily gives rise to microvoids, which is thus detrimental to the toughness and ductility of the alloy.

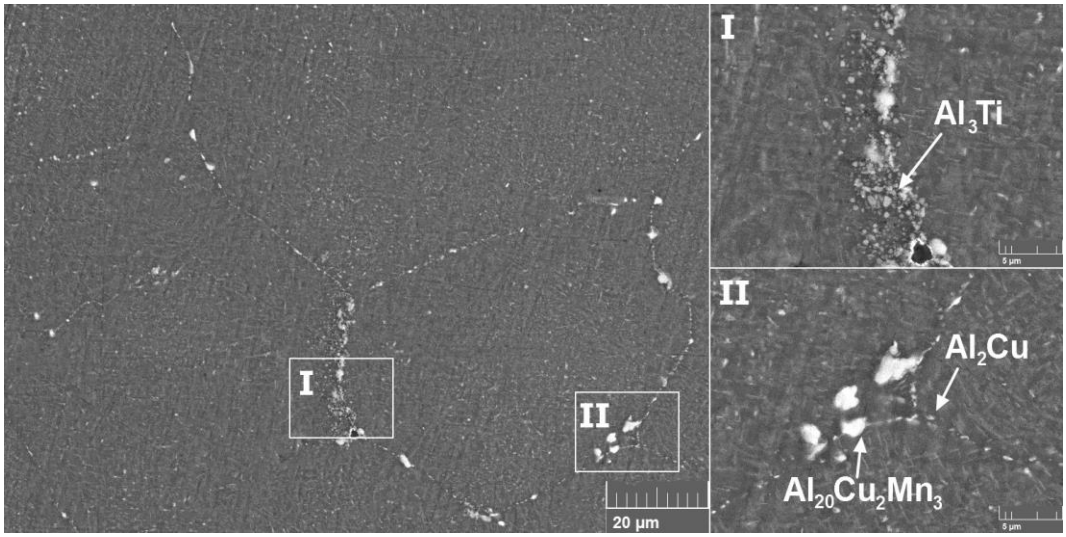

Figure 11. The inner microstructure of the test samples at MTS

The ductility of the alloy increases again to 18% under the 0.001/s strain rate at HTS. Accordingly, the microstructure of the samples at HTS is observed and shown in Figure 12. The fracture surface and metallographic microstructure are basically in agreement with the observations at MTS and include a rock-pattern fracture surface, Al_3Ti particles along with loose structures, homogeneously precipitated Al_2Cu dispersoids in the matrix, and obvious T phases in the grain boundaries. The Al_2Cu dispersoids and grain boundaries with T phases both become more obvious and coarse. Based on the analysis of the fracture strains at MTS, more grain boundary precipitates lead to worse ductility of the alloy. However, the fracture strains of samples at HTS

actually increase by more than 15%. Moreover, the brittle facture at the grain boundary at MTS transforms to a ductile fracture at HTS. The different fracture modes indicate that the mechanism of ductility is not the same.

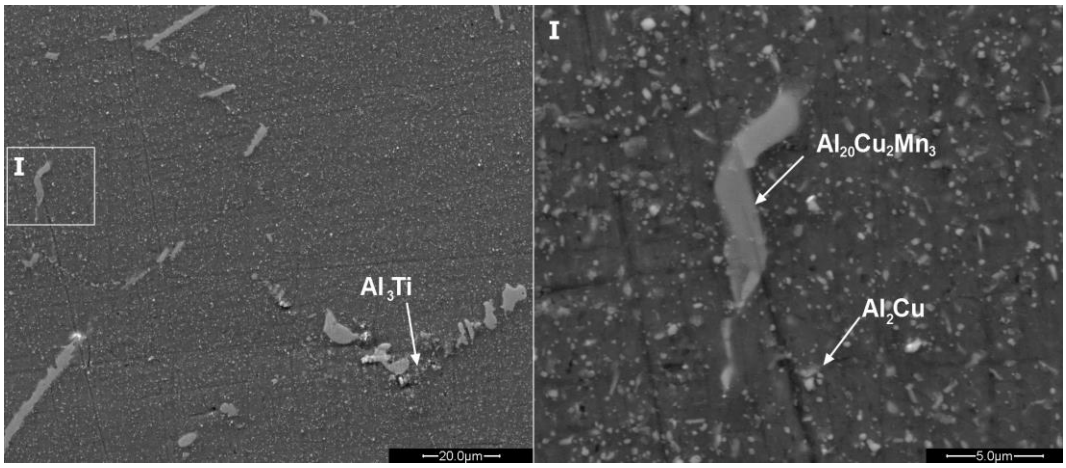

Figure 12. The inner microstructure of test samples at HTS

Discussion

4.1 Competitive effect of temperature and precipitation on ductility

The Al-Cu-Mn phase diagram in the Al-rich region is shown in Figure 13. The aluminum corner contains Al_2Cu, Al_6Mn and a ternary compound usually designated as the T phase ($Al_{20}Cu_2Mn_3$). According to previous data on casting alloys containing approximately 5% Cu, the concentration of manganese in the solid supersaturated solution during solidification can reach 2%(Belov et al., 2005), which is much higher than 0.5% Mn in ZL205A. The major deviation from equilibrium during solidification is due to the formation of non-equilibrium (Al) + Al_2Cu eutectics and a supersaturated solid solution of Mn in (Al). The decomposition of the latter during the reheating process to over 573-773K leads to the formation of Mn-containing precipitates, represented mainly by $Al_{20}Cu_2Mn_3$ (T phase).

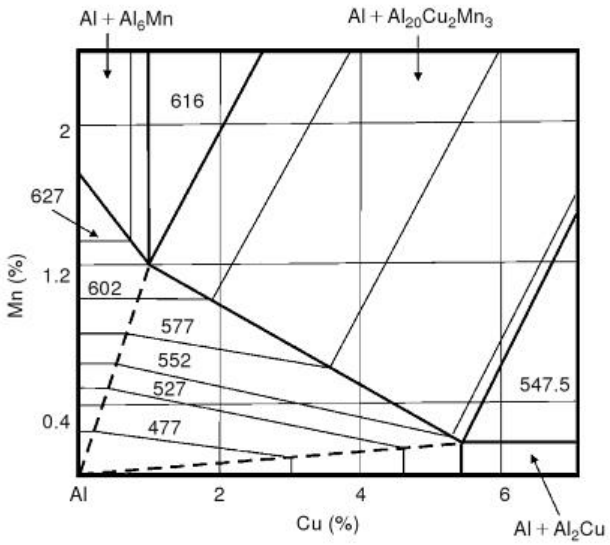

Figure 13. Phase diagram of Al-Cu-Mn at the aluminum rich corner of solidus(Belov et al., 2005)

Based on the Al-Ti phase diagram(Witusiewicz et al., 2008), Al_3Ti particles can easily sink and aggregate during solidification, leading to the segregation of white Al_3Ti. Al_3Ti segregation is difficult to avoid and is generally accompanied by microvoids and micro-porosity(Wang et al., 2014). Al_3Ti particles can almost not be solid solutionized and will not change during the heat treatment process. Therefore, it could not be the reason for spoon-shaped variation of ductility. Al_2Cu phases are homogeneously precipitated and uniformly distributed in the matrix. The amount of Al_2Cu precipitates increases gradually with experimental temperature. Hence, the existence of Al_2Cu also cannot cause the phenomenon of ductility variation. $Al_{20}Cu_2Mn_3$ phases do not exist at LTS, and precipitate considerably on grain boundaries at MTS and HTS, weakening the bonding of grain boundaries. Consequently, it is almost certain that the grain boundary T phases dominate the huge decline of ductility of as-quenched ZL205A alloy.

Without the influence of grain boundary precipitates, the ductility of alloys gradually increases with the increase of temperature and decreases with the increase of strain rate(Li and Ghosh, 2003). Because of dynamic recovery and dynamic recrystallization, the strength of $2^1/_4$Cr-1Mo steel(Booker et al., 1977) declines greatly at elevated temperatures, and the ductility obviously increases, as shown in Figure 15. The ZL205A alloy is softened with the increase of temperature, thus improving the ductility of the alloy. Dynamic recovery and dynamic recrystallization play an

increasingly important role on the deformation behavior of the alloy when the samples are stretched at elevated temperatures. Especially when the temperature increases to near the solid-solution temperature, the ductility greatly improves. The grain boundary is traditionally considered to be a strengthening factor, in other words, the bonding force in grain boundaries is higher than in the matrix. Therefore, intergranular fracture could occur if only grain boundaries are weakened. Generally, there are two basic reasons for weakened grain boundaries(Vasudevan and Doherty, 1987): 1) the presence of microstructures of the alloy and 2) the influence of high temperature and conditions.

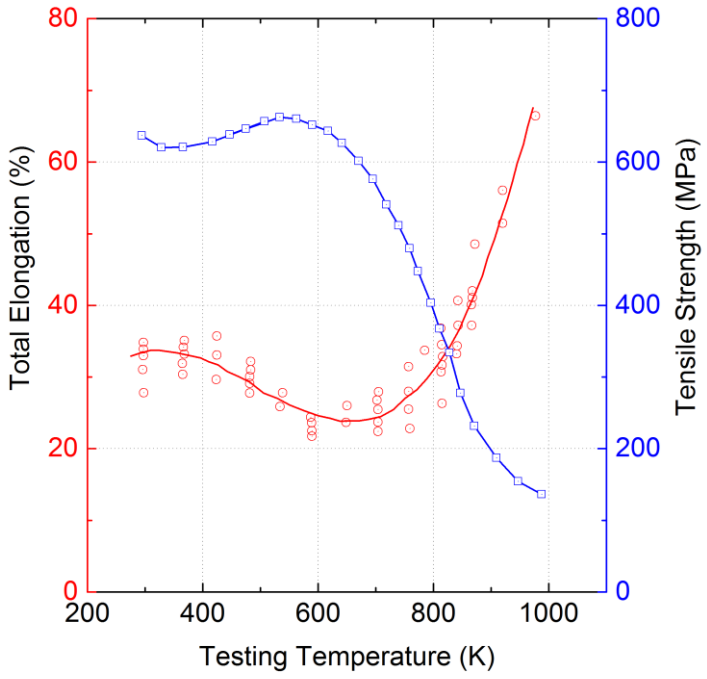

Figure 14. Effect of test temperature on ductility and tensile strength of steel

The obvious grain boundary T phases at MTS, i.e., the discrete rod-like particles, are the main reason for the weakened bonding force of the grain boundary, leading to huge decline of fracture strain and the grain boundary brittle fracture (GBBF). On the other hand, although the grain boundary precipitates at HTS are coarse and reduce the fracture strains of samples considerably, temperature has a more important impact on softening the alloy and increasing its fracture strain and ductility. Besides, the high temperature close to solution temperature at HTS hugely weakens the bonding of grain boundaries, leading to the grain boundary ductile fracture (GBDF). Therefore,

the variation of ductility of as-quenched ZL205A alloy results from the combined effects of both temperature and grain boundary precipitates.

Figure 15 shows that the fracture strains change not only with the test temperature but also with the strain rate. The fracture strain decreases as the strain rate increases at LTS, while the fracture strain increases with the increase in the strain rate at MTS and HTS. This observation can be explained by considering grain boundary precipitates. At LTS, grain boundary precipitates are truly little and negligible; as a result, a higher strain rate allows dislocations to generate and glide more easily and quickly, so ductility becomes worse in agreement with previous studies(Chen et al., 2013; Zhang et al., 2007). In addition, the fracture strain of samples slightly increases with the temperature at LTS, as a result of dynamic recovery. At MTS and HTS, a higher strain rate means a shorter experiment time, resulting in less precipitates being nucleated, especially grain boundary T phases. Therefore, the fracture strains are higher when the strain rate is larger. This phenomenon verifies the hypothesis that the combined effect of thermal softening and grain boundary precipitates is the primary reason for the variation in the fracture strain and ductility of as-quenched ZL205A.

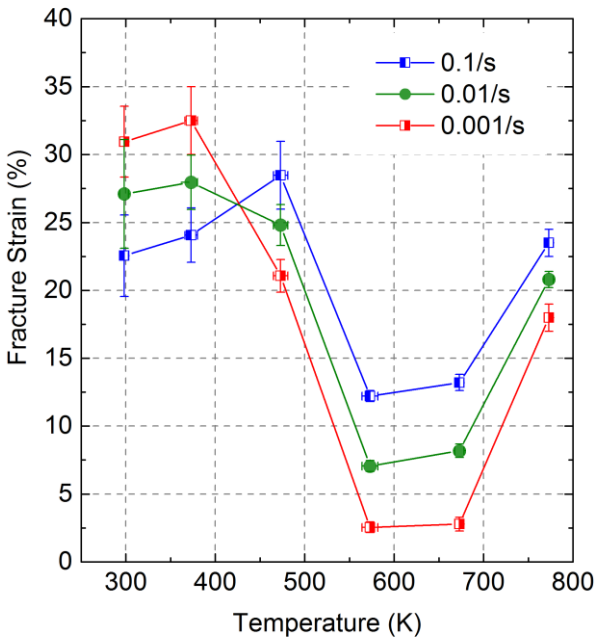

Figure 15. Fracture strain curves under different strain rates

4.2 A mathematical model of ductility on temperature and strain rate

Under the experimental conditions, it is believed that the competitive effect between thermal softening and grain boundary precipitates leads to the variation in the fracture strain. With the increase of temperature, on one hand, dynamic recovery and dynamic recrystallization reduce the strength of the matrix and increase the ductility of the matrix; on the other hand, an increasing amount of T phases nucleate and grow on the grain boundaries, resulting in a great decline of ductility and strength of the grain boundary. Typically, a large fracture strain of over 18% at HTS is due to the increase of ductility of the matrix, while the rock-pattern fracture surface is due to the decline of ductility of the grain boundary.

The ductility of as-quenched ZL205A is expressed by the fracture strain, denoted as ε_f (T, $\dot{\varepsilon}$). In the experiments, temperature and strain rate are independent variables. According to the competitive hypothesis of thermal effects and grain boundary precipitation, the ductility $\varepsilon_f(T,\dot{\varepsilon})$ can be expressed as Equation 3:

$$\varepsilon_f(T,\dot{\varepsilon}) = f(T) + g(T,\dot{\varepsilon}) \tag{4}$$

where $f(T)$ characterizes the positive influence of temperature on the ductility of the matrix, and $g(T, \dot{\varepsilon})$ expresses the negative correlation between grain boundary precipitations with the ductility of grain boundary. Under higher temperatures, grain boundary precipitates nucleate more easily, and at a higher strain rate, the amount of grain boundary precipitates decrease due to a shorter time in the tensile process. The three strain rates adopted in the experiments (0.001/s, 0.01/s, 0.1/s) are represented as $\dot{\varepsilon}_1$, $\dot{\varepsilon}_2$, and $\dot{\varepsilon}_3$. The ratio function w is proposed as shown in Equation 4, which is only dependent on temperature T.

$$w\left(T\right) = \frac{\varepsilon_f\left(T,\dot{\varepsilon}_3\right) - \varepsilon_f\left(T,\dot{\varepsilon}_2\right)}{\varepsilon_f\left(T,\dot{\varepsilon}_2\right) - \varepsilon_f\left(T,\dot{\varepsilon}_1\right)} \tag{5}$$

The $w(T)$ curve is given in Figure 16, and the error bars are computed by using the error transfer formula. The values of w at all temperature levels basically remain constant at 1.0. When w is constant, indicating its independence of temperature, the influence of grain boundary precipitation on ductility could be decomposed into two parts. Therefore, the function $g(T, \dot{\varepsilon})$ could be expressed as the product of a temperature function $k(T)$ and a strain rate function $h(\dot{\varepsilon})$. Then, the ductility $\varepsilon_f(T, \dot{\varepsilon})$ can be redefined as shown in Equation 5.

$$\varepsilon_f\left(T,\dot{\varepsilon}\right)=f(T)+k(T)\cdot h(\dot{\varepsilon}) \qquad (6)$$

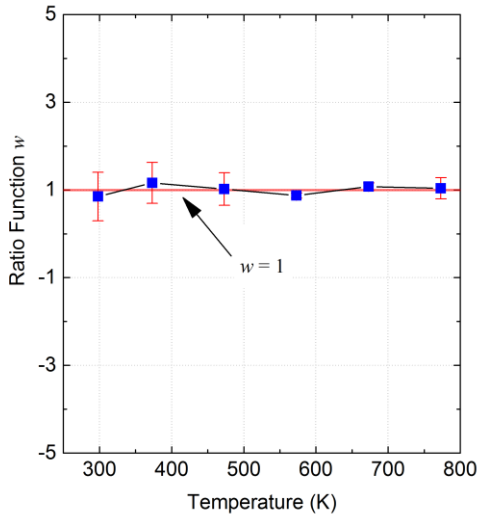

Figure 16. The relationship between w and elevated temperatures

It is worth noting that the constant relationship, w = 1.0, means a linear relationship between $h(\dot{\varepsilon})$ and $\ln(\dot{\varepsilon})$. Therefore, it is reasonable to assume the correlation $h(\dot{\varepsilon})=A\cdot\ln\left(\dot{\varepsilon}\right)+B$. Then,

$$\begin{aligned}\varepsilon_f\left(T,\dot{\varepsilon}\right)&=f(T)+k(T)\cdot\left[A\cdot\ln\left(\dot{\varepsilon}\right)+B\right]\\&=\left[f(T)+B\cdot k(T)\right]+\left[A\cdot k(T)\right]\cdot\ln\left(\dot{\varepsilon}\right)\\&=f^*(T)+k^*(T)\cdot\ln\left(\dot{\varepsilon}\right)\end{aligned} \qquad (7)$$

where $f^*(T)=f(T)+B\cdot k(T)$ and $k^*(T)=A\cdot k(T)$.

As a result, the temperature function $k^*(T)$ can be derived as shown in Equation (5).

$$k^*(T)=\frac{\varepsilon_f\left(T,\dot{\varepsilon}_1\right)-\varepsilon_f\left(T,\dot{\varepsilon}_3\right)}{h(\dot{\varepsilon}_1)-h(\dot{\varepsilon}_3)}=\frac{\varepsilon_f\left(T,\dot{\varepsilon}_1\right)-\varepsilon_f\left(T,\dot{\varepsilon}_3\right)}{\ln\left(\dot{\varepsilon}_1\right)-\ln\left(\dot{\varepsilon}_3\right)}. \qquad (8)$$

$k^*(T)$ and $f^*(T)$ can be plotted as shown in Figure 17. The function $k^*(T)$ characterizes the ability of precipitation to nucleate at a certain temperature. Thus, the trend of $k^*(T)$ increasing with the temperature conforms to expectations. Effect of grain boundary precipitation on ductility at 0.001/s is given as $g_1^*(T)=k^*(T)\cdot\ln\left(\dot{\varepsilon}_1\right)$, shown in Figure 17(a). $g_1^*(T)$ gradually declines with the temperature, and tends to steady after 600K. Accordingly, the function $f^*(T)$ could be represented by $f^*(T)=\varepsilon_f\left(T,\dot{\varepsilon}_1\right)-k^*(T)\cdot\ln\left(\dot{\varepsilon}_1\right)$, as shown in Figure 17(b). The function $f^*(T)$

characterizes the thermal effects for improving the ductility of as-quenched ZL205A, and overall, its value increases with the temperature. However, there are some fluctuations in the values of $f^*(T)$. The values of $f^*(T)$ gradually increase at LTS, which are in accordance with the dynamic recovery at LTS. Then, $f^*(T)$ slightly declines at MTS, which indicates that the grain boundary precipitates inhibit recovery and recrystallization in the material. After that, $f^*(T)$ increases sharply at HTS because dynamic recrystallization and creep behavior are dominant in the material behavior. Through comparative analysis of the plots of $g_1^*(T)$ and $f^*(T)$, it is confirmed that the dramatic drop of fracture strain at MTS mainly results from the effect of grain boundary precipitation, and the recovery of fracture strain at HTS is mostly on account of the high experimental temperature.

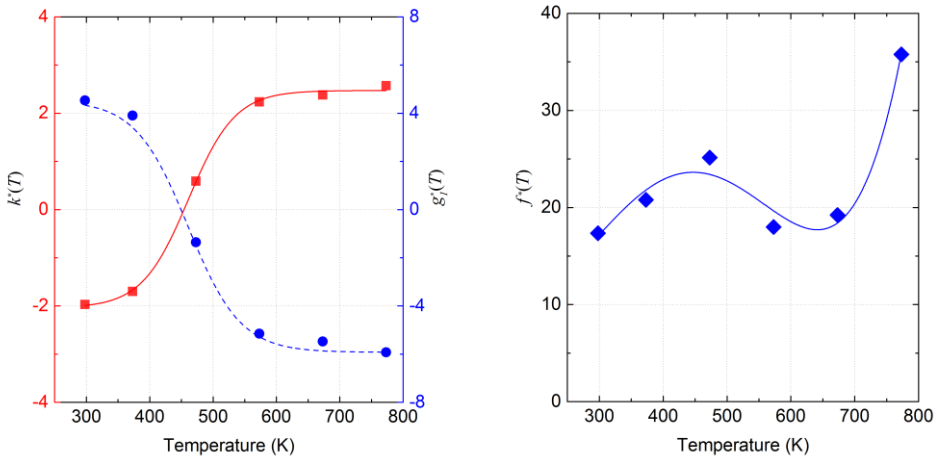

(a) $k^*(T)$ and $g^*(T)$ (b) $f^*(T)$

Figure 17. The relationship between the variables in the ductility model and temperature

Further experiments and relevant theoretic analysis are required to specifically determine $f^*(T)$ and $k^*(T)$. Additionally, the amount of T phases and Al_2Cu dispersoids during the experiments can be characterized using the TTT diagram of ZL205A, which can be used to define $k^*(T)$. Further research on this topic not only contributes to the explanation of the variation in the fracture strain and ductility of as-quenched ZL205A, but is also of great importance to comprehensively understand the relationship between the ductility of materials and process conditions.

Conclusions

In this paper, the ductility of as-quenched ZL205A was investigated in a temperature range of 298-773K and a strain rate range of 0.001-0.1/s. The fracture strain, which characterizes the ductility of as-quenched ZL205A, varied with temperature in "spoon" shape. The phenomena were quite unusual compared with traditional observations. Through analyzing the corresponding microstructure observations of fracture surfaces and inner microstructures, the ductility behavior at each temperature stage was determined by the combined effect of temperature and grain boundary precipitation.

At LTS, ZL205A exhibited good strength and ductility mainly due to a homogeneous solid-solution matrix and few precipitates. The samples at LTS showed typical ductile fracture with an orientation of 45 degrees to the loading direction, with a fracture strain of over 30%. At MTS, ZL205A lost its ductility and presented characteristics of brittleness. The formation of T phases ($Al_{20}Cu_2Mn_3$) at the grain boundaries played a primary role in intergranular fracture. The fracture strains still reached a minimal value of approximately 2%. At HTS, because it was close to the solid-solution temperature, dynamic recrystallization and creep behavior played a dominant role on the material behavior. The fracture strains increased noticeably to about 18%, even though the grain boundary T phases grew larger, which was detrimental to the ductility. The competitive relationship between the temperature and grain boundary precipitates was validated by the fracture strains under different strain rates. A higher strain rate meant that there was less time for the grain boundary T phases to nucleate and grow; thus, the smaller the amount of grain boundary T phases, the higher the fracture strains. The ductility model was proposed based on the analysis of experimental data and the linear relationship assumption between $h(\dot{\varepsilon})$ *and* $\ln\left(\dot{\varepsilon}\right)$. The ductility, $\varepsilon_f(T, \dot{\varepsilon})$, was deduced as follows:

$$\varepsilon_f\left(T,\dot{\varepsilon}\right) = f^*(T) + k^*(T)\cdot\ln\left(\dot{\varepsilon}\right)$$

The curves of $f^*(T)$ and $k^*(T)$ were plotted with the temperature.

Acknowledgements

This work was supported by the National Natural Science Foundation of China [grant number U1537202]. The authors declare that there is no conflict of interest.

References

Belov NA, Alabin AN and Matveeva IA. (2014) Optimization of phase composition of Al–Cu–Mn–Zr–Sc alloys for rolled products without requirement for solution treatment and quenching. *Journal of Alloys and Compounds* 583: 206-213.

Belov NA, Eskin DG and Aksenov AA. (2005) *Multicomponent Phase Diagrams: Applications for Commercial Aluminum Alloys,* Oxford: Elsevier Science, pp. 159-161

Besson J. (2009) Continuum models of ductile fracture: a review. *International Journal of Damage Mechanics* 19: 3-52.

Birol Y. (2007) Response to thermal exposure of the mechanically alloyed Al–Ti/C powders. *Journal of Materials Science* 42: 5123-5128.

Booker MK, Hebble TL, Hobson DO, et al. (1977) Mechanical property correlations for 214 Cr-1 Mo steel in support of nuclear reactor systems design. *International Journal of Pressure Vessels and Piping* 5: 181-205.

Chang W-S and Muddle BC. (1997) Trialuminide intermetallic alloys for elevated temperature applications—overview. *Metals and Materials* 3: 1-15.

Chen B, Flewitt PEJ, Cocks ACF, et al. (2015) A review of the changes of internal state related to high temperature creep of polycrystalline metals and alloys. *International Materials Reviews* 60: 1-29.

Chen BA, Liu G, Wang RH, et al. (2013) Effect of interfacial solute segregation on ductile fracture of Al-Cu-Sc alloys. *Acta Materialia* 61: 1676-1690.

Chen Z, Chen P and Ma C. (2012) Microstructures and mechanical properties of Al-Cu-Mn alloy with La and Sm addition. *Rare Metals* 31: 332-335.

Cvijović Z, Vratnica M and Cvijović-Alagić I. (2011) Effect of Alloy Purity on Fracture Behavior of Overaged 7000 Alloy Plates. *International Journal of Damage Mechanics* 20: 179-193.

Estey CM, Cockcroft SL, Maijer DM, et al. (2004) Constitutive behaviour of A356 during the quenching operation. *Materials Science and Engineering A* 383: 245-251.

Gao K, Song S, Li S, et al. (2016) Characterization of microstructures and growth orientation deviating of Al2Cu phase dendrite at different directional solidification rates. *Journal of Alloys and Compounds* 660: 73-79.

Horstemeyer MF, Lathrop J, Gokhale aM, et al. (2000) Modeling stress state dependent damage evolution in a cast Al–Si–Mg aluminum alloy. *Theoretical and applied fracture mechanics* 33: 31-47.

Li B, Shen Y and Hu W. (2011) Casting defects induced fatigue damage in aircraft frames of ZL205A aluminum alloy–A failure analysis. *Materials & Design* 32: 2570-2582.

Li C, Wang S and Jin Y. (1992) High resolution study of twins in Al20Cu2Mn3 phase. *Acta Materialia* 5: 227-230.

Li D and Ghosh A. (2003) Tensile deformation behavior of aluminum alloys at warm forming temperatures. *Materials Science and Engineering: A* 352: 279-286.

Lin YC and Chen X-m. (2011) A critical review of experimental results and constitutive descriptions for metals and alloys in hot working. *Materials & Design* 32: 1733-1759.

Liu H and Fu M. (2014) Prediction and analysis of ductile fracture in sheet metal forming—Part I: A modified Ayada criterion. *International Journal of Damage Mechanics* 23: 1189-1210.

Liu HJ, Fujii H, Maeda M, et al. (2003) Tensile properties and fracture locations of friction-stir-welded joints of 2017-T351 aluminum alloy. *Journal of Materials Processing Technology* 142: 692-696.

Majzoobi G-H, Fariba F, Pipelzadeh MK, et al. (2015) A new approach for the correction of stress–strain curves after necking in metals. *The Journal of Strain Analysis for Engineering Design* 50: 125-137.

Milman YV, Miracle D, Chugunova S, et al. (2001) Mechanical behaviour of Al 3 Ti intermetallic and L1 2 phases on its basis. *Intermetallics* 9: 839-845.

Newman ML, Robinson BJ, Sehitoglu H, et al. (2003) Deformation, residual stress, and constitutive relations for quenched W319 aluminum. *Metallurgical and Materials Transactions A* 34: 1483-1491.

Poole WJ, Wang X, Lloyd DJ, et al. (2005) The shearable–non-shearable transition in Al–Mg–Si–Cu precipitation hardening alloys: implications on the distribution of slip, work hardening and fracture. *Philosophical Magazine* 85: 3113-3135.

Raj R and Ashby M. (1975) Intergranular fracture at elevated temperature. *Acta Metallurgica* 23: 653-666.

Rakin M, Cvijovic Z, Grabulov V, et al. (2004) Prediction of ductile fracture initiation using micromechanical analysis. *Engineering Fracture Mechanics* 71: 813-827.

Samuel AM, Gauthier J and Samuel FH. (1995) Microstructural Aspects of the Dissolution and Melting of Al2Cu Phase in Al-Si Alloys during Solution Heat Treatment. *Metallurgical and Materials Transactions A* 27A: 1785-1798.

Samuel FH. (1998) Incipient melting of Al5Mg8Si6Cu2 and Al2Cu intermetallics in unmodified and strontium-modified Al–Si–Cu–Mg (319) alloys during solution heat treatment. *Journal of Materials Science* 33: 2283-2297.

Shi L, Yang H, Guo LG, et al. (2014) Constitutive modeling of deformation in high temperature of a forging 6005A aluminum alloy. *Materials & Design* 54: 576-581.

Siebel E and Schwaigerer S. (1948) On the mechanics of the tensile test. *Arch Eisenhuttenwes* 19: 145-152.

Simmons GW, Pao PS and Wei RP. (1978) Fracture mechanics and surface chemistry studies of subcritical crack growth in AISI 4340 steel. *Metallurgical Transactions A* 9: 1147-1158.

Toleuova A, Belov N, Smagulov D, et al. (2012) Quantitative analysis of the Al–Cu–Mn–Zr phase diagram as a base for deformable refractory aluminum alloys. *Metal Science and Heat Treatment* 54: 402-406.

Vasudevan AK and Doherty R. (1987) Grain boundary ductile fracture in precipitation hardened aluminum alloys. *Acta Metallurgica* 35: 1193-1219.

Wang W, Wang G, Hu Y, et al. (2016) Temperature-dependent constitutive behavior with consideration of microstructure evolution for as-quenched Al-Cu-Mn alloy. *Materials Science and Engineering: A* 678: 85-92.

Wang Y, Wu S, Xue X, et al. (2014) Formation mechanism and criterion of linear segregation in ZL205A alloy. *Transactions of Nonferrous Metals Society of China* 24: 3632-3638.

Wang Z-X, Fei Xue, Jian Lu, et al. (2010) Experimental and Theoretical Investigation of Size Effects on the Ductile/Brittle Fracture Toughness of a Pressure Steel. *International Journal of Damage Mechanics* 19: 611-629.

Westermann I, Pedersen KO, Børvik T, et al. (2016) Work-hardening and ductility of artificially aged AA6060 aluminium alloy. *Mechanics of Materials* 97: 100-117.

Westermann I, Pedersen KO, Furu T, et al. (2014) Effects of particles and solutes on strength, work-hardening and ductile fracture of aluminium alloys. *Mechanics of Materials* 79: 58-72.

Witusiewicz VT, Bondar AA, Hecht U, et al. (2008) The Al–B–Nb–Ti system: III. Thermodynamic re-evaluation of the constituent binary system Al–Ti. *Journal of Alloys and Compounds* 465: 64-77.

Yang X, Zhu J, Nong Z, et al. (2013) Constitutive Behavior of As-quenched Al-Cu-Mn Alloy. *Modern Physics Letters B* 27: 1-8.

Ye W, Shiping W, Lianjie N, et al. (2014) Optimization of low-pressure die casting process parameters for reduction of shrinkage porosity in ZL205A alloy casting using Taguchi method. *Proceedings of the Institution of Mechanical Engineers, Part B: Journal of Engineering Manufacture* 228: 1508-1514.

Zehnder AT and Rosakis AJ. (1990) Dynamic fracture initiation and propagation in 4340 steel under impact loading. *International Journal of Fracture* 43: 271-285.

Zhang M, Zhang W-w, Zhao H-d, et al. (2007) Effect of pressure on microstructures and mechanical properties of Al-Cu-based alloy prepared by squeeze casting. *Transactions of Nonferrous Metals Society of China* 17: 496-501.

Zhou J, Gao X, Hayden M, et al. (2012) Modeling the ductile fracture behavior of an aluminum alloy 5083-H116 including the residual stress effect. *Engineering Fracture Mechanics* 85: 103-116.

Zupanič F, Wang D, Gspan C, et al. (2015) Precipitates in a quasicrystal-strengthened Al-Mn-Be-Cu-alloy. *Materials Characterization* 106: 93-99.

Wang, Wenguang, Gang Wang, Yisen Hu, Guannan Guo, Tingting Zhou, and Yiming Rong. *Materials Science and Engineering: A* 678 (2016): 85-92.

Temperature-dependent constitutive behavior with consideration of microstructure evolution for as-quenched Al-Cu-Mn alloy

Wenguang Wang[1], Gang Wang[1,2], Yisen Hu[1], Guannan Guo[2], Tingting Zhou[3], Yiming Rong[4]

[1] State Key Laboratory of Tribology, Tsinghua University, Beijing, 100084, China

[2] Department of Manufacturing Engineering, Worcester Polytechnic Institute, Worcester, MA, 01609, USA

[3] Science and Technology on Surface Physics and Chemistry Laboratory, Jiangyou, 621908, China

[4] Mechanical and Energy Engineering Department, Southern University of Science and Technology of China, Shenzhen, 518055, China

Abstract

It is difficult to predict the deformation behavior of Al-Cu-Mn alloy during a quenching process due to the complex hardening mechanisms. In this paper, isothermal tensile tests were conducted under controlled experimental conditions (298 - 773 K and 0.001 - 0.1 /s strain rate). Observations on the microstructure of the alloy and tensile test analyses on stress-strain curves both verified that the deformation mechanisms differed drastically at 298 - 473 K and 573 - 773 K. Therefore, a temperature-dependent constitutive model was established to characterize the divergent flow behaviors of as-quenched Al-Cu-Mn alloy. In addition, the activation energy, Q, in the model is determined by the combined effect of dislocation forests and precipitate phases, various with different experimental conditions.

Keywords

[2] Corresponding author:
Gang Wang, State Key Laboratory of Tribology, Tsinghua University, Lee Shau Kee S&T Building A1003-3, Beijing, China. Email: gwang@tsinghua.edu.cn

As-quenched Al-Cu-Mn alloy; Precipitation; Dislocation forest; Arrhenius model; Activation energy

Introduction

Al-Cu-Mn cast alloy is widely used to produce large, thin-wall structures in the automobile and aerospace industries because of its light weight and high strength [1]. Before using the alloy in practical industry, proper heat treatment processes are usually applied to improve the mechanical properties of the Al-Cu-Mn alloy. Because of structural complexity and inevitable numerous casting micro-defects, e.g., micro-porosity and micro-segregation [2], workpieces of the alloy are very prone to heavy distortion during heat treatment, especially in the quenching process. Therefore, a step-quenching method is generally employed to decrease the quenching distortion of large workpieces [3]. Previous studies tried to predict quenching deformation via building a constitutive model of as-quenched Al-Cu-Mn alloy in a high temperature range [4-6]. Owing to the rapid cooling rate and wide temperature range of the quenching process, existing constitutive models are hardly sufficient to characterize the constitutive behavior of the as-quenched alloy in all temperature ranges [7, 8].

The Arrhenius model is a semi-physical constitutive model commonly used in the hot working field. The model was proposed by Sellars and Mctegart [9, 10] and developed from the empirical Zener-Hollomon model [11], which combines temperature and stress influences on dislocation motion. The thermal activation mechanism, a fundamental of the Arrhenius model, interprets the statistic process of dislocation thermal release over glide resistance. Recent studies have demonstrated that the hyperbolic-sine Arrhenius model is appropriate for Al alloys in a temperature range from $0.5T_m$ to T_m during quenching [12, 13], but the model fails to agree with experimental results in the low temperature range. In the Arrhenius model, the Zener-Hollomon parameter is proposed to characterize the activated effects of temperature and stress with the assumption of constant activation energy. Therefore, other glide mechanisms of dislocations, such as strain and precipitation hardening, are not taken into account in this model. Liu et al. revised the model by compensating for strain and

strain rate and fitting the activation energy, Q, as a polynomial function of strain to describe the strain hardening influence on the activation energy in engineering[14].

The activation energy reflects the energy required for dislocations to glide across obstacles, e.g., intermetallic particles or grain boundaries. The classical Arrhenius model only considers the effect of dynamic recrystallization and recovery, and the changing grain boundary was supposed to act as the primary obstacle to dislocations. As a result, the classical model is mostly effective for the aluminum alloys which satisfy the assumption of supersaturated homogeneous solid-solution state. For workpieces of Al-Cu-Mn alloy, precipitation during the quenching process is difficult to avoid, if the temperature is not cooled quickly enough. The difference of mechanical behaviors of the alloy at the high temperatures and low temperatures is also observed in Yang's research [15]. However, the relationship between microstructures and mechanical property variation with temperature is lacking in further investigation. More importantly, how microstructures affect the model parameters is particularly conducive to predicting quenching deformation of the alloy better and improving applicability of the constitutive model.

Estey et.al. [16]proposed that the diversity of mechanical behaviors of as-quenched alloys is probably relevant to the slight precipitation during experiments. The pinning effect of small precipitated particles on dislocations increases the energy of dislocation gliding, which results in variations in the activation energy [17, 18]. In addition, the different deformation mechanisms of aluminum alloys over different temperature ranges have an important impact on the activation energy, such as dynamic recovery at low temperatures and dynamic recrystallization at high temperatures. Sellars stated that the complexity of an aluminum alloy or the formation of a precipitate phase among the matrix may affect the activation energy of hot deformation [19]. Chemical concentration effects [20] and initial structure [21] have also been proven to have an effect on the activation energy. Therefore, the activation energy cannot be considered to be constant if the applicable scope of the constitutive model needs to be extended.

In this paper, a modified Arrhenius model has been used to predict the flow stress of the Al-Cu-Mn alloy over a wide temperature range (298 - 773 K). Additionally, the initial structures at different quenching temperatures and interactive motions of dislocation and precipitate phases at different temperatures were observed to determine microstructure effects on flow stress. The activation energy of hot deformation is given as a function of temperature and strain.

Experiments

Al-5%Cu-0.4%Mn is used in this experiment, and the detailed composition is given in table 1. The experimental samples were machined into a rod shape with two screw thread ends. At first, all samples were heated in a Muffle furnace at 813 K for 10 hours in order to obtain full solution treatment. After solution treatment, samples were taken out of the furnace and quenched in 11% UCON^{TM} quenchant. Next, tensile samples were stretched on an Instron 5985 at experimental temperatures (298 K, 373 K, 473 K, 573 K, 673 K, 773 K). Because the heat-up rate was great enough, the material state at experimental temperatures was able to simulate the conditions of step-quenching. The strain rates were 0.001 /s, 0.01 /s and 0.1 /s, which covered the possible values of strain rate during a quenching process[22].

Table 2 Main element composition of Al-5%Cu-0.4%Mn

Element	***Cu***	***Mn***	***Ti***	***Zr***	***Cd***	***B***	***V***	***Al***
wt%	*4.6 - 5.3*	*0.3 - 0.5*	*0.15 - 0.35*	*0.05 - 0.20*	*0.15 - 0.25*	*0.005 - 0.006*	*0.05 - 0.3*	*Bal.*

After tensile testing, specimens for TEM were prepared by mechanical and ion thinning methods. Their microstructure was examined on a high-resolution transmission electron microscope, TECNAI G2 20.

Results

Stress-strain curves

Figure 1 gives the stress-strain curves for as-quenched Al-Cu-Mn alloy in a temperature range of 298 to 773 K and strain rate range of 0.001 to 0.1 /s. The stress-strain curves show great differences at 298 - 473 K and 573 - 773 K. At low experimental temperatures (298 - 473 K), the flow stress is less sensitive to temperature and strain rate, but strain hardening behavior can be observed. However, at high experimental temperatures (573 - 773 K), the flow stress greatly declines with

an increase in temperature and rises with an increase in strain rate. In addition, at high temperatures, the alloy behaves as a steady flow beyond yield strength during the tensile tests without a typical strain hardening stage.

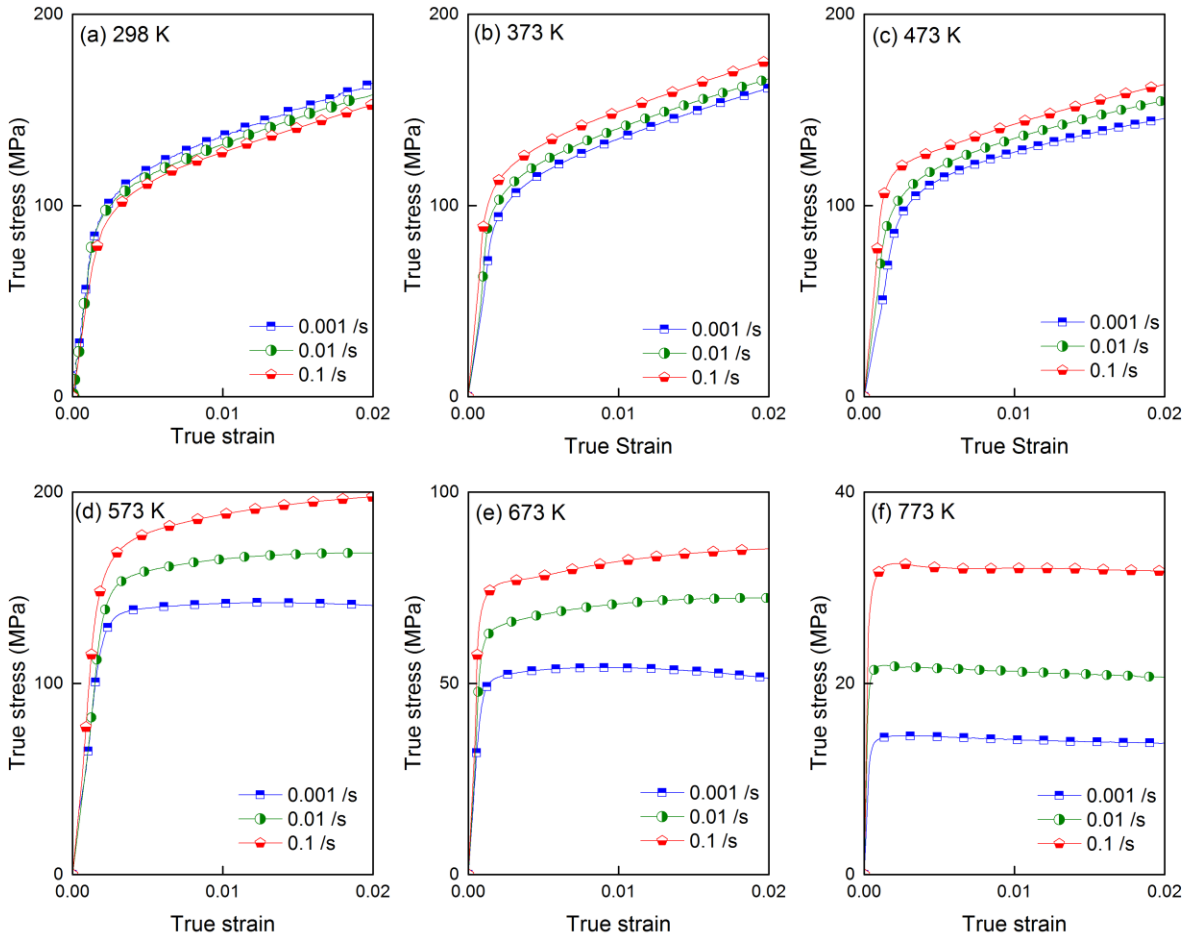

Figure 1. Stress-strain curves of as-quenched Al-Cu-Mn alloy

Figure 2(a) shows a plot of the strain hardening rate (SHR), $\theta(=d\sigma/d\varepsilon)$, vs. true strain, ε, at different temperatures. The SHR θ drops dramatically with strain and remains roughly stable with large strain (> 0.01). It is interesting that the SHR at 298 - 473 K is much higher than the value at 573 - 773 K. The SHR at 298 - 473 K finally stays in a constant state around zero, which indicates the alloy reaches a steady flow. However, the SHR at 573 - 773 K reaches a constant level at approximately 2500 MPa, which indicates strain hardening behavior in the strain range of 0 - 0.02.

To quantify the strain hardening response, the strain hardening exponent (SHE), n, was used to fit the tensile curves based on the Ludwik equation [5, 23]:

$$\sigma = \sigma_y + K\left(\varepsilon - \varepsilon_y\right)^n \qquad (1)$$

where, σ_y and ε_y are yield strength and strain of the material, and K is the strength coefficient. The n plot is shown in Figure 2(b) for all experimental conditions. A linear correlation between SHE and temperature was found for both 298 - 473 K and 573 - 773 K with reasonable approximation. However, the fitted lines were distinctly separate from each other in the temperature ranges. The SHE n at 298 - 473 K is about twice as large as that for 573 - 773 K. The results for SHR θ and SHE n highlight that there is a drastic difference in the strain hardening mechanism of as-quenched Al-Cu-Mn alloy at 298 - 473 K and 573 - 773 K.

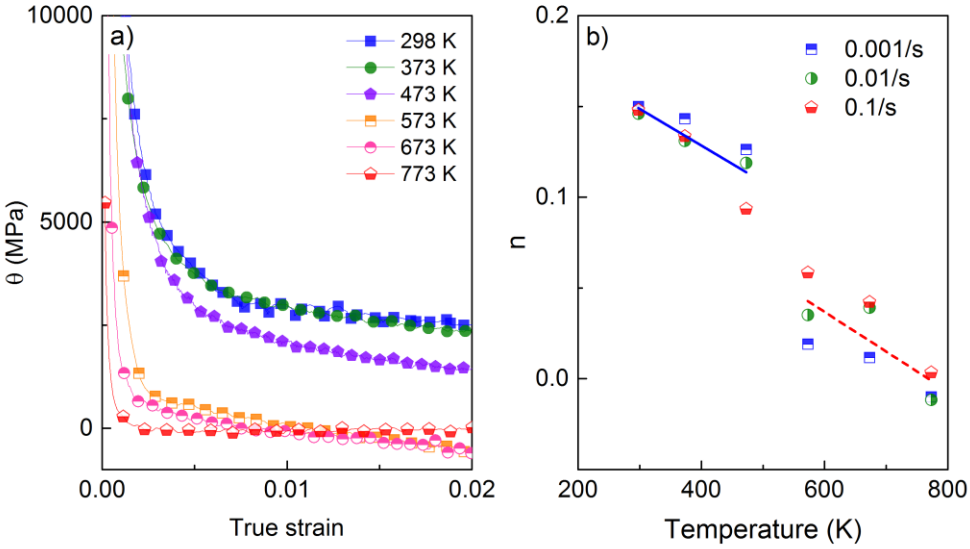

Figure 2. Strain hardening behavior of as-quenched Al-Cu-Mn alloy

The effects of strain rate and temperature on material flow behavior are illustrated in Figure 3. Strain rate sensitivity (SRS), m, is another important parameter that reflects the flow behavior of materials. The m values can be evaluated based on the following equation, which is quite similar to the Lindholm equation [24]:

$$\sigma/\sigma_{\min} = m\log\dot{\varepsilon} \qquad (2)$$

The flow stress is normalized by σ_{min}, the minimum value of flow stresses at the corresponding temperatures. The SRS plot of $\sigma_{0.01}/\sigma_{min}$ vs. $\log\dot{\varepsilon}$ is given in Figure 3(a), and the slope is the SRS m value. At 298 - 473 K, the SRS plots slowly shift, and the values of $\sigma_{0.01}/\sigma_{min}$ are close to one. This finding indicates that flow stress is less sensitive to strain rate at low temperatures. It is worth noting that the flow stress shifts downward at 298 K. This unusual phenomenon is quite complex and will be discussed later. At 573 - 773 K, $\sigma_{0.01}/\sigma_{min}$ increases dramatically at larger strain rates

as the temperature increases. Therefore, flow stress at high temperatures is increasingly sensitive to the strain rate. The relationship between SRS, *m*, and temperature, *T*, is shown in Figure 3(b). Correspondingly, the trends at 298 - 473 K and 573 - 773 K completely differ from each other. At 298 - 473 K, the SRS is low and increases slowly, while at 573 - 773 K, the SRS climbs sharply with increasing temperature.

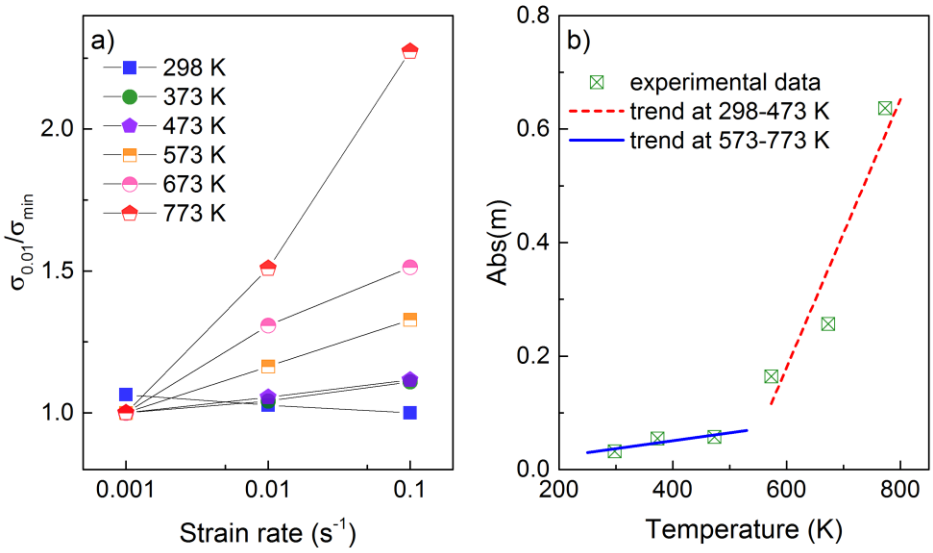

Figure 3. Strain rate sensitivity of as-quenched Al-Cu-Mn alloy

The strain hardening exponent, *n*, and the strain rate sensitivity, *m*, play very important roles in characterizing the deformation behavior, which is closely related to the microstructures. The distinct differences in the SHE and SRS plots imply dissimilarities in the low temperature range (298 - 473 K) and high temperature range (573 - 773 K). Therefore, to better represent the stress-strain behavior of as-quenched Al-Cu-Mn alloy, the constitutive model should be analyzed separately at 298 - 473 K and 573 - 773 K. The constitutive behavior in the transitive temperature range (473-573 K) should be a linear combination of the behavior at 473 K and 573 K.

Constitutive model

The total constitutive model for the whole temperature range (298 - 773 K) is proposed to be the following:

$$\dot{\varepsilon} = \begin{cases} F_1(\sigma, \varepsilon, T) & 298K \le T \le 473K \\ a \cdot F_1(\sigma, \varepsilon, T) + b \cdot F_2(\sigma, \varepsilon, T) & 473K < T < 573K \\ F_2(\sigma, \varepsilon, \mathrm{T}) & 573K \le T \le 773K \end{cases} \quad (3)$$

where, a and b can be determined by the corresponding proportion of the specific temperature in the 473 - 573 K range and $F_1(\sigma,\varepsilon,T)$ and $F_2(\sigma,\varepsilon,T)$ are the Arrhenius models at 298 - 473 K and 573 - 773 K, respectively. The Arrhenius model is useful for predicting the flow stress of aluminum alloy during a hot working process. The Zener-Hollomon parameter combines the effects of strain rate and temperature on deformation in an exponent-type equation. The hyperbolic law between the Zener-Hollomon parameter is employed for better approximations at all stress levels. Thus, the flow stress can be written as a function of the Zener-Hollomon parameter. The basic Arrhenius model can be represented as

$$\dot{\varepsilon} = A[\sinh(\alpha\sigma)]^{\eta} \exp\left(-\frac{Q}{RT}\right) \quad (4)$$

$$\mathrm{Z} = \dot{\varepsilon} \exp\left(\frac{Q}{RT}\right) \quad (5)$$

$$\sigma = \frac{1}{\alpha} \ln\left[\left(\frac{Z}{A}\right)^{1/\eta} + \sqrt{\left(\frac{Z}{A}\right)^{2/\eta} + 1}\right] \quad (6)$$

in which, $\dot{\varepsilon}$ is the strain rate (s^{-1}), R is the universal gas constant (8.31 J· $mol^{-1}K^{-1}$), T is the absolute temperature (K), Q is the activation energy of hot deformation (kJ· mol^{-1}), σ is the flow stress (MPa) for a given strain, and A, α and η are the material constants.

To obtain exact parameter values for the Arrhenius model, the natural logarithm of Equation (4) is given as:

$$\ln Z = \ln A + \eta \ln[\sinh(\alpha\sigma)] \quad (7)$$

Figure 4 shows the plots of ln$Z$ vs. ln[sinh($\alpha\sigma$)] for 298 - 473 K and 573 - 773 K, respectively. The completely separate lines confirm the difference in the constitutive behaviors of as-quenched Al-Cu-Mn alloy in the two temperature ranges.

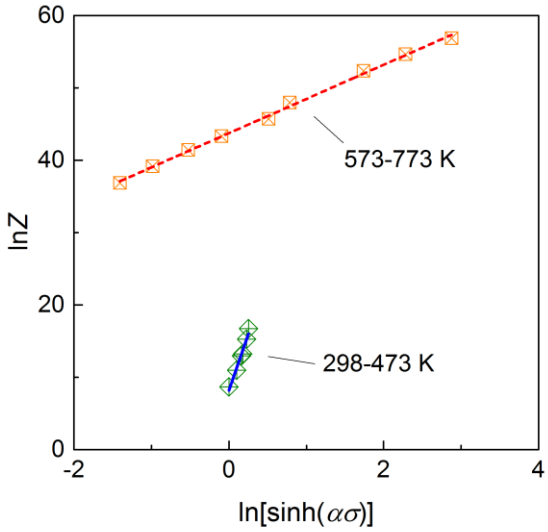

Figure 4. Variations of the Zener-Hollomon parameter with flow stress

Finally, at 298 - 473 K, the Arrhenius model, $F_1(\sigma,\varepsilon,T)$, of as-quenched Al-Cu-Mn alloy at 0.2% strain was obtained and is given as Equation (8). The parameters of the model at strain rates of 0.2 - 2.0% were obtained as polynomial functions of strain, using Lin's method [14].

$$\dot{\varepsilon} = 8.54 \times 10^{-5}[\sinh(0.0084\sigma_{0.2})]^{24.71} \exp\left(-\frac{1.360 \times 10^3}{8.314T}\right) \qquad (8)$$

The values calculated at 298 K, 373 K and 473 K based on the model agreed with the experimental results with a mean relative error of 4.3%, shown in Figure 5. The calculated values cannot describe the negative strain rate sensitivity of stress-strain behavior at 298 K, as shown in Figure 5(a). The calculated values at 0.001 /s and 298 K are in good agreement with the experimental results. However, as the strain rate increases, the calculated values increase based on an Arrhenius-type prediction, which is contrary to the experimental results. At other temperatures (373 K and 473 K), the model predicts the experimental results well.

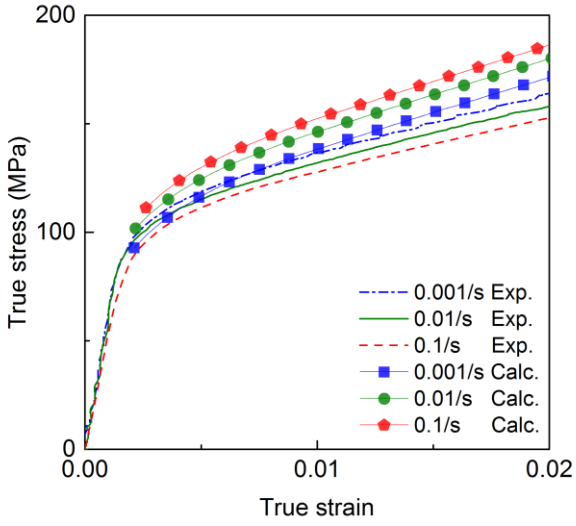
200
100
0
True stress (MPa)
0.00
0.01
0.02
True strain
0.001/s Exp.
0.01/s Exp.
0.1/s Exp.
0.001/s Calc.
0.01/s Calc.
0.1/s Calc.

(a) 298 K

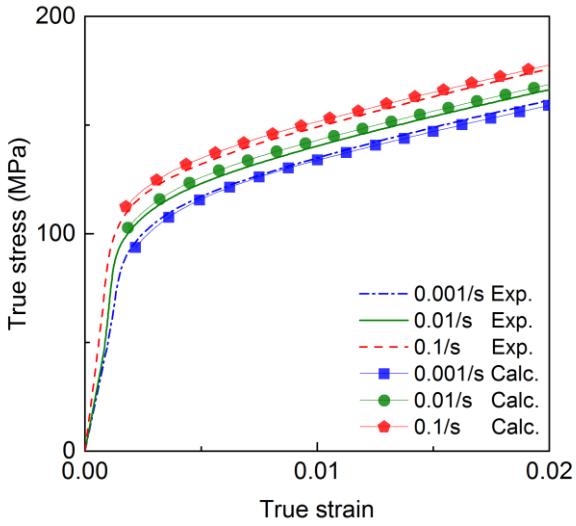
200
100
0
True stress (MPa)
0.00
0.01
0.02
True strain
0.001/s Exp.
0.01/s Exp.
0.1/s Exp.
0.001/s Calc.
0.01/s Calc.
0.1/s Calc.

(b) 373 K

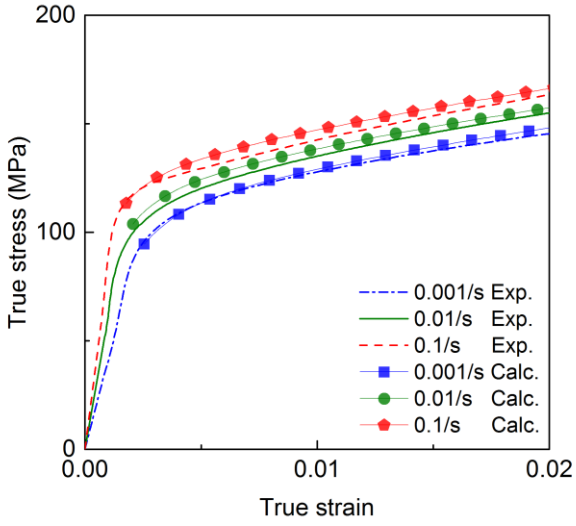

(c) 473 K

Figure 18. Comparison of calculated values with experimental results at 298 - 473 K

At 573 - 773 K, the Arrhenius model, $F_2(\sigma,\varepsilon,T)$, of as-quenched Al-Cu-Mn alloy at 0.2% strain was obtained and is given as Equation (9). Accordingly, the model parameters at a strain rate of 0.2% to 2.0% were also obtained as polynomial functions of strain.

$$\dot{\varepsilon} = 2.89 \times 10^{28}[\sinh(0.0152\sigma_{0.2})]^{8.145} \exp\left(-\frac{3.98 \times 10^5}{RT}\right) \qquad (9)$$

The comparison of calculated values and experimental results at 573 - 773 K with a mean relative error of 2.1% is shown in Figure 6.

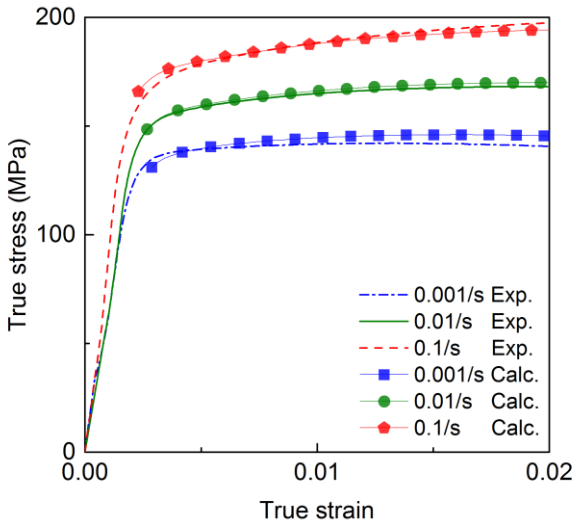

(a) 573 K

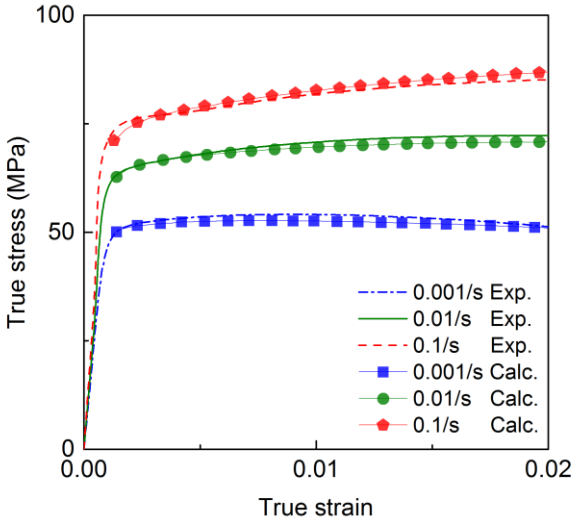

(b) 673 K

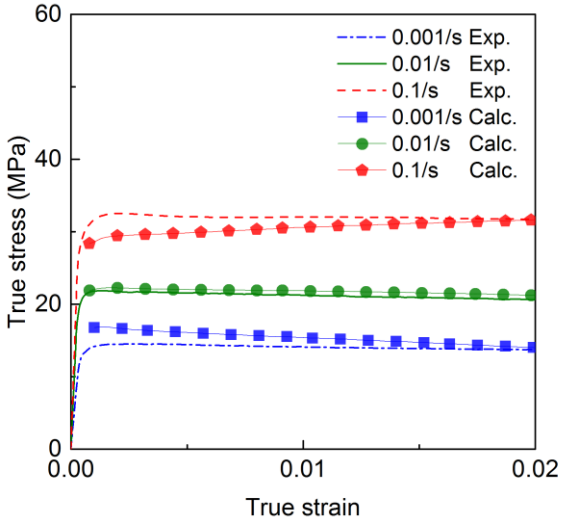

(c) 773 K

Figure 19. Comparison of calculated values with experimental results at 573 - 773 K

Therefore, for the whole temperature range (298 - 773 K), a constitutive model was built and is shown as Equation (3). The model is comprised of two separated Arrhenius models, ($F_1(\sigma,\varepsilon,T)$ for 298 - 473 K and $F_2(\sigma,\varepsilon,T)$ for 573 - 773 K, and a transition model for 473 - 573 K.

Discussion

Microstructure evolution

The change in the constitutive behaviors of as-quenched Al-Cu-Mn alloy over the temperature ranges is closely related to the variation in the microstructures of the

alloy. Remarkably diverse microstructures of as-quenched Al-Cu-Mn alloy are shown in Figure 7 at different temperatures. At 373 K, the matrix exhibits a homogeneous state with rare second precipitation particles, and numerous entangled dislocation forests can be clearly observed. At 573 K, tiny precipitation particles are evident, and the dislocation forests are significantly reduced. The tiny, acicular particles were shown to be Al_2Cu precipitation by EDS analysis, shown in Figure 8. The blocky particles were shown to be intermetallic Al_3Ti, which could exist in the form of a twin, as shown in Figure 7(d). Al_3Ti is a type of impurity generated during the casting process and does not change during heat treatment [25]. At 773 K, there is distinct rod-like precipitation in the matrix and almost no visible dislocation forests. Therefore, as the experimental temperature increases from low to high, the alloy microstructures gradually transform from a dislocation forest dominant state into a precipitation dominant state.

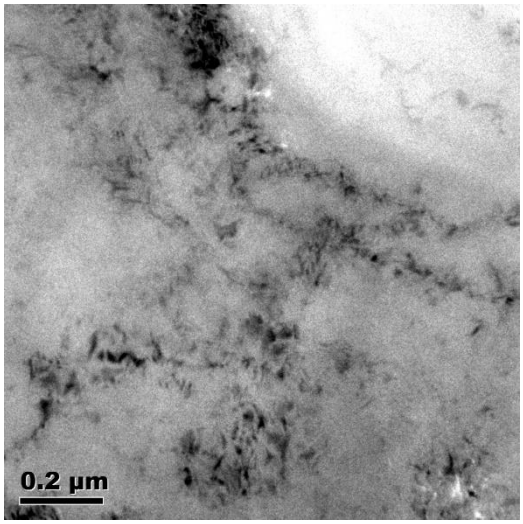

(a) 373 K, 0.001/s

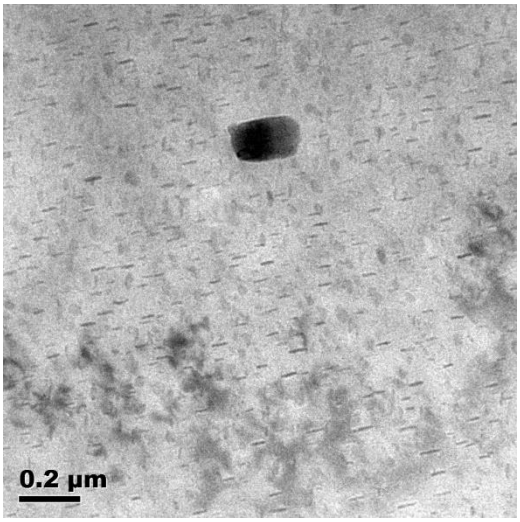

(b) 573 K, 0.001/s

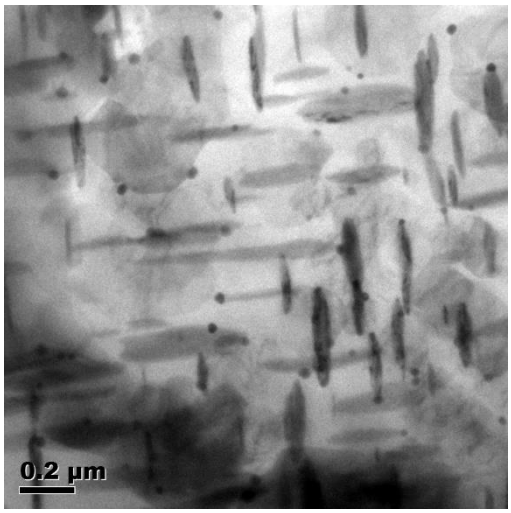

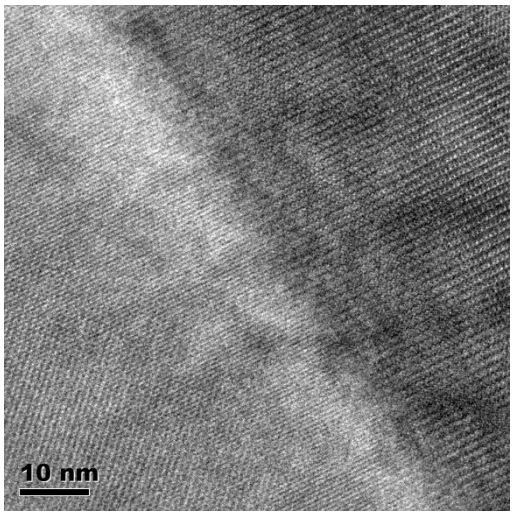

(c) 773 K, 0.001/s (d) HRTEM of Al_3Ti particles

Figure 7. TEM observation of as-quenched Al-Cu-Mn alloy microstructures

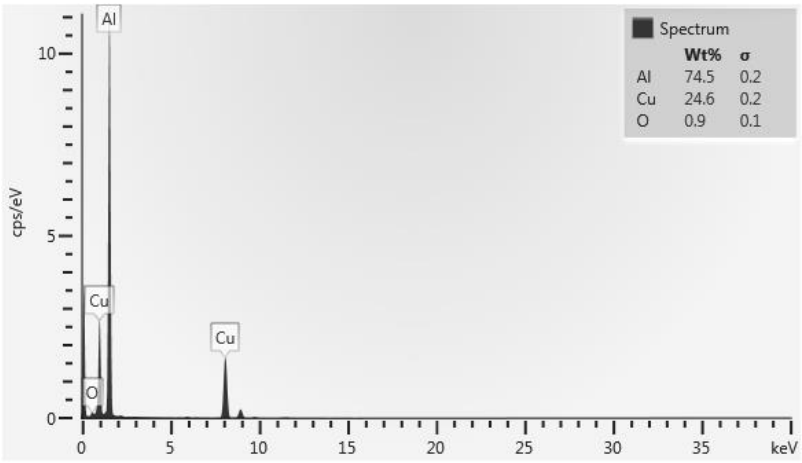

Figure 8. EDS analysis of the tiny acicular particles at 573 K

Dislocation forests and precipitation hardening are the two major hardening mechanisms of as-quenched Al-Cu-Mn alloy. When a gliding dislocation encounters a forest or other dislocation, the dislocation junctions will give a temperature independent contribution to the flow stress. The components of the Burgers vector do not play a role in the flow stress for repulsive dislocation trees [26]. Precipitation strengthening is achieved by producing a particulate dispersion of obstacles to the dislocation movement. The flow stress increases beyond the resistance, and dislocations will bypass the particles either by Orowan looping or cross-slip [27]. The flow stress increment by dislocation bowing leads to the Orowan equation, $\Delta\tau=Gb/L$, which is linearly dependent on the Burgers vector. As a result of different hardening mechanisms, resulting from distinct microstructures, the deformation behavior of as-quenched Al-Cu-Mn alloy exhibits various trends at different temperatures.

Temperature-dependent thermal activation energy

The dramatic difference between the thermal activation energy Q of the alloy at 298 - 473 K and 573 - 773 K is displayed in Figure 9. Therefore, the assumption that the activation energy Q is independent of temperature is not applicable to as-quenched Al-Cu-Mn alloy. The activation energy Q is the energy required when a thermal release of dislocations occurs at obstacles (thermal activation). Under many circumstances, the activation energy is closely related to temperature [28].

For as-quenched Al-Cu-Mn alloy, the activation energy Q reaches more than 3×10^5 J at 573 - 773 K and only approximately 1×10^4 J at 298 - 473 K. Indeed, the simplified assumption for the activation energy Q in the Arrhenius model makes it easier to obtain approximate values from experimental data. However, the activation energy Q is affected by experimental conditions and is most sensitive to temperature. The activation energy Q is essentially determined by the microstructures of the material [13], such as dislocation forests and precipitation.

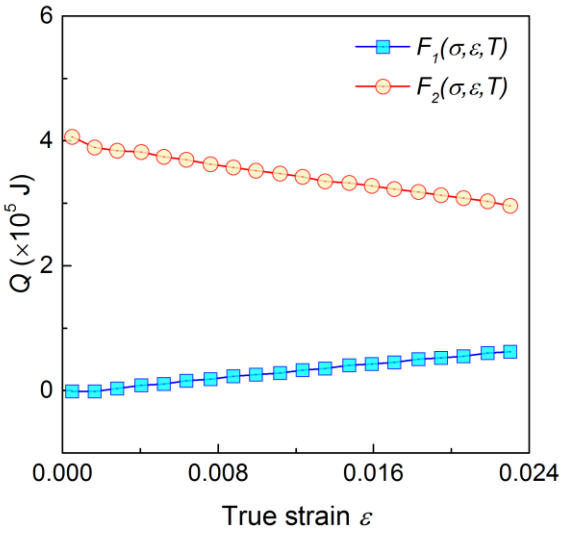

Figure 9. Thermal activation energy in $F_1(\sigma,\varepsilon,T)$ and $F_2(\sigma,\varepsilon,T)$

The comparison between microstructures in Figure 7 and activation energy in Figure 9 indicates that precipitation leads to an increase in the activation energy of the material, and dislocation forests decrease the activation energy. Upon accumulation of plastic strain, activation energies at 298 - 473 K and 573 - 773 K begin to drastically diverge. One possible explanation for this is that a larger plastic strain means longer experimental time, thus, the microstructure of the material gradually changes at the same time. At 298 - 473 K, because of high super-saturation in the matrix, some tiny precipitation may nucleate over a longer period of time, leading to a slow increase in the activation energy. At 573 - 773 K, the precipitation barely increases with low super-saturation in the matrix. However, massive dislocations are activated and entangled with new dislocation forests at higher plastic strains, resulting in a gradual decline in the activation energy. Presently, the competitive relationship between the effects of the dislocation forests and the precipitation on the activation energy is quite complex and still needs further study.

For complex commercial aluminum alloy, e.g., the Al-Cu-Mn alloy in this paper, the analysis of the macroscopic and microscopic aspects of deformation is still challenging. The activation energy is a significant physical parameter of the material, but, in most cases, it is calculated based on idealized assumptions, such as in the Arrhenius model. Kocks[29] proposes the activation area, Δa, to describe thermal activated dependence on obstacle hardening mechanisms. The activation area is defined as

$$\Delta a \equiv -\frac{1}{b}\frac{\partial \Delta G}{\partial \sigma} \qquad (10)$$

where ΔG is the activation free enthalpy, b is the Burgers vector, and σ is the applied stress.

Use of the $b^2/\Delta a$ vs. σ plot to determine the dominant strengthening mechanism of a material is illustrated in Figure 10. The slope of the $b^2/\Delta a$ plot is proportional to the activation work for dislocations sliding across obstacles [30] and is sensitive to dislocation forests. The steep slope at low temperatures indicates that the dislocation-dislocation interactions act pivotal parts in the hardening mechanism. At 298 - 473 K, the dislocations are relatively athermal with steep slopes, and, therefore, the flow stress is less sensitive to strain rate and temperature. Along with the experimental temperature, the effect of dislocation forest hardening gradually decreased. At 573 - 773 K, the activation work for dislocation strengthening is likely to be much smaller, as a result of dominant precipitation hardening.

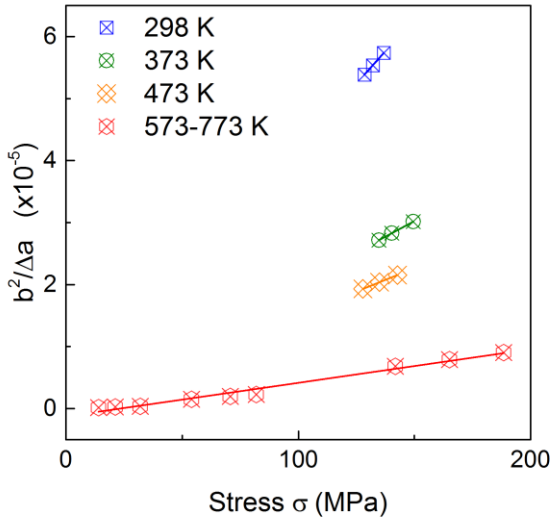

Figure 10. Effect of temperature on the slope of a $b^2/\Delta a$ plot

Strain rate sensitivity

Figure 11 shows variations in the parameter η of $F_1(\sigma,\varepsilon,T)$ for 298 - 473 K and $F_2(\sigma,\varepsilon,T)$ for 573 - 773 K. The parameter exhibits completely opposite trends with strain in different models, which again verifies the huge difference between the deformation at 298 - 473 K and 573 - 773K. $1/\eta$ characterizes strain rate sensitivity in the Arrhenius model and is defined as follows:

$$\left.\frac{\partial \ln[\sinh(\alpha\sigma)]}{\partial \ln \dot{\varepsilon}}\right|_{T,\varepsilon} = \frac{1}{\eta} \qquad (11)$$

The value of η at 298 - 473 K is far higher than the value at 573 - 773 K, indicating the alloy is more sensitive to strain rate at higher temperatures. The result corresponds with the analysis in Figure 3. However, the SRS $|m|$ of as-quenched Al-Cu-Mn alloy is not constant but increases with the experimental temperature. Although the parameter η in the Arrhenius model cannot change, variation of η with different temperature ranges is in agreement with the SRS $|m|$. The reason why the Arrhenius model cannot describe the finding is because the activation energy Q in the Arrhenius model is supposed to be a constant. If the activation energy Q were a function of strain rate, $Q=Q(\ln\dot{\varepsilon})$, then,

$$\left.\frac{\partial \ln[\sinh(\alpha\sigma)]}{\partial \ln \dot{\varepsilon}}\right|_{T,\varepsilon} = \frac{1}{\eta}\left(1 + \frac{1}{RT}\frac{\partial Q}{\partial \ln \dot{\varepsilon}}\right) \qquad (12)$$

Therefore, the activation energy Q should decline along with strain rate. A larger strain rate leads to denser dislocation forests, which bring about a decline in the activation energy.

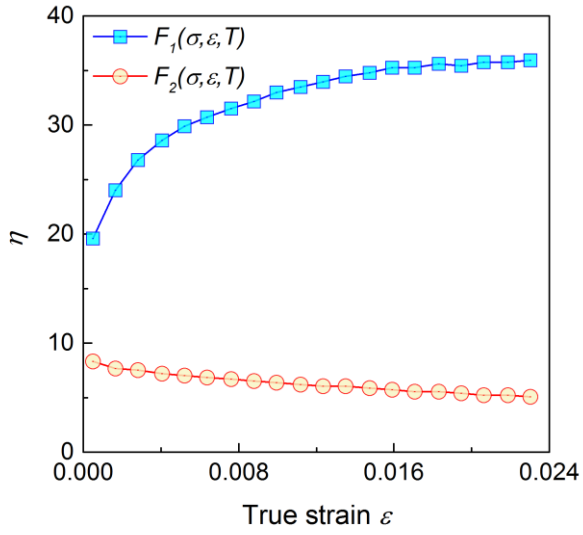

Figure 11. Comparison of parameters in $F_1(\sigma,\varepsilon,T)$ for 298 - 473 K and $F_2(\sigma,\varepsilon,T)$ for 573-773 K

The negative strain rate sensitivity in Figure 1 and Figure 2 is also observed in other aluminum alloys [31, 32]. Such behavior may reduce the ductility of materials and affect its formability. The negative strain rate sensitivity is generally explained by dynamic strain aging (DSA). The microscopic mechanism of DSA has been proposed by Picu [33] based on the concept of strength variation in the dislocation junctions due to the presence of solute clusters on forest dislocations. At high strain rates, when the average time is short, the clusters are too small to produce an effective enhancement of the obstacle strength. Because it is related to solute diffusion, DSA is thermally activated. The transition temperature from negative to positive $|m|$ is between 298 K and 373 K. This phenomenon corresponds with the observations of Picu et al. [34] and Ling et al. [35]. The negative strain rate sensitivity does not appear at high temperatures due to structural changes, such as precipitation, which could change the features of the dislocation motion rate controlling obstacles.

Conclusions

A set of isothermal tensile tests on as-quenched Al-Cu-Mn alloy were conducted over a range of temperatures (298 - 773 K) and strain rates (0.001 - 0.1 /s), which cover the actual ranges in practice. Based on observations of the alloy microstructures and analysis on the stress-strain curves, different microstructures (dislocation forests are dominant at low temperatures, while precipitation is dominant at high temperatures) result in the divergence of hardening mechanisms and deformation behaviors over different temperature ranges.

Finally, an Arrhenius-type constitutive model was proposed for the whole temperature range and was in good accordance with the experimental data. The model includes three parts, $F_1(\sigma,\varepsilon,T)$ for 298 - 473 K, $F_2(\sigma,\varepsilon,T)$ for 573 - 773 K and a transition model for 473 - 573 K.

$$\dot{\varepsilon}_{298-473K} = 8.54 \times 10^{-5}[\sinh(0.0084\sigma_{0.2})]^{24.71} \exp\left(-\frac{1.360 \times 10^3}{8.314T}\right)$$

$$\dot{\varepsilon}_{573-773K} = 2.89 \times 10^{28}[\sinh(0.0152\sigma_{0.2})]^{8.145} \exp\left(-\frac{3.98 \times 10^5}{RT}\right)$$

The strain hardening and strain rate sensitivity behaviors of the alloy at low and high temperatures were also reflected in variations of the parameter, η, in different models.

In this paper, the activation energy Q was not constant and varied with temperature, strain rate and plastic strain. Experimental conditions influence the microstructures of the alloy and thus affect the activation energy value. It is reasonable to conclude that the activation energy has a positive correlation with precipitation and a negative correlation with dislocation forests.

Acknowledgments

This work was supported by the National Natural Science Foundation of China [grant number U1537202].

The authors declare that there is no conflict of interest.

References

[1] M. Zhang, W.-w. Zhang, H.-d. Zhao, D.-T. Zhang, Y.-Y. Li, Effect of pressure on microstructures and mechanical properties of Al-Cu-based alloy prepared by squeeze casting, Transactions of Nonferrous Metals Society of China 17(3) (2007) 496-501.

[2] B. Li, Y. Shen, W. Hu, Casting defects induced fatigue damage in aircraft frames of ZL205A aluminum alloy–A failure analysis, Materials & Design 32(5) (2011) 2570-2582.

[3] S.-d. Liu, Y. Zhang, W.-j. Liu, Y.-l. Deng, X.-m. Zhang, Effect of step-quenching on microstructure of aluminum alloy 7055, Transactions of Nonferrous Metals Society of China 20(1) (2010) 1-6.

[4] X. Yang, J. Zhu, Z. Nong, M. Ye, Z. Lai, Y. Liu, Constitutive Behavior of As-quenched Al-Cu-Mn Alloy, Modern Physics Letters B 27 (2013) 1-8.

[5] M. Roy, D. Maijer, L. Dancoine, Constitutive behavior of as-cast A356, Materials Science and Engineering: A 548 (2012) 195-205.

[6] Y. Peng, G. Wang, T. Zhu, S. Pan, Y. Rong, Dynamic mechanical behaviors of 6082-T6 aluminum alloy, Advances in Mechanical Engineering 5 (2013) 878016.

[7] M. El Mehtedi, F. Musharavati, S. Spigarelli, Modelling of the flow behaviour of wrought aluminium alloys at elevated temperatures by a new constitutive equation, Materials & Design 54 (2014) 869-873.

[8] Y.C. Lin, X.-m. Chen, A critical review of experimental results and constitutive descriptions for metals and alloys in hot working, Materials & Design 32 (2011) 1733-1759.

[9] C.M. Sellars, W.J. Mc Tegart, Hot Workability, International Metallurgical Reviews 17 (1972) 1-24.

[10] C.M. Sellars, Recrystallization of Metals during Hot Deformation, Philosophical Transactions of the Royal Society A: Mathematical, Physical and Engineering Sciences 288(1350) (1978) 147-158.

[11] C. Zener, J.H. Hollomon, Effect of Strain Rate Upon Plastic Flow of Steel, Journal of Applied Physics 15(1) (1944) 22.

[12] X.W. Yang, Z.H. Lai, J.C. Zhu, Y. Liu, D. He, Hot compressive deformation behavior of the as-quenched A357 aluminum alloy, Materials Science and Engineering B 177 (2012) 1721-1725.

[13] L. Shi, H. Yang, L.G. Guo, J. Zhang, Constitutive modeling of deformation in high temperature of a forging 6005A aluminum alloy, Materials & Design 54 (2014) 576-581.

[14] Y.C. Lin, M.-S. Chen, J. Zhong, Constitutive modeling for elevated temperature flow behavior of 42CrMo steel, Computational Materials Science 42(3) (2008) 470-477.

[15] X.W. Yang, Multi-field coupling models and deformation prediction of aluminum alloy large complicated workpieces during heat treatment, School of Materials Science and Engineering, Harbin Institute of Technology, Harbin, 2013.

[16] C.M. Estey, S.L. Cockcroft, D.M. Maijer, C. Hermesmann, Constitutive behaviour of A356 during the quenching operation, Materials Science and Engineering A 383(2) (2004) 245-251.

[17] U.F. Kocks, H. Mecking, Physics and phenomenology of strain hardening: the FCC case, Progress in Materials Science 48 (2003) 171-273.

[18] U.F. Kocks, A.S. Argon, M.F. Ashby, Thermodynamics and kinetics of slip, Progress in Materials Science 19 (1975).

[19] C. Sellars, W.J. McTegart, On the mechanism of hot deformation, Acta Metallurgica 14 (1966) 1136-1138.

[20] S.F. Medina, C.A. Hernandez, General expression of the Zener-Hollomon parameter as a function of the chemical composition of low alloy and microalloyed steels, Acta Materialia 44(1) (1996) 137-148.

[21] Y. Deng, Z. Yin, J. Huang, Hot deformation behavior and microstructural evolution of homogenized 7050 aluminum alloy during compression at elevated temperature, Materials Science and Engineering A 528(3) (2011) 1780-1786.

[22] M.L. Newman, Modeling the behavior of a type-319 aluminum alloy during quenching, Automotive Engineering, University of Illinois at Urbana-Champaign, Illinois, 2002, p. 14.

[23] N. Afrin, D.L. Chen, X. Cao, M. Jahazi, Strain hardening behavior of a friction stir welded magnesium alloy, Scripta Materialia 57(11) (2007) 1004-1007.

[24] N. Tahreen, D.L. Chen, M. Nouri, D.Y. Li, Effects of aluminum content and strain rate on strain hardening behavior of cast magnesium alloys during compression, Materials Science and Engineering: A 594 (2014) 235-245.

[25] W.-S. Chang, B.C. Muddle, Trialuminide intermetallic alloys for elevated temperature applications—overview, Metals and Materials 3(1) 1-15.

[26] G. Schoeck, R. Frydman, The Contribution of the Dislocation Forest to the Flow Stress, physica status solidi (b) 53(2) (1972) 661-673.

[27] T. Gladman, Precipitation hardening in metals, Materials science and technology 15(1) (1999) 30-36.

[28] P.S. Follansbee, U.F. Kocks, A constitutive description of the deformation of copper based on the use of the mechanical threshold stress as an internal state variable, Acta Metallurgica 36 (1988) 81-93.

[29] R.A. Mulford, Analysis of strengthening mechanisms in alloys by means of thermal-activation theory, Acta Metallurgica 27(7) (1979) 1115-1124.

[30] R. Mulford, U. Kocks, New observations on the mechanisms of dynamic strain aging and of jerky flow, Acta Metallurgica 27(7) (1979) 1125-1134.

[31] H. Zhang, K.T. Ramesh, E.S.C. Chin, High strain rate response of aluminum 6092/B4C composites, Materials Science and Engineering: A 384(1–2) (2004) 26-34.

[32] A. Rusinek, J.A. Rodríguez-Martínez, Thermo-viscoplastic constitutive relation for aluminium alloys, modeling of negative strain rate sensitivity and viscous drag effects, Materials & Design 30(10) (2009) 4377-4390.

[33] R.C. Picu, A mechanism for the negative strain-rate sensitivity of dilute solid solutions, Acta Materialia 52(12) (2004) 3447-3458.

[34] R. Picu, G. Vincze, F. Ozturk, J. Gracio, F. Barlat, A. Maniatty, Strain rate sensitivity of the commercial aluminum alloy AA5182-O, Materials Science and Engineering: A 390(1) (2005) 334-343.

[35] C.P. Ling, P.G. McCormick, Strain rate sensitivity and transient behaviour in an AlMgSi alloy, Acta Metall Mater 38(12) (1990) 2631-2635.

Guo, Guannan, et al. "A Brief Review of Precipitation Hardening Models for Aluminum Alloys." *Proceedings of the 2nd World Congress on Integrated Computational Materials Engineering (ICME)*. Springer, Cham, 2013.

A BRIEF REVIEW OF PRECIPITATION HARDENING MODELS FOR ALUMINUM ALLOYS

Guannan Guo[1], Qigui Wang [2], Gang Wang[3], Yiming Rong[1,3]

[1] Worcester Polytechnic Institute, Manufacturing Engineering, Worcester, MA 01609 USA

[2] GM Powertrain Materials Technology, Pontiac, MI, USA

[3] Tsinghua University Precision, Instruments and Mechanology, Beijing China

Keywords: A356, aging, yield strength, modeling, precipitate hardening

Abstract

This paper briefly reviews the precipitation hardening models in aluminum alloys. Several well-accepted precipitation and strengthening models are compared with experimental data of aluminum A356 alloy. The differences among various models are presented and further improvements of precipitation hardening models are discussed.

1 Introduction

Aluminum alloys are increasingly used in structural applications because of their lightweight, relatively low manufacturing cost, and high strength to weight ratio particularly after heat treatment. Most aluminum alloys, like A356 used for critical structures are usually subjected to aging precipitation hardening. The main reason for aluminum alloy strengthening is the formation of the precipitates, act as point obstacle to inhibit the motion of the dislocation. The early period of aging is governed by the dislocation mechanism of shearing while the dislocation mechanism of bypassing dominates the later period of aging. The type, size and volume fraction of precipitates depend upon the alloy compositions and heat treatment conditions. In Al-Mg-Si

system, like A356 alloy, Mg/Si precipitates are the dominated strengthening phases after aging.

Modeling of precipitation hardening has been extensively studied in past years [1-7]. Several well-known strengthening models for aluminum alloys are reproduced in this paper. The model predictions are compared with experimental data of A356 aluminum alloy. The differences among various precipitation and hardening models are presented and further improvement of hardening models are proposed.

2 Microstructure Models

Mean value approach and discrete value approach are two types of models in the literature to predict the size or volume fraction of the precipitate particles. The mean value method does not consider the particle size distribution, [1, 3, 5, 6], taking all the particles as the same. The discrete value approach considers the particle size distribution based on selected radius classes. [9]

2.1 Mean Value Approach

In the mean value approach, the modeling of precipitates follows the classical nucleation and growth theory. [4] The basic principle for the growth of precipitate particles is diffusion mechanism of solution element. In each period, volume fraction and the mean radius of particles follow different growth kinetics.

Table 3 Input Data for Figure 1

C0	Ce	Cp	D(Diffusion coefficient m^2/s)	γ(surface energy J/m^2)	V(volume per atom m^3)	a(lattice parameter nm)	T(K)
0.06	0.01	1	$5.0*10^{-20}$	0.13	$1.6*10^{-29}$	0.404	433

Table 1 gives the experiment data for mean value approach method, where C0, Ce, Cp is the initial solute concentration, equilibrium solute concentration and solute concentration in precipitate. Figure 1 gives the result.

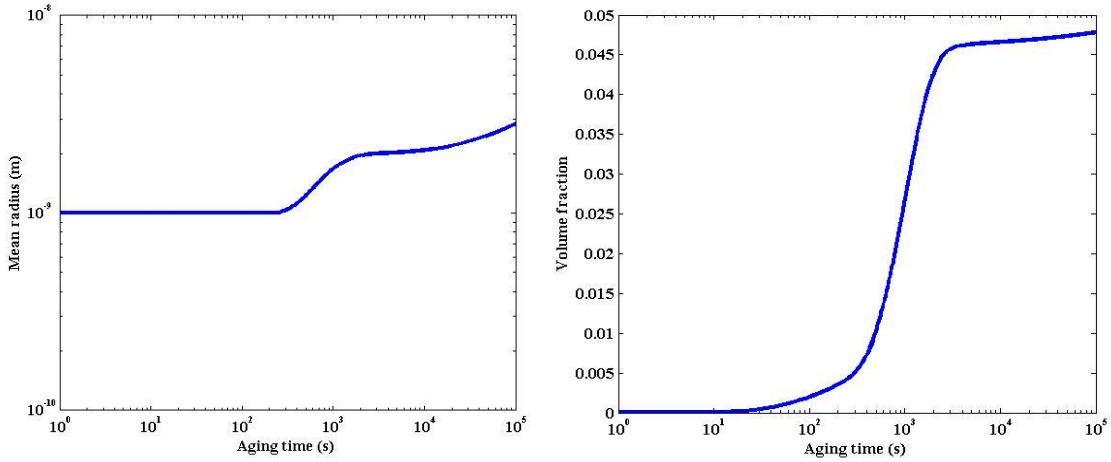

Figure 1 The mean particle size and volume fraction predicted by A.Deschamps's model

The nuclei remain at the critical radius at the nucleation stage. And the nucleation rate drop to zero when no extra solute element remains in the solid solution. Growth period is corresponded with the dramatically increased mean radius of precipitates, meanwhile the volume fraction increases. In coarsening period, the radius slowly increases and the volume fraction almost remain the same at peak value.

2.2 Discrete value approach

New formed nuclei at each time step are grouped and the size evolution of each group is tracked. The following plots (Figure 2) showing the changes of mean radius, volume fraction and particle size distribution during aging are based on this approach.[10]

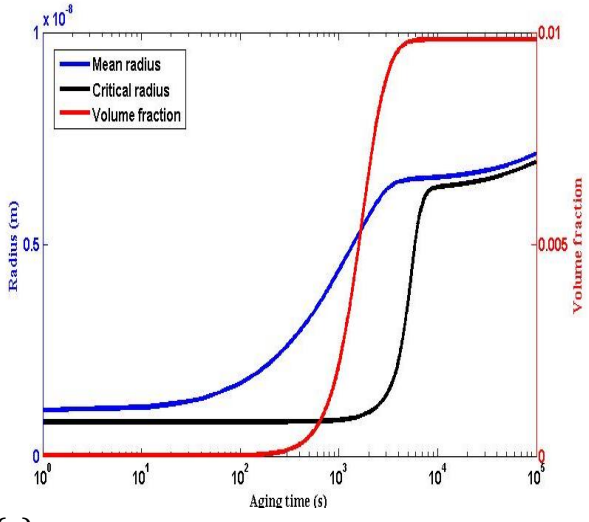

(a)

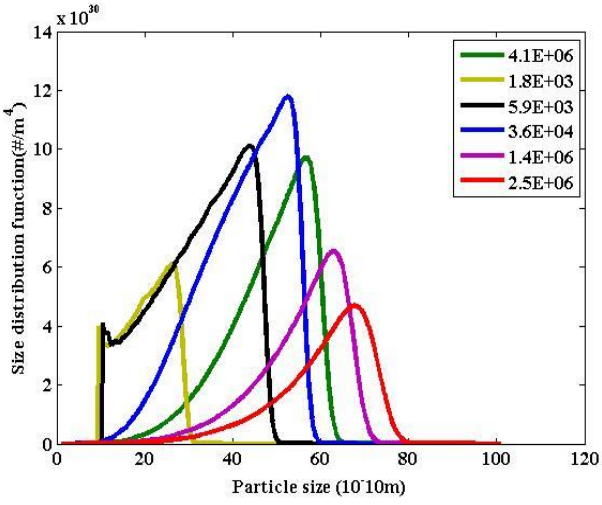

(b)

Figure 2 The mean radius, critical radius, density distribution and volume fraction of aluminum alloy A356 at 443K, and different aging time, predicted by Myhr's model

With the density distribution at each radius group, the total density at each time and the mean radius can be calculated by summing up all groups. The volume fraction can be then derived based on the assumption of spherical precipitate particles.

3 Yield Strength Model

3.1 Either shearing or bypassing mechanism considered

Considering the particle radius, there are two types of dislocation hardening mechanisms- shearing and bypassing. Both mechanisms follow the similar strengthening prediction, which is given below [10]:

$$\sigma = \frac{MF}{bL} = Cr^m f^n \quad (1)$$

where M is the Taylor factor, F represents the average obstacle force, b is the burgers vector and L is the average space of particles. C is the coefficient decided by material and aging conditions, r and f represent the mean radius and volume fraction of the precipitates, respectively. m and n are different for shearing and bypassing mechanism. In Liu's model, particles are considered to strengthen the matrix via bypassing mechanism.

3.2 Combined shearing and bypassing mechanism

Ashby and Shercliff combined shearing and bypassing mechanism using the harmonic value of shearing and bypassing strength. [1] Deschamps' model and Myhr's model separate the shearing mechanism and bypassing mechanism with critical radius, applying corresponding equations in different periods. [4] At the beginning of the aging process, the particles are small and coherent with matrix; the dislocation can shear these particles. [14] At peak aging and over-aged conditions, particle size is large and incoherent with matrix and bypassing mechanism dominates deformation. [13]

4 Results and Discussion

4.1 Modeling of precipitate evolution during aging

Difficulty in building good microstructure model is how to quantify the nucleation, growth and coarsening period. Critical radius, defined as the minimum radius for stable particle, is one way to separate growth and nucleation periods, which is widely used in many models. However, it is hard to identify when the coarsening period begins since the radius grows continuously with no obvious change in short period of time. Deschamps defines coarsening portion to calculate the growth and coarsening particles fraction: [4]

$$f_{coarse} = 1 - \mathrm{erf}\left(4\left(\frac{R}{R_0}\log\left(\frac{C}{C_e}\right) - 1\right)\right) \quad (2)$$

Volume fraction can be another way to build the microstructure model without considering radius. Figure 3 gives the volume fraction evolution and yield strength change curve predicted by Ashby's model. Lloyd also predicted volume fraction by JMAK model which was calibrated using TEM.

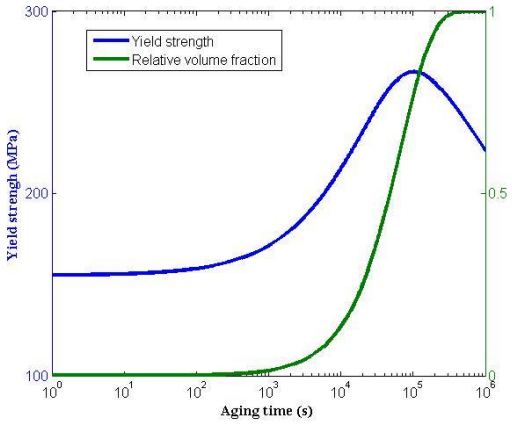

Figure 3 Yield strength and volume fraction for Al-Mg-Si at 443K

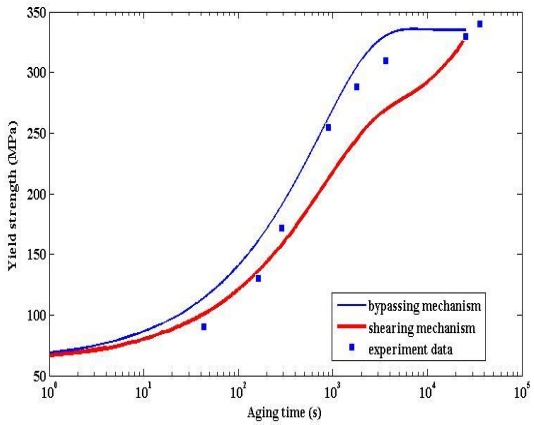

Figure 4 Shearing and bypassing mechanism for A6111 aging at 453K

4.2 Modeling of yield strength

As mentioned above, the shearing and bypassing mechanisms are strongly related with the radius of particles. Lloyd made a comparison when considering only shearing mechanism or bypassing mechanism. [12] In Figure 4, the experimental data lie between the two prediction lines, which indicate that there should be a method to

combine two dislocation mechanisms in order to make the prediction more reliable. Ashby's model takes the harmonic value of shearing strength and bypassing strength which matches well with experimental data before peak-aging, but not good in overaging period.

The orientation and the shape of precipitates also affect the yield strength. [13] Liu considers this effect in his model when predicting Al-Mg-Si alloy aging behaviors, [7] following the method given by Zhu et al. to evaluate the yield strength based on bypassing mechanism. [8]

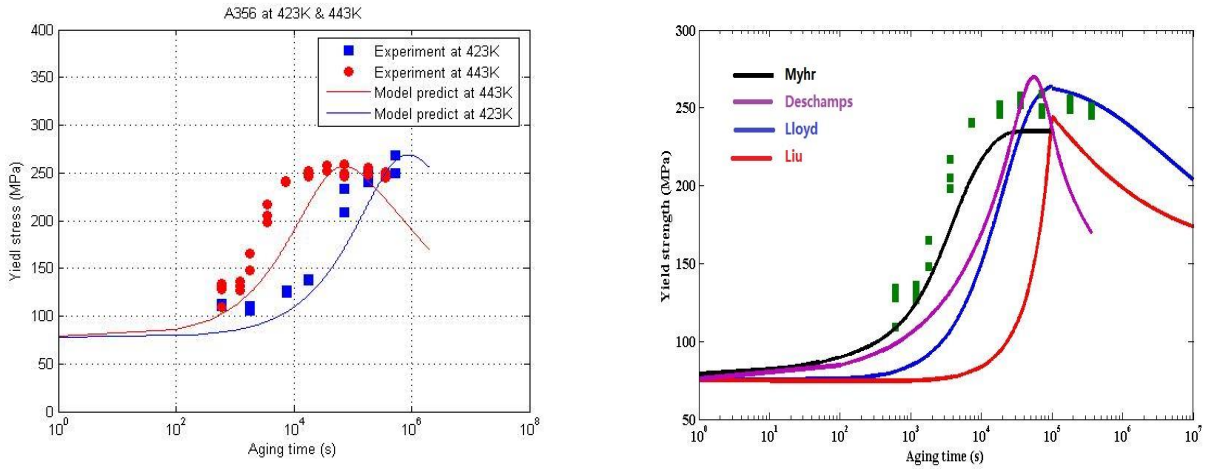

(a) (b)

Figure 5 (a) Ashby's model;(b) Lloyd, Liu, Deschamps & Myhr's model for A356 at aging temperature 443K, the green square dots are experiment data;

Figure 5 compares the yield strength predictions from various models including Ashby, Loyld, Liu, Deschamps and Myhr's model with experimental data of A356 alloy aged at 443K. It can be seen that Liu's model has the largest deviation from the experimental data and Ashby and Myhr's models match well with the experimental data.

5 Future works

Microstructure model is critical to the precipitate hardening prediction. Mean or discrete value approaches are developed well for the spherical shape precipitates. However, the actual shape of the precipitate particles in aluminum alloys is not spherical. Following the principle of the discrete value approach, it seems that the

length and the radius of the precipitate particles can be considered to be two-axis coordinate to classify the group of particles. A better method to distinguish the growth and coarsening periods in order to separate the shearing and bypassing mechanisms is needed. In discrete value approach, each group can be considered as a unity to analyze its contribution to the yield strength by comparing with the critical radius.

6. Acknowledgement

This work is financially supported by Materials Technology Department of GM Global Powertrain Engineering.

Reference:

1 H.R Shercliff and M.F. Ashby, *Acta mater*, Vol 38, No. 10, pp. 1789-1802, 1990

2 M. Perez, M. Dumont and D. Acevedo-Reyes, *Acta mater* 56(2008) 2119-2132

3 A. Deschamps, *Acta mater*, Vol 47, No. 1, pp 281-292, 1999

4 A. Deschamps, *Acta mater*, Vol 47, No. 1, pp 293-305, 1999

5 S. Esmaeili, *Acta mater* 51 (2003) 2245-2257,

6 A. Bahrami, *Metallurgical and Materials Transactions A*, 09 August 2012

7 G. Liu, G.J. Zhang, X.D. Ding, J. Sun, K.H. Chen,. *Materials Science and Engineering A*

8 A.W Zhu, E.A Starke, Jr, "Stress aging of Al-Cu Alloys: Computer Model", *Acta mater*. 49(2001)3063-3069

9 S. Esmaeili, D.J. Lloyd, *Metallurgical and Materials Transactions A*, Vol 34A, March 2003.

10 O.Myhr, *Acta mater*. 48(2000)1605-1615,

11 S. Esmaeili, D.J. Lloyd, *Acta mater* 51(2003) 2243-2257,

12 M. Ferrante and R.D. Doherty, *Acta mater* Vol. 27 pp. 1603-1614

13 O.R.Myhr, S.J. Andersen, *Acta mater*.49(2001) 65-75

14 M. Song, Metallurgical and Materials Transactions A, 443(2007) 172-177

To be submitted to Materials Performance and Characterization

Modeling the yield strength of an A356 aluminum alloy during the aging process

Guannan Guo[1], Qigui Wang [2], Yiming Rong[1,3]

[1] Worcester Polytechnic Institute, Manufacturing Engineering, Worcester, MA 01609 USA

[2] GM Powertrain Materials Technology, Pontiac, MI, USA

[3] Mechanical and Energy Engineering Department, Southern University of Science and Technology of China, Shenzhen 518055, China

1 Introduction of the precipitate hardening models

Aluminum alloys are widely used in automotive industry because of their high mechanical performance and lightweight. The precipitate hardening process is an important heat treatment technique to improve the yield strength of aluminum alloys. It is generally acknowledged that the precipitate phase formed during the aging process strengthens the matrix by blocking the dislocation motions. [1] Mobile dislocations can shear coherent or semi-coherent smaller precipitate particles or bypass the larger incoherent precipitate particles, which makes different strength contributions to the matrix. Thus, the dislocation density will be increased by the interactive motion of precipitate phase and dislocations. [2] Most aging hardening models have applied process parameters, such as aging conditions, to relate with the final mechanical properties, such as hardness or yield stress. In these simulations, the process parameters are first used to calculate the precipitate phase morphology and volume distribution, and then these microstructure data are used to calculate the yield stress. [3, 4]

Precipitate phase formation is affected by aging conditions and aluminum alloy components. In general, one primary precipitate phase may make a dominant contribution to strengthen the matrix, which is usually fully coherent within the

matrix and has the dominant volume fraction at the peak-aged state. [1] For a giving alloy composition, the aging sequence under different aging conditions can be characterized by TEM and DSC curves to determine the prime strengthening precipitate phase. Based on the experimental data, the crystallographic parameters, orientations, dimensions and particle space distributions of the precipitate phase are obtained, and the related thermodynamic parameters can be derived based on first principles theory. [5, 6]

The chemical concentration, aging time and temperature are input data to evaluate the volume fraction of the precipitate phase. The variation of the solute element concentration can change the final yield stress under the same aging conditions. The activation energy and equilibrium volume fraction for the precipitate phase is a function of the temperature, which inhibits or stimulates the formation of the precipitate phase. TEM and isothermal calorimetric experiments can be used to obtain the volume fraction of the prime precipitate phase. While the TEM image only reflects the volume distribution at a selected section, the DSC curve for a specific material gives the exothermic and endothermic peaks and the heats released or absorbed, corresponding with the precipitation or dissolution, respectively. [11] After obtaining the activation energy for the prime precipitate phase, the classic JMAK equation could be adapted to calculate the volume fraction of the precipitate phase:

$$f = f_{eq} exp(-k(T)t)^n \quad (1)$$

Where f_{eq} is equilibrium volume fraction, T is temperature, k(T) is transformation kinetic as a function of temperature and Q_a is active energy. t is transformation time and n is a materials relate parameter. The mathematical presentation of k(T) is given as followed:

$$k(T) = k_0 exp\left(-\frac{Q_a}{RT}\right) \quad (2)$$

When taking all the particles as spheroids for simplification, the volume of the precipitate particles can be easily calculated. The volume fraction increases very slightly at the beginning part of the aging process; meanwhile, the precipitate particles nucleate during this period. Then, the volume fraction rapidly rises to the peak value, which represents the pure growth period of the particles. After the peak-aged state, the

volume fraction is assumed to maintain the peak value. The smaller particles dissolve into the matrix and larger particles continue to grow, which leads to the total volume fraction remaining the same during the overaged period. However, the volume of the prime precipitate phase will decrease during the transformation from the coherent and semi-coherent stage to the incoherent stable phase. The volume fraction calculations in previous models are all concentrated on the prime precipitate phase without considering the phase transformation from primary precipitate phase to other phases. In this paper, a new aging model of A356 alloy is proposed consider the volume fraction change of primary strengthening precipitate phases. The new model will fulfill at least the following functions:

a) To determine the volume fraction transformation from the metastable phase to the stable phase and obtain the volume fraction evolution of each phase;
b) To modify the volume change due to the loss of the metastable precipitate phase. The volume fraction of the metastable precipitate phase during the aging process should be the original value minus the fraction transformed to the stable phase.

2 Experiments

In this project, A356 is chosen as test materials to accomplish aging experiments. The chemical content of A356 is given as followed:

Table 1 A356 chemical composition

Element	Cu	Mg	Si	Ti	Mn	Zn
Wt%	~0.2(max)	0.2~0.4	6.5~7.5	0.25	0.1	0.1

The heat treatment process of A356 is typical T6 heat treatment. Samples are heated to 540C solution temperature and keep for 10 hours, then take out the samples and quickly quench to room temperature. The as-quenched samples are kept in fridge for avoiding natural aging. Then samples are taken out to reheat various aging temperature: 150C, 160C and 170C for 10min, 20min, 30min, 1 hour, 2 hours, 5 hours, 10 hours, 20 hours, 50 hours and 100 hours. The aged samples quench in air to room temperature after aging process and conduct quasi-tensile tests. The 0.2% offset yield strength of samples under different aging conditions are obtained for experimental fitting and validation.

3 Precipitate hardening model of A356 alloy

Before establishing precipitate hardening model of A356 alloy, the primary strengthening precipitate should be determined in order to obtain related materials parameters. In this section, the aging sequence and primary strengthening precipitate of A356 are discussed and confirmed. Then, applying JMAK equations, the volume fraction of primary strengthening precipitate is used to predict the yield strength of A356 under different aging conditions. After obtaining needed microstructure parameters, the calculation of yield strength is given as consequence. The strengthening mechanism is obeyed bypassing mechanism corresponded with strong obstacle particles during underaged and peak aged states.

3.1 A356 aging sequence and the primary strengthening precipitate

There is a generally accepted aging sequence for casting the A356 aluminum alloy: SSS(supersaturated solid solution)α →GP zones (spheres or needles) →β″(needles) →β′ (rods) →β (plates, Mg_2Si or non-stoichiometric Mg_xSi_y). At the peak aged stage, the primary strengthening precipitate in the cast A356 aluminum alloy is the Mg_5Si_6 (β″) precipitate phase, which is different from the Mg_2Si (β′) phase previously reported. Therefore, in order to apply the thermal growth model, the precipitate phase lattice parameter and related thermal constant should be calculated based on the β″ precipitate phase.

Mg_2Si rods such as the β′ phase precipitate from β″; meanwhile, volume loss during the transformation because of the phase change will occur. Considering different precipitate phases may exist during the aging process, we should obtain knowledge of those possible precipitate phases. The following table gives the lattice parameters of possible precipitate phases in the Al-Mg-Si alloy system:

Table 2 Possible precipitate phases of Al-Mg-Si alloy aging process

Phase	Lattice parameter (nm)
GP-zones, Mg_4AlSi_6	a=1.48, b=0.405, c=0.648, β=105.3°
β″, Mg_5Si_6, Monoclinic	a=1.516, b=0.405, c=0.674, β=105.3°
β′, $Mg_{1.8}Si$, Hexagonal	a=b=0.715, c=0.405, γ=120°
β, Mg_2Si, Cubic	a=0.6354
U1, $MgAl_2Si_2$	a=b=0.405, c=0.674, γ=120°
U2, $Al_4Mg_4Si_4$	a=0.675, b=0.405, c=0.794

Based on the aging sequence, the β″ phase precipitates from the GP-zones. Thus, the volume changes contributed by β″ are calculated directly by the volume loss from the GP-zones to β″. However, there will be some β′ phase formulated from β″, which means the volume of β″ should be subtracted from the transformed β′ phase to modify the value before calculating the growth contribution of the β″ phase. Additionally, the volume of the β′ phase also needs to be subtracted from the volume of the β phase, since in the latter periods of the aging process, the β′ phase will turn into the β phase. In addition to the aging sequence, the Mg/Si content ratio and aging conditions also affect the precipitate phase distribution. The concentration of Mg is approximately 0.31%~0.34%, while the Si concentration is 0.7%. Some works have also noted the phase fraction of these precipitate phases may be changed because of the chemical concentration and aging conditions. In the T6 heating condition, the β″ phase is the prime precipitate phase with a high volume fraction when the aging time is less than half an hour, while the β′ phase only forms slightly. When the aging time prolongs 3 hours, the prime precipitate phase is the β′ phase, and almost no β″ phase exists. The following chart given by C.D. Marioara in 2006 shows the phase volume fractions at different aging times of these precipitate phases:

Table 3 Si/Mg ratio and aging treatment effect on the prime precipitate phase volume fraction

Si/Mg ratio	Aging treatment	Prime precipitate phase
2	3 h	97% U1 phase(Al_2MgSi_2)
1.25	10 min	76% β″
	3 h	26% β′, 65% U2($Al_4Mg_4Si_4$)
0.8	10 min	100% β′
	3 h	97% β′

In this paper, the volume loss of primary strengthening precipitates is the phase transformation from β″ phase to β′ phase. Since T6 aging process is applied in this experiment, β phase which is usually formed in over aging process is not included in phase transformation. This phase transformation also explains the overestimation of yield strength at peak aging.

3.2 Volume fraction of primary strengthening precipitates

The primary strengthening precipitate is β″ of A356 alloy in aging process. In this work, the volume fraction of the precipitate phase is used as an input to predict the final yield stress. The basic equation of the volume fraction applied JMAK equation:

$$f_r = 1 - exp(-k(T)t)^n \quad (3)$$

This equation can be applied to the pre-aged aluminum alloys in isothermal or non-isothermal aging processes. For the present work, with our A356 experiment, the isothermal aging process is mainly taken into consideration. Parameter *n* in equation 3 is determined based on the shape and composition of the precipitates. Parameter *k* is a temperature dependent constant, which is calculated by a form of the Arrhenius-type relationship. The JMAK equation is adapted to predict the relative volume fraction change of the precipitates during the nucleation and growth process.

Based on JMAK equation's assumption, the volume fraction of primary strengthening precipitates remains constant at peak state and after. However, with prolonging the aging process, some of the meta-stable precipitates will form from primary strengthening precipitates, which reduces the volume fraction of primary strengthening precipitates. Ford's patent proposed a method to optimize heat treatment via predicting thermal growth of the precipitate phases.

The second term is the volume fraction of the precipitate phase, which is calculated based on the JMAK equation. This term is determined by the thermally dependent equilibrium phase fraction of the precipitate phase $f_{eq}(T)$, and the temperature-dependent kinetic growth coefficient. The function $f_{eq}(T)$ utilizes the computational thermodynamic method, considering the complexities of the precipitation-hardened alloys, and is only dependent on temperature.

The temperature-dependent kinetic growth coefficient *k(T)* is used to predict the volume at different heating times. The following equations show k values of the primary precipitate phase β'' and transformed phase β' of A356 alloy:

$$k_{\beta'} = 8750\, exp\left(-\frac{90000}{RT}\right) \quad (4)$$

$$k_{\beta''} = 19000\, exp\left(-\frac{76000}{RT}\right) \quad (5)$$

After obtaining the above terms, the volume fraction of the precipitate phase, after considering the transformation from the precipitate phase to the stable phase, can be modified as:

$$f_r^{\beta''} = 1 - exp\left[-k_{\beta''}(T)t\right] \quad (6)$$

$$f_r^{\beta'} = 1 - exp\left[-k_{\beta'}(T)t\right] \quad (7)$$

$$f_r = f_r^{\beta''} - f_r^{\beta'} \quad (8)$$

Since the precipitate phases will tend to grow or transform before being stabilized and bring detritus deformation to the alloy system, the volume fraction for the primary precipitate phase is not constant as previous assumption claimed. The combination of the volume evolution and transformation among the precipitate phases during the aging process can reduce the volume fraction of primary strengthening precipitate. Therefore, the relative volume fraction of primary strengthening precipitate, which is used as input data, is obtained from the difference between the value calculated from equation 6 and 7.

3.3 Modeling of yield strength of A356 in underaged process

The yield strength model of A356 is composed of three terms: the intrinsic strength of aluminum (σ_i); the solid solution strength (σ_{ss}) and precipitate strength (σ_{ppt}). They are summarized by following equation:

$$\sigma = \sigma_i + \sigma_{ss} + \sigma_{ppt} \quad (9)$$

Generally, the intrinsic yield strength of aluminum matrix is treated as constant during aging process. The strength contribution of solid solution is affected by the transformed volume fraction of primary strengthening precipitates, which are nucleated from solid solution. Esmaeili gave the mathematical relationship between solid solution strengthening and volume fraction of primary strengthening phase:

$$\sigma_{ss} = \sigma_{0ss}(1 - f_r)^{2/3} \quad (10)$$

The strengthening mechanism of A356 in aging process is governed by the interactive motion of precipitate particles and dislocations. Based on different size of precipitate particles played as obstacles to mobile dislocation, the strengthening mechanism can be categorized as strong or weak strengthening depending on dislocation breaking angle. When the breaking angle is smaller than 120°, the mobile dislocation could by-

passing this kind of precipitate particle (which is called strong obstacles) and leave a dislocation loop behind so that increasing dislocation density. When the breaking angle is larger than 120°, the mobile dislocation will be cut when encountering with precipitate particles, in this circumstance, such particles are called small obstacles. During underaged period, the precipitate strengthening mechanism is governed by strong obstacles strengthening. The contribution of precipitate strengthening is calculated by following equation:

$$\sigma_{ppt} = \frac{MF}{bL} \quad 11$$

where M is the Taylor factor, b is magnitude of the Burgers vector, F is the average force of a particle and L is the average space of the particles. The average obstacle strength F has a simple linear relationship with the average radius of the differently shaped or oriented precipitates, and the average spacing L is defined as the planar center-to-center distance between the strong particles or adapted to Freidel statistics for a triangular array of weak obstacles, which is related to the volume fraction of the precipitate phase. [7-9] At peak-aging, Equation 11 may be rewritten as:

$$\sigma_{ppt} = Af_r^{\frac{1}{2}} \quad 12$$

where A is a constant related to the material, and f_r represents the relative volume fraction of the precipitate phase. [10] Under this condition, the yield stress is only dependent on the volume fraction, regardless of the morphology of the precipitate phases. Constant A will be calibrated by yield strength at peak aged state. The average obstacle strength is taken as a simple linear relationship with the average radius of the differently shaped or oriented precipitates, and the average spacing is defined as the planar center-to-center distance between the strong particles or adapted by Freidel statistics for a triangular array of weak obstacles. Therefore, the total yield strength is obtained as followed:

$$\sigma = \sigma_i + \sigma_{0ss}(1 - f_r)^{2/3} + Af_r^{\frac{1}{2}} \quad 13$$

The flow chart of modified precipitate hardening model for A356 is pictured as followed:

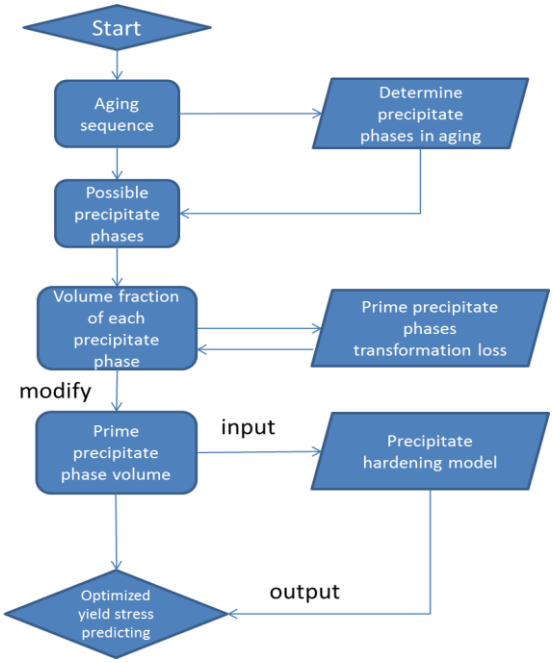

Figure 1 Flow chart of modified precipitate hardening model for A356

3.4 Simulation results compare between original precipitate hardening model and modified model

Based on original precipitate hardening, the volume fraction of primary strengthening precipitates remains constant at and after peak aged state. The strengthening mechanisms at under aged and over aged period are different. In this project, the under aged aging process is concerned. Figure 2 gives the simulation results obtained from original model. It can tell from the figure that the simulation results predict large underestimation at 150C compared with experimental data while give overestimation at 170C. Since during under aged state, the strong strengthening mechanism is used to calculate the yield strength, the volume fraction of primary strengthening phase should be the only reason to cause this derivation. If the volume fraction of primary strengthening precipitate is the only concerned parameter, the deviation of

experimental results and simulation results cannot be eliminated.

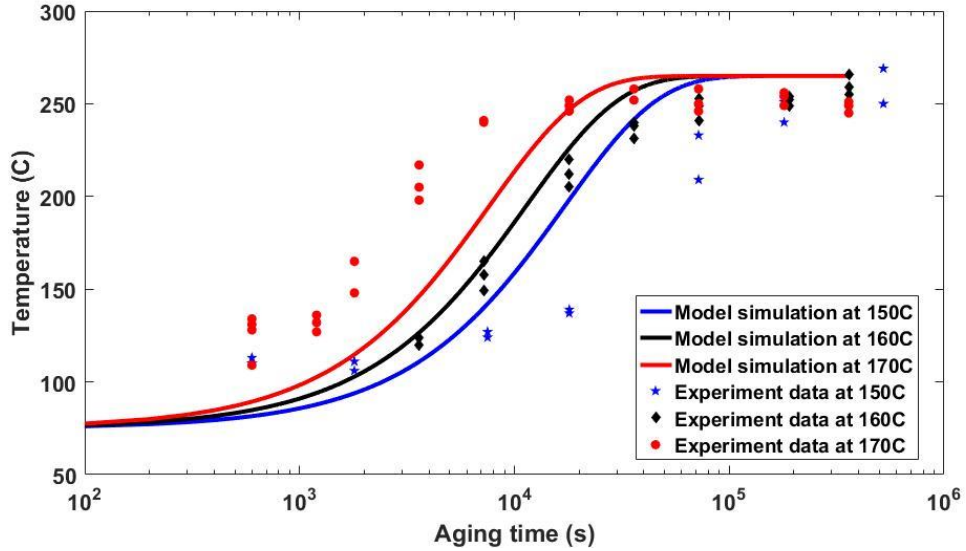

Figure 2 Yield strength prediction results by original model at different aging conditions

When applying the optimized model, the difference kinetic parameters of primary strengthening precipitate $\beta''$and transformed precipitate β' can help to improve the accuracy of volume fraction value at both lower temperature and high temperature. The needed parameters for optimized model are given in Table 2 and the simulation results for A356 are given in Figure 3:

Table 2 The value of parameters used in optimized model

Adjusted parameters used in optimized model	Value
σ_i	10MPa
σ_{0ss}	42MPa
A	240MPa

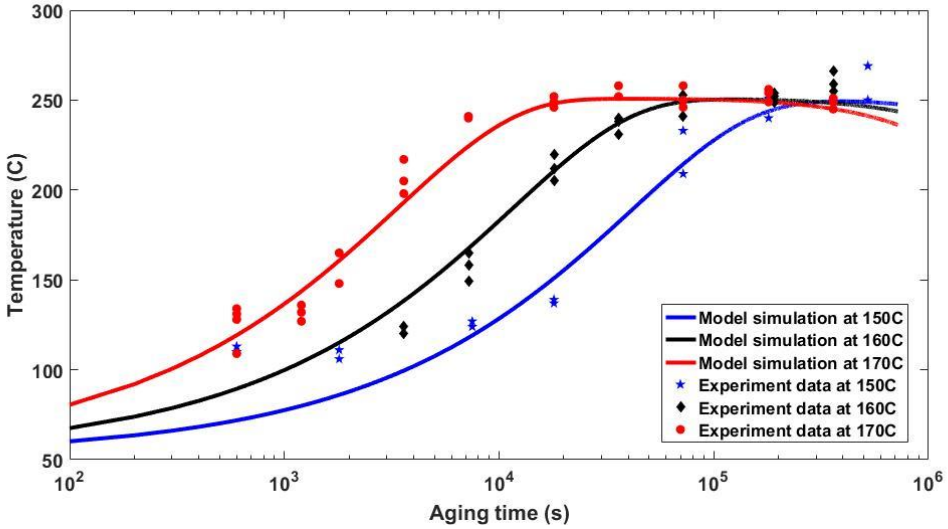

Figure 3 Yield strength predicted by optimized model for A356 at different aging temperatures

It can be seen from the figure that the predicted results match well with the experimental data. While the previous precipitate hardening model is overestimated during the over-aging period, the modified model shows the drop of the yield stress since the difference volume fraction of primary precipitate and transformed precipitate reduce at 150C. At 170C, the overestimation of original simulation results also eliminate because of more primary precipitate occurred in under aged state than transformed precipitate compared with low temperature.

4 Summary

The precipitate hardening model based on JMAK equation is reviewed and applied to predict A356 aging response behaviors. The volume fraction is used as an input to study the microstructure evolution, according to the JMAK equation. It is concluded that applying the JMAK equations is much easier to do, and a satisfactory simulated result can be obtained from the original model. However, the simulated result is overestimated in the over aged period at high temperature while underestimated in under-aged period. The volume fraction of the prime strength precipitate for hardening is considered to remain the same since there is no newly formed precipitate particles in pure growth period in under-aged period and large precipitate particle will consume small particles in over-aged period. While in reality, the transformation among the prime precipitate phase and the other precipitate phases or stable phases can lead to extra volume losses during the whole aging process. Therefore, the modification of the volume fraction should be considered. In this project, the

optimized method of volume fraction is learnt from thermal growth model based on Ford's patent. By applying this model, the volume change due to the newly formed precipitates in the aging process and the volume fraction of each phase can be calculated. The differences in volume transformation kinetics of primary strengthening precipitate β'' and transformed precipitate β'can adjust such derivation. The optimized precipitate hardening model is presented in this report.

References

1 Jacobs, M. H. "Precipitation hardening." *TALAT Lecture: Interdisciplinary Research Centre in Materials The University of Birmingham, UK* (1999): 2-10.

2 Anjabin, N., and A. Karimi Taheri. "Microstructure based modeling of flow behavior of Al-Mg-Si alloy at different temper conditions." *Materials Science and Technology* 29.8 (2013): 968-974.

3 Shercliff, H. R., and M. F. Ashby. "A process model for age hardening of aluminum alloys—I. The model." *Acta Metallurgica et Materialia* 38.10 (1990): 1789-1802.

4 Zhu, A. W., and E. A. Starke Jr. "Strengthening effect of unshearable particles of finite size: a computer experimental study." *Acta materialia* 47.11 (1999): 3263-3269.

5 Marinara, C. D., et al. "Post-β ″phases and their influence on microstructure and hardness in 6xxx Al-Mg-Si alloys." *Journal of materials science* 41.2 (2006): 471-478.

6 Ravi, C., and C. Wolverton. "Comparison of thermodynamic databases for 3xx and 6xxx aluminum alloys." *Metallurgical and Materials Transactions A* 36.8 (2005): 2013-2023.

7 Gerold V. In: Nabarro FRN, editor. Dislocations in Solids,vol. 4. Amsterdam, The Netherlands: North Holland Publ. Co.; 1979. p. 219.

8 Ardell AJ. Metall Trans A 1985;16A:2131.

9 Lloyd DJ. In: Proceedings of the 7th Int Conf on the Strength of Metals and Alloys, I.C.S.M.A.-7, Montréal, Canada, vol. 3. Oxford: Pergamon Press; 1985. p. 1745.

10 Esmaeili, S., D. J. Lloyd, and W. J. Poole. "A yield strength model for the Al-Mg-Si-Cu alloy AA6111." *Acta Materialia* 51.8 (2003): 2243-2257.

11Esmaeili, S., and D. J. Lloyd. "Modeling of precipitation hardening in pre-aged AlMgSi (Cu) alloys." *Acta materialia* 53.20 (2005): 5257-5271.

12 Perez, Michel, M. Dumont, and Daniel Acevedo-Reyes. "Implementation of classical nucleation and growth theories for precipitation." *Acta materialia* 56.9 (2008): 2119-2132.

13 Deschamps, A., and Y. Brechet. "Influence of predeformation and ageing of an Al–Zn–Mg alloy—II. Modeling of precipitation kinetics and yield stress." *Acta Materialia* 47.1 (1998): 293-305.

14 Myhr, O. R., and Øystein Grong. "Modelling of non-isothermal transformations in alloys containing a particle distribution." *Acta Materialia* 48.7 (2000): 1605-1615.

15 Liu, Gang, et al. "Modeling the strengthening response to aging process of heat-treatable aluminum alloys containing plate/disc-or rod/needle-shaped precipitates." *Materials Science and Engineering: A* 344.1 (2003): 113-124.

16 Allison, John, and Christopher Wolverton. "Method of optimizing heat treatment of alloys by predicting thermal growth."

Contribution

In the paper of "Competitive relationship between thermal effect and grain boundary precipitates on the ductility of an as-quenched Al–Cu–Mn alloy", the experiments including tensile tests and observations of fracture surface under SEM are conducted. The phenomena that ductility of Al-Cu-Mn alloy change a lot when at low temperature and high temperature ranges is observed in tensile tests during different temperatures. Then, a series of tensile tests under different strain rates and temperatures are conducted, which proves temperature has dominant impact on ductility behaviors. The observations of fracture surface via SEM show there are precipitates gathered at the grain boundary, and such precipitates, which are identified with EDS, are confirmed to reduce bonding energy of neighbor grains. Thus, the ductility reduction at high temperature range can be explained by precipitates formation.

In the paper of "Temperature-dependent constitutive behavior with consideration of microstructure evolution for as-quenched Al-Cu-Mn alloy", a modified constitutive model is proposed to describe mechanical behaviors of as-quenched Al-Cu-Mn alloy from room temperature to high temperature (up to 500C). Stress-strain curves obtained tensile tests behaves different pattern at the low temperature range and the high temperature range. Arrhenius type constitutive model with Zenor-Hollomon parameters is modified since the classical version of this model is only valid at high temperature range with the assumption that hot deformation energy remains constant. My contribution in this paper is release the assumption so that hot deformation energy is a function of temperature. At low temperature, the forest dislocations dominates the deformation properties and precipitates formed at high temperature interact with mobile dislocation and reduce bonding energy of grains affect deformation behaviors at high temperature range. At last, the final temperature-dependent constitutive models are established in three temperature ranges, low temperature range, transition temperature range and high temperature range.

In the paper of “A brief review of precipitate hardening models for aluminum alloy”, my work is focus on previous classical precipitate hardening models for aluminum alloy and categorized them into mean value approach and discrete value approach based on the simulation method of morphology and volume fraction of precipitate phases. The regeneration of classical models is accomplished with experiment data of A356 offered by General Motors Company.

At last, a modified precipitate hardening model is put forward to obtain more accurate simulation results of A356 aging response behaviors. The volume fraction of primary strengthening precipitate β'' is adjusted by considering the volume loss caused by phase transformation. The β' phase will nucleate from β'' phase so that the total volume fraction of β'' is reduced. The optimized mode gives perfect fitting results compared with experiment data.